Vibrational studies of Cyanobacteriochromes

Experimental construction for cryogenic measurements

Author:	W.J.M. Franse
Date:	03-06-16
Number of pages:	79 (Incl. 27 pages of Appendices)
1e Coach HHS:	R.A. Mantel
2e Coach HHS:	A.J. Lock
Internship Mentor:	Prof. D.S. Larsen

Scriptieverslag

Gegevens Student

Naam:	W.J.M. Franse
Studentnummer:	12114979
Adres:	A.L. Dyserinckstraat 96 2032 RE, Haarlem

Gegevens Onderwijsinstelling

Instelling:	De Haagse Hogeschool Vestiging Delft, opleiding Technische Natuurkunde
Adres:	Rotterdamseweg 137, 2628 AL, Delft
	015-260 6200
1e Coach:	R.A. Mantel
Contactgegevens:	r.a.mantel@hhs.nl
2e Coach:	A.J. Lock
Contactgegevens:	a.j.lock@hhs.nl

Gegevens stageverlenende instelling

Instituut:	University of California, Davis Larsen Lab
Afdeling:	Chemistry
Adres:	Shields Ave. 1 CA, 95616, Verenigde Staten
Contactgegevens:	+1 530-752-1011
Stageperiode:	08-02-16 t/m 03-06-16
Stagebegeleider:	Prof. D.S. Larsen
Contactgegevens:	dlarsen@ucdavis.edu (530) 754-9075

"Science, my lad, is made up of mistakes, but they are mistakes which it is useful to make, because they lead little by little to the truth."

– **Jules Verne**

Abstract

Cyanobacteriochromes (CBCRs) are phytochrome-related photoreceptor proteins, which transform protein structure when illuminated by a particular color of light. During this photo-conversion, the CBCRs convert from one stable state into another, via the evolution through several intermediate states. To investigate the nature of the intermediate and terminal states, the time-resolved vibrational spectra of these states were to be characterized by combining a liquid nitrogen cryostat with a Fourier Transform InfraRed (FTIR) spectrometer.

The research work done in this thesis shows steps that were taken to build a FTIR cryokinetics set-up. Effort was dedicated toward optimizing FTIR detection for both room temperature and for temperature dependent measurements.

This required constructing a home-made liquid nitrogen purging system to purge the FTIR instrument of water vapor and CO_2. To further avoid these interfering signals, a moving rod was developed to move either the protein sample or buffer material in and out of the detector's beam pathway to measure new background spectra. Hence, a temperature dependent background scan was taken repeatedly to eliminate the detector's drift ($(2.4\pm0.3) \cdot 10^{-4}$ [min^{-1}]) and interference of water vapor and CO_2. By using an aperture of 4 mm with 4 cm^{-1} resolution, along with the author's handmade automated system, 10 scans are made every minute to keep track of the kinetic traces of the protein during cryo-cooling.

Room temperature experiments revealed that CBCRs undergo secondary structural changes in the region of 1625-1550 cm^{-1}, where β-sheet-α-helix transformation takes place. In addition, it was found that CBCRs exhibits significantly more activity (e.g., hydrogen-bonding break or changing local dielectric constants) in the A-ring C_1=O ((1715 ± 2) / (1713 ± 1) cm^{-1}) and D-ring C_{19}=O ((1736 ± 1) / (1732 ± 1) cm^{-1}). This is in contrast to other cyanobacterial phytochromes, which have no activity in this region.

Nederlandse Samenvatting

Cyanobacteriochromen (CBCR) zijn fytochroom-gerelateerde fotoreceptor eiwitten, die van eiwitstructuur veranderen wanneer deze belicht worden met bepaalde kleuren licht. Tijdens deze foto-conversie transformeren de CBCRs van de ene stabiele staat naar de andere, via het doorlopen van verschillende tussenproducten. Om de trillingsenergieën en kinetische sporen te meten van zowel de tussenproducten als de terminale staten, zal een vloeibare stikstof cryostaat worden gebruikt in combinatie met een Fourier Transform InfraRed (FTIR) spectrometer.

Het onderzoekswerk dat is uitgevoerd in deze scriptie laat zien welke stappen zijn ondernomen om een FTIR cryokinetic set-up te bouwen. Inspanning werd gewijd aan het optimaliseren van de FTIR om kamertemperatuur en temperatuur afhankelijke metingen te verrichten.

Dit vereiste de bouw van een zelfgemaakte vloeibare stikstof zuiveringssysteem om de FTIR cryokinetics experimenten te zuiveren van waterdamp en CO_2. Om deze stoorsignalen verder te voorkomen is een op-en-neer bewegende stang ontwikkeld dat zowel eiwitmonsters als buffermateriaal in en uit de detector's stralingspad haalt om nieuwe achtergrond spectra te nemen. Door dit te doen wordt een temperatuur afhankelijke achtergrond scan herhaaldelijk genomen om zowel de drift van de detector ($(2{,}4 \pm 0{,}3) \cdot 10^{-4}$ [min^{-1}]) als de interferentie van waterdamp en CO_2 te elimineren in de spectra. Door een apertuur van 4 mm doorsnee met een resolutie van 4 cm^{-1} te gebruiken, samen met een zelfgemaakt automatisch systeem, worden er 10 scans per minuut opgenomen om de kinetische sporen van het eiwit gedurende cryogene koeling te kunnen volgen.

Bij de kamertemperatuur experimenten bleek dat CBCRs een secundaire structurele verandering ondergaan in het gebied van 1625-1550 cm^{-1}, waarbij een β-sheet-α-helix transformatie plaats vindt. Ook werd vastgesteld dat CBCRs meer activiteit vertonen (door bijvoorbeeld breking van waterstofbindingen of wijzigingen van plaatselijke diëlektrische constanten) in de A-ring $C_1 = O$ ((1715 ± 2) / (1713 ± 1) cm^{-1}) en D-ring $C_{19} = O$ ((1736 ± 1) / (1732 ± 1) cm^{-1}). Dit is tegengesteld aan cyanobacterio fytochromen, dit in dit gebied geen activiteit vertonen.

Table of Contents

1. Introduction

To obtain a bachelor degree at The Hague University of applied sciences a student needs to complete a graduation assignment within an organization or university. The author accomplished this by doing research work in the Larsen Lab in the Chemistry Department at the University of California, Davis (UC Davis). The main focus of the Larsen Lab is to explore the ultrafast processes (fs-ns) of photoreceptors and other light sensitive proteins which serve central roles in light activated biological functions. A fundamental question for many photoreceptors is how the absorption of a photon within a protein is transformed into the complex responses required for biological functions.

Currently, the Larsen Lab at UC Davis [1] is one of many labs that study photosynthetic organisms. Photosynthetic organisms such as phytochromes and cyanobacteria can offer valuable information in harvesting solar energy and consume CO_2 during photosynthesis. Photosynthetic organisms, in general, have evolved mechanisms to optimize solar energy harvesting. These organisms use photosensory proteins to measure the light environment and report findings through biochemical signals, allowing proper biochemical responses to the environment. To remain functional during dawn or dusk, while harvesting dim light, the light-harvesting systems of the organisms are regulated to preserve an optimum quantum yield. To do so, the cyanobacteria have developed photosensory proteins to adjust their metabolism in response to the quantity and quality of ambient light. Similarly, the photosensory process in cyanobacteria could be useful in developing methods to optimize, regulate and generate electricity in organic photovoltaics.

The Larsen Lab at UC Davis focus their research on understanding how cyanobacteria convert light energy into chemical energy. To achieve this, both the biological functions and structures of the molecules involved are required. To successfully develop cyanobacteria as a new form of energy production studies in the regulation and optimization of energy storage within a model cyanobacteriochrome (CBCR) photoreceptors is the first step. In collaboration with the Lagarias Lab in the Microbiology Department at UC Davis, the Larsen Lab chose to focus on cyanobacteriochrome (CBCR) from *Nostoc punctiforme*.

CBCRs have the ability to self-assemble a thermally stable dark state, in the absence of light, using a linear tetrapyrrole (bilin) protein chromophores. Light absorption triggers these bilins to change structure (photo-isomerization), which can persist from seconds to weeks. In other words, shining light begins a transformation from one state to another. CBCRs are usually found as a subcomponent within larger signaling molecules. Photo-conversion between the two photostates triggers changes in local structures, which changes the signaling output domains that interface with cellular signal networks. These photoreceptors help cyanobacteria to self-regulate light harvesting in response to different light conditions. These photosensors are thus excellent components for synthetic systems that allow regulation of target genes or pathways of interest in response to the color or intensity of light.

The Larsen Lab uses spectroscopic techniques to examine biological structures and functions when particular colors of light are illuminated upon the CBCRs. Ultrafast spectroscopic techniques are used to study the efficiency of photon capture, examine the reaction pathways of photoconversion, and characterize photochemical and biochemical events in signal transduction within the photosensors. Studies [2] revealed that between the two photostates are multiple intermediate states, usually with relatively short lifetimes in the order of pico-/nanoseconds. In addition, the Larsen group also studies the visible/ultraviolet, far-red and ns-ms room temperature properties of these photosensory proteins.

The research work done in this thesis focused on a new study: the vibrational spectral energies of the photo- and intermediate states of the photosensory proteins. Wherein a method is developed to measure the vibrational spectra, obtain vibrational information on the photosensitive proteins and work towards building a new set-up. The goal for this set-up is to perform vibrational energy measurements on the photosensitive proteins at cryogenic temperatures. This is achieved by using Fourier Transform InfraRed (FTIR) spectroscopy techniques and equipment. A FTIR spectrometer is used to perform both room temperature and temperature dependent measurements. These experiments give information on the CBCR's behavior, such as: spectral differences between terminal and intermediate states, response on temperature and the dynamics of transitions between states.

By cryo-cooling the proteins, the intermediate states are 'trapped' to extend their lifetime. To measure the kinetic traces of the changing states multiple scans should be taken during cryo-cooling. To do so, a FTIR spectrometer is combined with an optical cryostat, which cools the photosensitive proteins down to cryo-temperatures (~150 K). When trapped, measurements are performed with the FTIR spectrometer to collect vibrational data. This process is referred to as FTIR cryokinetics. Once data is collected multi-dimensional analyzes, such as global analysis, should be used to process the time and temperature dependent intermediate spectra. This thesis will describe a way to build towards the FTIR cryokinetic measurement for the red/green CBCR NpR6012g4.

The methods described and tested in this thesis open a new path for the Larsen Lab to measure different photosensitive proteins in the future. While developing methods, programs, set-ups and procedures for these experiments, explained all throughout this thesis, the main goal is to:

Build a set-up for taking vibrational spectra of photosensitive proteins' photo- and intermediate states at cryogenic temperatures.

So, what is needed to build such a set-up? During construction, yet unknown vibrational spectral information is collected from different proteins used for the room temperature and temperature dependent measurements. FTIR room temperature measurements, performed on the proteins NpF2854g3 and Anacy 4718g3, are carried out to develop the static part of the cryokinetic measurements. Followed by the temperature dependent measurements on the protein Cph1, and constructing the temperature dependence part of the FTIR cryokinetics set-up.

All experiments and proteins represent as examples for future FTIR experiments on different proteins. However, to build towards the cryokinetic set-up the three subjects, described below, are dealt with:

First, understanding of the known theory and equipment, which describes theories on phytochromes, CBCRs, FTIR spectrometer/program & operation, advantage of FTIRs, vibrational spectral information and the known data, so far, on the proteins.
Second, the experimental set-up and procedure, describing: which settings give, relatively, the most information on the vibrational bands, desirable and achievable scanning time of spectrometer, cryostat operation, sample preparation for sufficient scans and set-up for measurement methods and procedures for static room temperature, temperature dependent and cryokinetic measurements.
Final, process and interpreting the results, which depicts: theory/usage of global analysis & van't Hoff equations, making a correlation between FTIR cryokinetic, UV-VIS cryokinetic and other known data of the photosensitive proteins.

2. Theory on CBCRs, FTIR and data processing

2.1 Phytochromes and cyanobacteria chromes

In this section phytochromes and CBCRs are discussed: what has been discovered to date, which states occur, what is the photocycle and a brief explanation on some (bio)chemical terms are given throughout the paragraphs. The protein NpR6012g4 is used as example throughout this paragraph. The other proteins used in this thesis have different properties, found in Appendix A.1, but the principle explained in here stays the same.

2.1.1 Phytochrome and the Phytochrome family

Phytochromes [2] are a family of pigment-containing proteins (photoreceptors) that uses specific wavelengths of light to regulate plant growth and development. A phytochrome switches back and forth between two isomeric forms [3]. It is commonly sensitive to red and far-red light regions of the visible spectrum. One isomer, P_r (inactive), absorbs red light and the other isomer, P_{fr} (active), absorbs far-red light. The two forms of the phytochrome are photo-reversible and the interconversion of one form to the other acts as a control mechanism to regulate various events. Figure 2-1 shows a schematic of the (de)activation mechanism of a phytochrome protein.

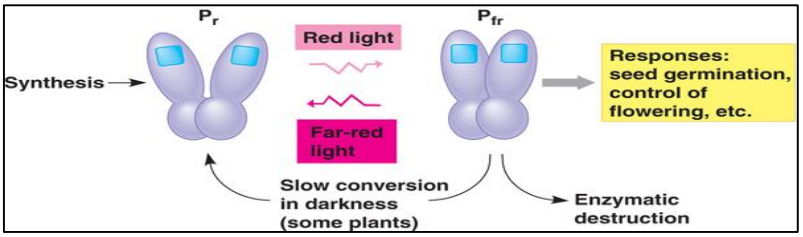

Figure 2-1: The phytochrome protein is originally synthesized in the P_r (dark) form. When red light enters the cell, it converts some of the P_r into P_{fr}. In some plants, the P_{fr} then enters the nucleus, binds to proteins that associate with DNA, activates / inhibits transcription of specific genes. [4] The figure is a simplified representation and unlike the ones used in this thesis.

Besides plants, the phytochrome family has grown to include any related biliprotein (pigments) from many different organisms, with substantial structural and spectroscopic variety [5]. Phytochromes are categorized as followed:

(1) All photoreceptor proteins which bind an open chain tetrapyrrole as cofactor and photo-switchable sensor.
(2) After light absorption, photo-conversion takes place between the dark adapted and the light induced state.

Some phytochrome bacteria such as, cyanobacteria, are also able to fix nitrogen. Meaning that there are two ways for energy production: carbon fixation via photosynthesis, and hydrogen production via nitrogen fixation (see Appendix A.2). The produced hydrogen can be used as a new source of energy while the fixed carbon is converted into biofuels. Nitrogen-fixing cyanobacteria can also form a symbiosis with plants. Being able to make such a symbiosis offers secondary benefits to global energy usage, because the plant partner will not be needing nitrogen from fertilizers.

Cyanobacteriochromes (CBCRs) is a sub-family related to phytochromes. The CBCR sub-family contains a variety of proteins from different species; each reacting to a different wavelength λ of light. Figure 2-2 shows the diversity within the CBCR sub-family.

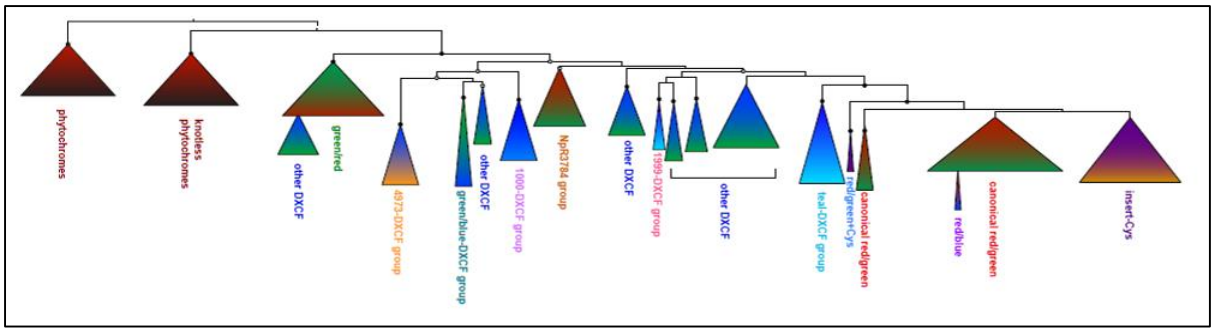

Figure 2-2: Schematic family tree of the sub-family: Cyanobacteriochrome (CBCR). [6]

One CBCR, commonly used in the Larsen Lab, is *Nostoc punctiforme* [7], which is a nitrogen-fixing filamentous cyanobacteria. Several subfamilies of protein photoreceptors, within the *N. punctiforme* strain, respond to the visible and near-infrared regions of the electromagnetic spectrum. Other subfamilies can also respond to blue/ultraviolet light. This means that, family members within *N. punctiforme*, cover the spectrum from the NIR to the UV.

2.1.2 Photostates, intermediates and photocycles

NpR6012g4 is a cyanobacteriochrome in the canonical Red/Green family and originates from *N. punctiforme*. Since NpR6012g4 is mostly used in the lab for its qualitatively high illumination responses, its known/proposed properties shall be used to explain the photostates, intermediates and photocycles.

NpR6012g4 photo-converts between a red-absorbing ground state (*P*r) and a green-absorbing photoproduct (*P*g). In the dark, the protein stabilizes in its (ground) dark-state with the bilin in the 15Z configuration. When illuminated with red light (λ_r=650nm), photo-conversion starts and produces a photoproduct with a 15E bilin. The photo-conversion requires a rearrangement of the atoms within the protein, which is referred to as isomerization. The photoproduct can thermally return to the 15Z dark state via a process known as dark reversion. Dark reversion can also be stimulated by illumination with green light (λ_g=540nm). Figure 2-1 explained the same conversion in plants in paragraph 2.1.1. A schematic of NpR6012g4's conversion is shown in figure 2-3.

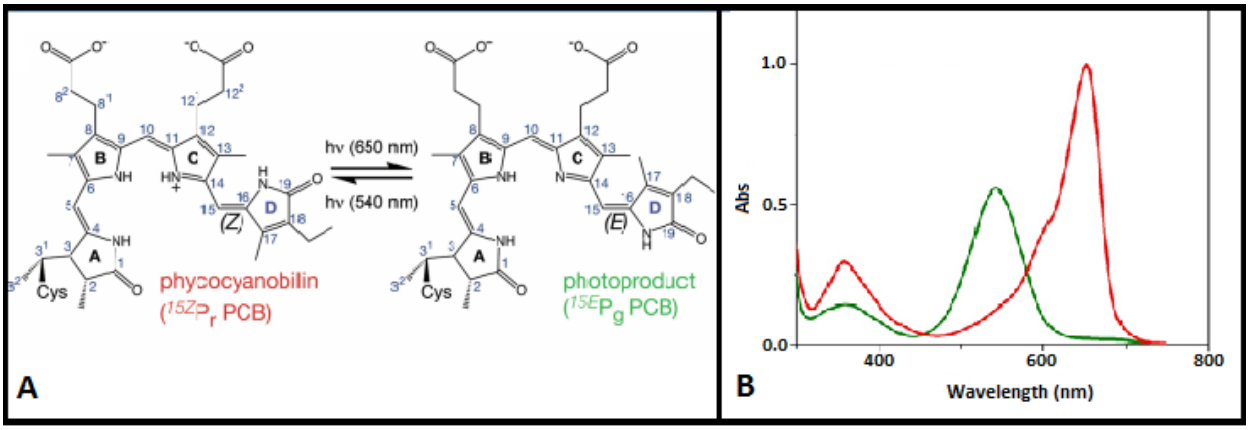

Figure 2-3: (A) **chromophore is protonated in the red-absorbing 15Z P_r ground-state (left) but deprotonated in the green-absorbing 15E P_g light-state (right)** [7] **(B) (visible) Absorption spectrum of Npr6012g4 in 15Z (red) and 15E (green) state.**

Figure 2-3(A) shows that the isomerization takes place at the $C_{15/16}$ double bond, which results into a rotation in the D-ring of the bilin, a Z-E configuration. Figure 2-3(B) depicts that the two states have different absorption spectra in the visible light region of the electromagnetic spectrum.

Switching from the red-absorbing state to the green-absorbing photoproduct is called the *forward reaction* and backwards the *reverse reaction*. Doing both in a row completes a cycle, which is often reverted to as the photocycle. Previous researches suggest that there are multiple intermediate states between the two described states [1,7]. These intermediates are referred to as Lumi or Meta states, each with minor variation in its configuration, and lifetime τ of ps-ns in contrast to the red/green states which can last from seconds to weeks. Figure 2-4 shows a schematic of the photocycle with intermediates of the forward reaction from P_r to P_g.

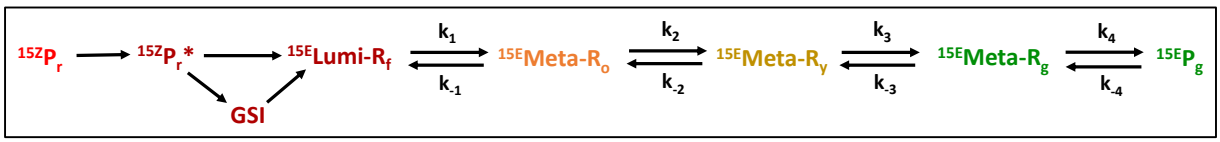

Figure 2-4: Integrated forward reaction of NpR6012g4's photocycle constructed from primary dynamics, secondary dynamics, and cryokinetics data. Red P_r-state and green P_g-state with a Lumi and multiple Meta states. The GSI state is another ground state of the P_r and P_r^* is an excited state. [8]

A potential energy diagram of the forward reaction is shown in figure 2-5. It is possible to excite the ground state of the P_r to a higher state when enough energy is added by illumination. After excitation there are two possibilities:

(1) the excited state falls back to the ground state, or
(2) falls in an intermediate state, like Lumi-R_f.

Figure 2-5 also shows that each intermediate 'sits' in an energy well. So, thermal energy is needed to 'push' the intermediate over an activation barrier and form a new intermediate.

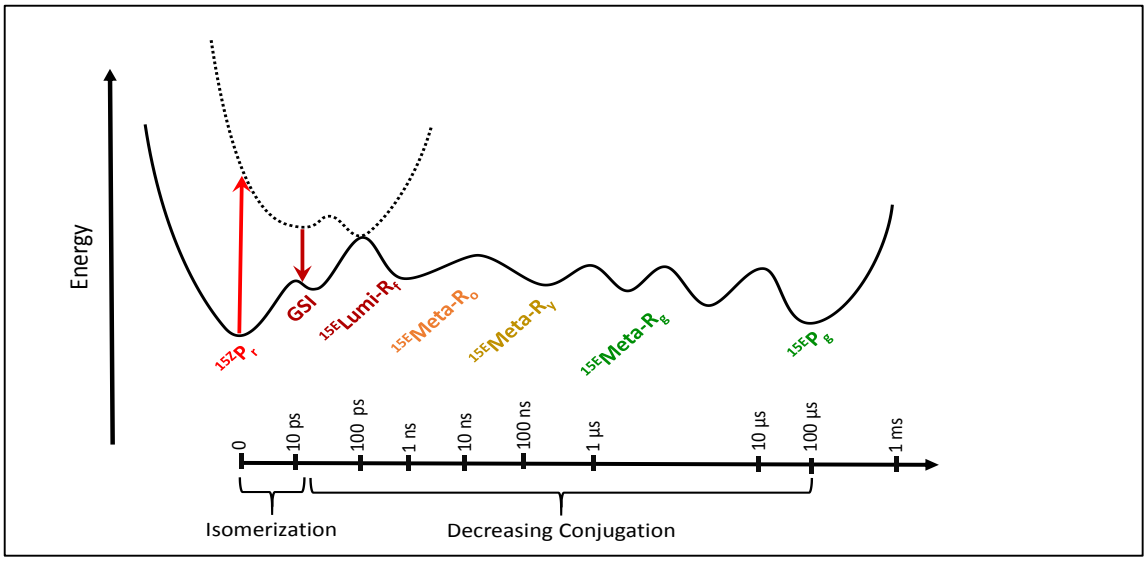

Figure 2-5: Schematic showing the forward reaction from P_r to P_g with multiple intermediates. On the y-axis is the energy E, x-axis the time needed for the P_r - P_g configuration. From left to right is also the isomerization from Z to E (not shown). Dotted line is the excited state of the protein. [8]

Since the intermediates have relatively short lifetimes, it is difficult to measure the spectra properly. One way is to use ultrafast techniques, [1,7] the other is cryotrapping by cryokinetic measurements. In these measurements, CBCR protein samples are cryo-cooled within an optical cryostat (down to ~150 K), and illuminated to generate trapped intermediates of the photocycle. Increasing the temperature 'pushes' the trapped photogenerated populations into the intermediates. Spectral changes during approach to equilibrium can be analyzed by using global analysis and transition state theory. The fractional occupations at thermal and chemical equilibrium are related by respective enthalpy differences (ΔH) via the van't Hoff equation. The analysis and equations will be discussed in section 2.3.

2.2 Vibrational, IR, spectra and FTIR technique

This section discusses vibrational spectra and FTIR spectroscopy, explaining: the principles of IR spectroscopy, calculating vibrational energies, read and interpret spectra. The section is concluded with an explanation on FTIR technique, method and the Michelson-interferometer.

2.2.1 Vibrational and Infrared spectroscopy

IR spectroscopy is a technique used in laboratories for analyzing materials. When illuminating IR light through samples the IR radiation is either partially absorbed or transmitted. The measured spectrum gives a 'fingerprint' of the sample's molecular structure, which is unique to the measured sample. The fingerprint represents the absorption bands which correspond to the vibrational frequencies of the atomic bonds within the sample. The information that IR spectroscopy provides is: identifying unknown materials, determining quality or consistency of samples, determining the amount of components in mixtures and gives information about sample's structures and vibrational energies.

The principle of IR spectroscopy [9] is based on the interaction between infrared radiation and atomic vibrations in molecules and ions. IR radiation is either absorbed or emitted (after absorbing) by atomic bonds when the radiation frequency corresponds to the frequency of the vibration due to the dipole moment of the molecule. The energy of the absorbed radiation can be found from Plank's equation when the radiation frequency corresponds to the frequency of the oscillating dipole moment, since [10]:

$$E = \frac{hc}{\lambda} = h\nu \qquad (1).$$

With Plank's constant h [$6.63 \cdot 10^{-34}$ J·s], speed of light c [$3.00 \cdot 10^{8}$ m·s^{-1}], wavelength λ [nm] and frequency ν [s^{-1}] (corresponding to molecular vibration frequency). The frequency of a diatomic bond is calculated using classical mechanics with [9]:

$$\nu = \frac{1}{2\pi}\sqrt{\frac{k_{AB}}{\mu_{AB}}}, \qquad \text{with: } \frac{1}{\mu_{AB}} = \frac{1}{m_A} + \frac{1}{m_B} \qquad (2).$$

Where k_{AB} is a force constant, determined by the strength of the atomic bond. μ_{AB} is the reduced mass of system A-B, with masses m_A and m_B. The derivation for this formula is found in Appendix A.3.

Absorbing radiation with the exact frequency as the oscillating dipole moment results into an increase of amplitude in the detected vibration band. In general, the atomic bonds / molecules 'losses' the extra energy by collisions or photon emission.

To understand IR spectroscopy, the above described (classic) model is sufficient. However, a more accurate description of the molecular vibrations is given by quantum mechanics supported by wave functions. As seen in formula 3 [9]:

$$E_n = \left[n + \frac{1}{2}\right] h\nu \qquad (3).$$

The energy of a vibration in the harmonic oscillator model has a discrete set of values with n as the vibrational quantum number, with values: 0,1,2…

The molecule still holds a vibrational energy E_n when $n = 0$ (ground state), whereby the molecule vibrates with ½ $h\nu$, even at absolute zero (0 K), see figure 2-6. It also shows that only energy states with an integer number of $h\nu$ an allowed, meaning that the molecule not only vibrates at ν, i.e. resulting in overtones. Even though, the quantum mechanical approach is more accurate, the classical approach still leads to almost the same positions of the absorption bands.

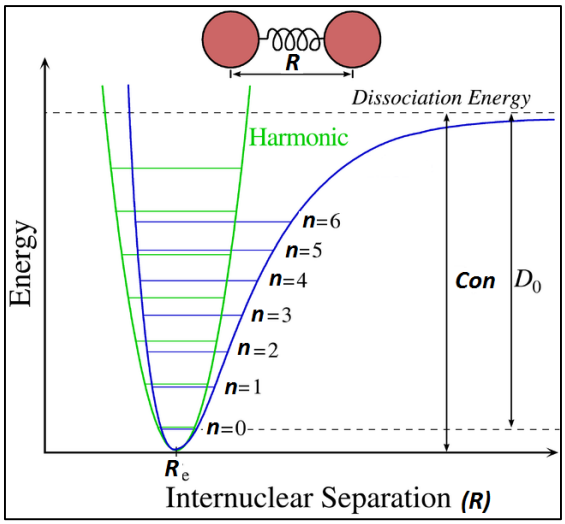

Figure 2-6: Schematic of energy and separation between imaginary atom pair. Energy *E* plotted against inter-nuclear separation *R*. It is shown that for every vibrational quantum number *n* the atoms vibrate further from each other with a higher energy. *Con* is the difference between *the bottom of the potential well* and the dissociation energy, D_0 is the dissociation energy from the ground state and R_e is the equilibrium distance between the two atoms. [11]

IR radiation has wavelengths λ greater than 800 nm and are categorized in: near infrared (NIR; 0.4-5.0 µm), Mid-infrared (MIR; 5.0-25 µm) and far-infrared (FIR; 25-1000 µm) [9].

With MIR [12], the energy is equivalent to the molecule's vibrational energy level (fig. 2-7). This means that the molecules in the ground state absorb MIR-rays and can make transitions to the first excited state. Such transitions are only permitted when frequency corresponds to changing dipole moment frequency (explained above) and the vibrational quantum number *n* changes by ± 1 (fundamental tones). Vibrations with an integer *n* of ±2 and up are equivalent to harmonic tones (forbidden transitions).

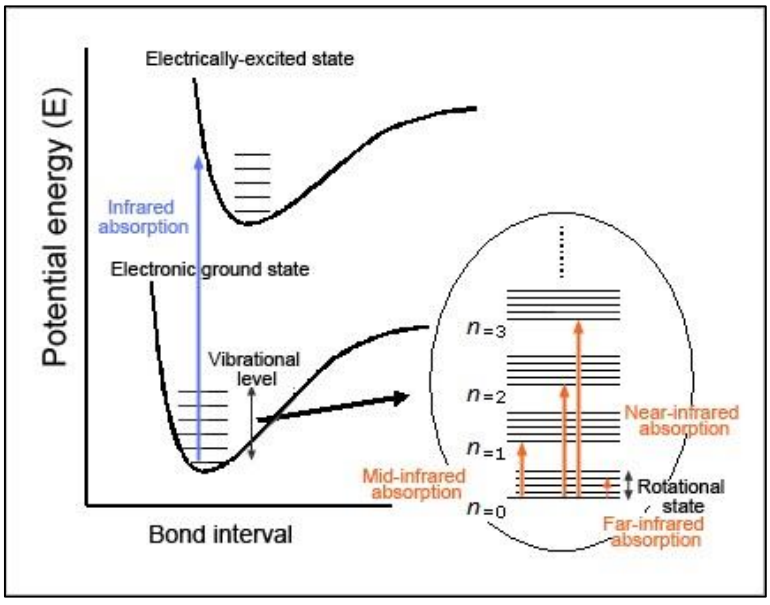

Figure 2-7: Scheme of a molecule's energy in its electrically-excited state (above) or ground state (below). (Potential) energy *E* is plotted against bond interval *R*. Figure also shows (zoom-in) the influence of absorbing MIR, NIR or FIR rays in correspondence to fundamental tones, respectively, overtones/forbidden transitions and rotational energy states. [11]

In IR spectroscopy it is common to characterize the radiation with wavenumbers ν [cm^{-1}] instead of wavelengths, calculated with formula 4 [10].

$$\nu = \frac{1}{\lambda} \qquad (4).$$

From the previous story, it would be expected to see sharp lines in the vibrational spectrum at wavenumbers corresponding with the frequencies of the normal modes (fundamental tones).

However, broad absorption bands are found, which is seen in the spectrum of liquid water (fig. 2-8). The line dilatations are mostly caused interactions between molecules in solutions [9]. Most IR spectrometers send multiple wavelengths (frequencies) and differences with the surroundings give wider bands. For more information on characteristic vibrations, see Appendix A.4.

Line dilatations do not cause problems for positioning the absorption bands of the molecules. However, these widened lines may overlap bands of interest, which might cause sample data being 'buried' by the used medium (buffer material). Therefore, when preparing a sample, the medium (-concentration) should be taken in account.

Figure 2-8 gives an idea of generally presenting IR absorption spectra. The x-axis, showing wavenumbers, is set from right to left and the y-axis gives the transmittance *T* [-], replaceable by absorbance *A* [-]. The scale on the x-axis is convenient since this is linear in energy *E* (formulas 1 & 4).

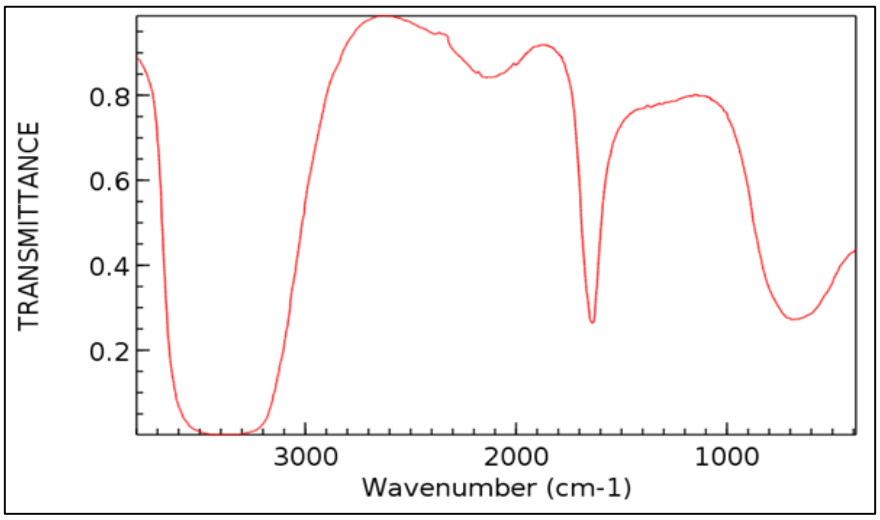

Figure 2-8: IR spectrum of water, where transmittance *T* [-] plotted against wavenumber *v* [cm^{-1}]. Water has a respectively wide peak around 3300 cm^{-1} due to OH (a)symmetric stretch, a smaller spike at 1600 cm^{-1} due to OHO bending, and a combined peak at 2100 cm^{-1}. Peak at 700 cm^{-1} is unclear. [13]

As in many other spectroscopic techniques, Beer's law [9] is also applicable in IR. Where the extinction E_x is proportional to the sample's: extinction coefficient ε, thickness b and concentration C, given in formula 5 [9]. The formula derivation can be found in Appendix A.5.

$$E_x = \log_{10}\frac{I_0}{I_t} = -\log_{10} T = \varepsilon C b \qquad (5).$$

The right amount of sample is of importance, too much sample and the data gets 'cut-off', as all the light is absorbed (fig. 2-8 at 3300 cm^{-1}), not enough sample gives no signal or 'useless' data. The most accurate measurements are accomplished with transmittances *T* between 70 and 30% [9].

In addition, the atomic movements in a polyatomic molecule [14] are regarded as a superposition of a number of harmonic vibrations. For nonlinear molecules, there are 3*N*-6 (*N* number of atoms) different independent molecular vibrations possible and 3*N*-5 for linear molecules. These vibrations are the normal modes of the molecule, accompanied by a change

in dipole moment. The molecule is able to absorb IR radiation, which makes the vibration Infrared-active.

In a normal mode all atoms with the same frequency move around an equilibrium position and pass this position at the same time. The frequencies of the normal modes are determined by the masses of all atoms in the molecule and their force constants. The frequencies of different normal mode vibrations are in general different.

However, as a result of the symmetry within the molecule two or more normal modes could have the same frequency. The most common vibrational motions are: (a)symmetric stretching, rocking, bending, wagging and twisting. Appendix A.4 shows motion examples.

2.2.2 FTIR spectroscopy

Fourier Transform InfraRed (FTIR) spectroscopy [15] is a common used method of IR spectroscopy. The major advantage FTIRs have, in contrast to its predecessors, is speed. FTIR is a method for measuring multiple IR frequencies simultaneously instead of individually like Dispersive IRs. FTIRs can measure spectra in matter of seconds rather than minutes. This is made possible by using a Michelson-interferometer.

The Michelson-interferometer [16] consist two perpendicular mirrors and a beam splitter. The beam splitter is designed to split an incoming beam of light into two, one half is transmitted and the other half reflected. The split beams travel towards the two mirrors, a movable and a stationary mirror. The transmitted and reflected light beams strike the stationary and movable mirror. After reflection by the mirrors the two beams recombine with each other at the beam splitter. Figure 2-9 shows a schematic of the interferometer and the beam pathways.

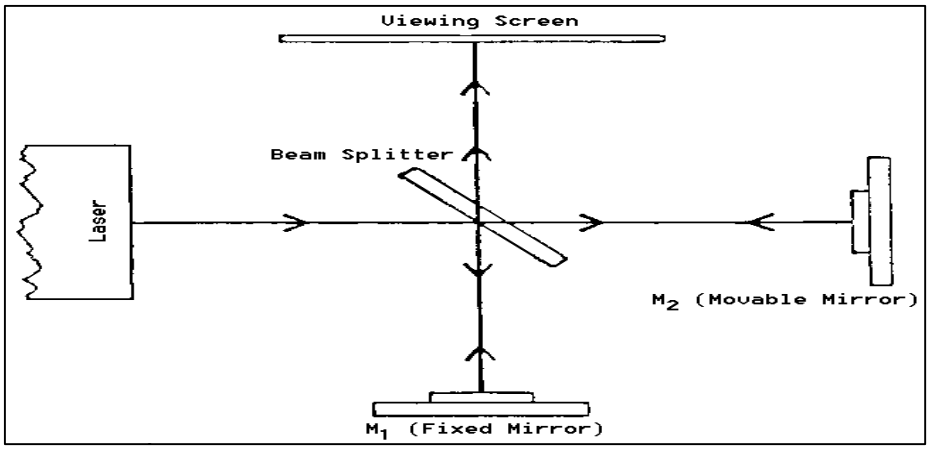

Figure 2-9: Schematic of a Michelson-interferometer. On the left a laser radiates light into a beam splitter, which splits the beam towards a stationary (M_1) and a movable mirror (M_2). After reflection the two beams recombine in the beam splitter and travel towards the viewing screen, which can be replaced by a sample or detector. [17]

Now two events can occur [18]: in the first case, the distances from the beam splitter to the two mirrors are the same (zero path difference: ZPD) or they differ from each other. In the second case, the light beam striking the movable mirror travels a longer distance than the one striking the stationary mirror. The displacement of the movable mirror is represented by Δ. The extra distance that the light beam travels (optical path difference: OPD) is represented by δ. The mirror displacement should be multiplied by 2 (back and forth moving beam). Therefore [10],

$$\delta = 2\Delta \qquad (6).$$

Back in the beam splitter interference occurs between the two light beams. Constructive when OPD is the multiples of the wavelength, see formula 7, and destructive when OPD is the half wavelength (with or without added multiples of wavelength), see formula 8.

$$\delta = 2\lambda n \qquad \text{Where } n = 0,1,2,.. \qquad (7).$$

$$\delta = (n + \tfrac{1}{2})\lambda \qquad \text{Where } n = 0,1,2,.. \qquad (8).$$

Constructive interference gives a maximum intensity signal while destructive gives a minimum intensity signal. These are the two extreme situations. In a FTIR spectrometer the movable mirror is constantly moving back and forth. This results in a cosine wave, which plot is defined as an interferogram.

Every data point (function of moving mirror position *X*) in an interferogram contains information about every infrared frequency coming from the source. Resulting in simultaneously measured frequencies as described above.

By using Fourier transformations, the interferogram can be 'decoded' to collect information of the individual frequencies. Fast Fourier Transformations (FFT) as depicted in formula 9 [18] are used to transform the interferogram from time domain to frequency domain. Since the CPU in the FTIR spectrometer does all the calculations and the only interest goes to the position of each frequency/wavenumber, the Fourier transformations will not be further discussed.

$$X_k = \sum_{n=0}^{N-1} x_n e^{-i2\pi k \frac{n}{N}} \qquad (9).$$

In this equation there are N outputs X_k, each requiring a sum of N terms, x_n are complex input numbers of n terms and i is the square root of -1.

The interferogram is converted into an IR absorption spectrum, a schematic is depicted in figure 2-10. In general, IR absorption spectra the Transmittance T [-] is plotted against wavenumber ν [cm^{-1}]. Formulas 10 and 4 [9,10] show how to calculate the Transmittance T and, respectively, wavenumber ν as shown in figure 2-10.

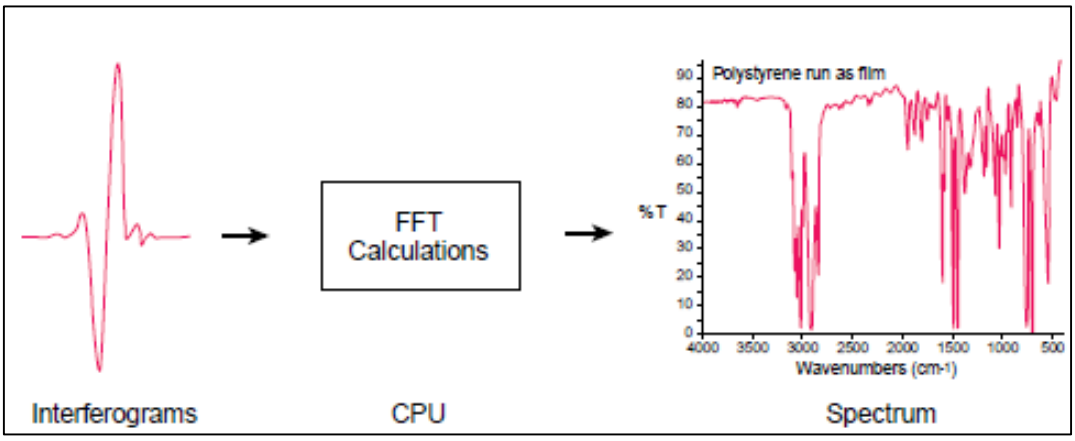

Figure 2-10: Schematic of the conversion of the interferograms, through the computer's FFT Calculations, resulting in an IR spectrum. Wherein Transmittance *T* is plotted against Wavenumber *ν*. [15]

$$T = \frac{I}{I_0} \qquad (10),$$

wherein, I [W] is the transmitted intensity and I_0 [W] the original intensity. Absorbance A [-], commonly used in IR spectra, is calculated from the Transmittance T, see formula 11.

$$A = -\log_{10}(T) \qquad (11).$$

Other components built in the FTIR spectrometer are: laser, laser source, detector, sample compartment and computer/software. These components are briefly discussed in paragraph 3.1.1.

Another well-known technique used to observe atomic vibrations is Raman-spectroscopy [9], based on the inelastic scattering of monochromatic light. The advantages of Raman-spectroscopy, contrary to FTIR, are: water could be used as diluent, glass/quartz are optional optics, no special detectors needed, less absorption bands overlaps, symmetric vibrations (N_2) are 'visible' and intensity is directly proportional to concentration and laser power.

On the other hand, FTIR: is sensitive to minor structural differences, optical throughput is higher resulting in lower noise levels, mechanical simplicity (one moving mirror), measures ratios of intensity (independent of laser power) and it has better detection limits.

FTIR and Raman-spectroscopy are complementary techniques. Unfortunately, there are less known Raman-spectra than IR-spectra. This and the fact that FTIR is relatively faster, easier in use and more sensitive to minor differences (intermediates) are the reasons why FTIR is chosen for this research.

2.3 Multi-dimensional analysis of *λ, t, T*

In FTIR cryokinetics measurement, the photosensitive proteins change state while approaching thermal and chemical equilibrium. The concentrations of intermediate and terminal states increase or decrease at different rates simultaneously. To keep track and analyze the spectral changes for the cryokinetics (or any kinetics), global analysis is used to derive microscopic forward and reverse rate constants as the protein equilibrates. The fractional occupations at thermal and chemical equilibrium are related by respective enthalpy differences (ΔH) via the van't Hoff equation. The basics of global analysis and van't Hoff equation are explained in the paragraphs below.

2.3.1 Basics of global analysis

Global analysis is a compartmental-model-based analyzing technique that fits multidimensional data globally. Mathematical details of this technique are described in papers of van Stokkum et al. [19] and Holzwarth [20]. Global analysis is used, for example, to construct a reasonable mechanism, extract spectral features, and determine lifetime constants of the intermediates in time-resolved data. Global analysis is not only applicable to time-resolved signals, it is also applied to different variables, such as temperature and pH.

By analyzing the kinetic traces from the extracted spectral range, global analysis intends to resolve: the number of compartments n_{comp}, or states, the spectra of those compartments, and associated concentration profiles and lifetimes for each corresponding intermediate state.

The compartmental aspect of decomposing the data is described below [21], which is analogous to the Beer-Lambert law, see Appendix A.5:

$$\Delta Abs(\lambda, t) = \sum_{l=1}^{n} c_l(t)\Delta\varepsilon_l(\lambda) \qquad (12)$$

The $\Delta\varepsilon_l$ is the difference in extinction coefficient between the l^{th} compartment and ground-state, i.e. representing a difference spectrum of the l^{th} compartment. The $c_l(t)$ is the concentration of l^{th} compartment at time t. Thus the signal ΔAbs is a superposition of signals from n_{comp} compartments (or intermediate populations). The n_{comp} is estimated with the use of sequential model analysis, described in paragraph 2.3.2.

The compartmental kinetic model with n_{comp} compartments is described by [21]:

$$\frac{dc}{dt} = Kc(t) + j(t) \qquad (13).$$

The off diagonal elements of transfer matrix *K* describe the microscopic rate constants leading to transitions between compartments (or intermediates). The diagonal elements of *K* contain the total decay rates of each compartment. The concentrations of each compartment could be described by a vector $c(t)=[c_1(t)...c_{ncomp}(t)]^T$. The vector $j(t) = i(t)\ [1\ x_2\ ...\ x_{ncomp}]^T$, input of the system, with $i(t)$ the IRF (impulse response function, i.e. laser pulse) and x_l representing a possible extra input to compartment *l*. Formula 12 is solved analytically.

As described above, $\Delta\varepsilon$ represents the difference spectra of spectral species (intermediates), which is termed **S**pecies-**A**ssociated-**D**ifference-**S**pectra (SADS). For light-induced and dark-adapted experiments the spectral differences ΔA are obtained by formulas 14 and, respectively, 15 [8]. Where *A* is the absorption spectra (replaceable by transmission) at time *t*, wavelength λ and temperature *T*.

$$\Delta A(\lambda, t, T) = A(\lambda, t, T) - A_{ref}(\lambda, t = \infty, T) \qquad (14)$$

$$\Delta A(\lambda, t, T) = A(\lambda, t, T) - A_{ref}(\lambda, t = 0, T_1) \qquad (15).$$

The goal of using global analysis is to extract SADS, the lifetime for each single step within the reaction, concentration of the intermediates, and connectivity schemes between different spectral species. By interpreting these parameters correctly, a physical mechanism of the chemical reaction could be constructed. Other valuable information could also be obtained, such as: ground-state heterogeneity, excited-state energy barrier, and dynamic equilibrium.

When the kinetic model does not describe the time-resolved reaction correctly, the false difference spectra extracted from such model are not SADS but a linear combination of the true SADS [19].

2.3.2 Sequential analysis description

First, in the use of global analysis, an estimation of the number of compartments n_{comp} and their corresponding lifetime constants (time required for the intermediate concentration to decrease to 1/e of its original value) is made, which adequately fits the whole data. To extract these data, a sequential model is build. Schematics of photochemical reactions are presented in figure 2-11.

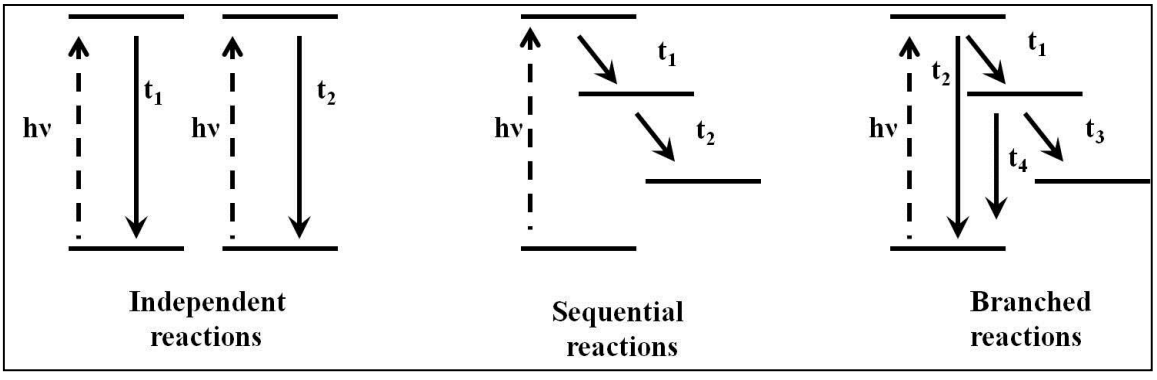

Figure 2-11: Comparison between different types of photochemical reactions, from left to right, independent reactions, sequential reactions and branched reactions. [22]

In the sequential model (populations in spectral compartments flow in sequence, i.e., comp 1 → comp 2 → … comp *n*), the extracted difference spectra of each compartment is termed **E**volution-**A**ssociated-**D**ifference-**S**pectra (EADS), which is a superposition of the SADS. Thus, EADS describe the spectral evolution of a time-resolved data set. The connectivity matrix *K* and initial populations *x* for n_{comp} = 4 could be described as in formula 16 [21]:

$$K = \begin{bmatrix} 0 & 0 & 0 & 0 \\ \tau_{12} & 0 & 0 & 0 \\ 0 & \tau_{23} & 0 & 0 \\ 0 & 0 & \tau_{34} & \tau_{44} \end{bmatrix}, \quad x = \begin{bmatrix} 1 \\ 0 \\ 0 \\ 0 \end{bmatrix} \qquad (16)$$

Where τ_{12} is the rate constant from comp 1 to comp 2 and τ_{23} is the rate constant from comp 2 to comp 3, etc. The n_{comp} is varied and the goodness of fit is evaluated by comparing the fit to the data for n_{comp} =1, 2, …

By numerical fitting, several models can fit the data. Using, for example, 5 and 6 lifetime constants might both provide sufficient fits with similar quality. Generally, a simpler model is preferred if goodness of fit are similar, following Occam's razor: *not postulating a mechanism that is more complex than is required unless there is solid or external evidence suggesting otherwise*. Which is based on the main assumption that all intermediates must have non-negative absorption at all times.

The sequential analysis is useful to estimate the number of compartments for the reaction, and also provides the unbiased, model-free spectral analysis to provide information for the more sophisticated target based global analysis. Target analysis is used when the assumption of a branched reaction is present (right fig. 2-11) and is therefore not used or described in this thesis.

2.3.3 Van t' Hoff equation and plot

The temperature dependence of microscopic rate constants can be described with a model containing thermodynamic parameters. Measurements at multiple different temperatures offers an opportunity to identify and estimate both forward and backward microscopic rate constants [23,24], thus enabling estimation of free energy differences Δ*G*.

Δ*G* is the change of Gibbs (free) energy [25] for a system and is the difference in the energy between reactants and products. Δ*G* is unaffected by external factors that change the kinetics of the reaction. The Gibbs energy is defined as [25]:

$$\Delta G = \Delta H - T\Delta S \qquad (17)$$

For systems at chemical equilibrium, Δ*G* holds [25]:

$$\Delta G = -RTln(K) \qquad (18).$$

Where Δ*H* is the change in enthalpy, *T* the temperature [K], Δ*S* is the change in entropy of the system, *R* is the gas constant [8.314 $J \cdot K^{-1} \cdot mol^{-1}$] [10] and *K* is the equilibrium constant of a system. Combining and rewriting the equations above gives the van't Hoff equation [26]:

$$ln(K) = -\frac{\Delta H}{RT} + \frac{\Delta S}{T} \qquad (19).$$

For a reversible reaction, the equilibrium constant can be measured at a variety of temperatures. This data can be presented in a graph where ln(K) is plotted against T^{-1}, giving a so called van 't Hoff plot (see fig. 2-12). When the range in temperature is small enough the ΔH and ΔS are essentially constant, therefore giving a linear plot.

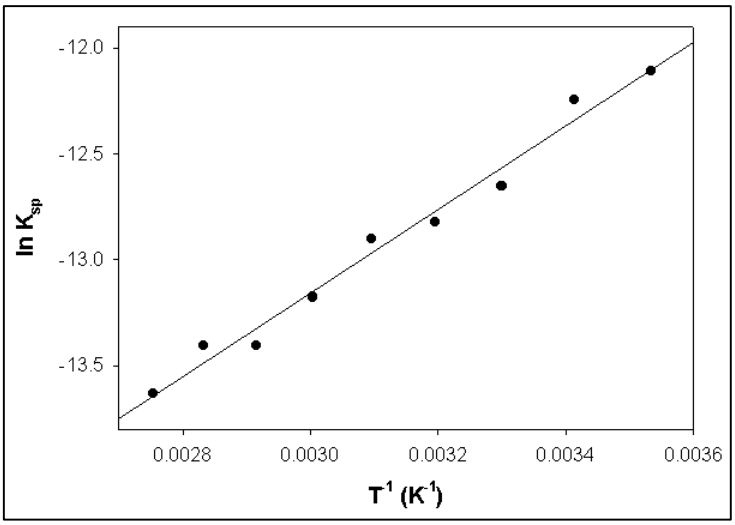

Figure 2-12: A van't Hoff plot example of $Ca(OH)_2$, wherein ln(K) is plotted against T^{-1}. [26]

Via the van't Hoff plot's slope and interception with the y-axis, both ΔH and ΔS are obtain by: $\Delta H = -R \cdot slope$, [26] ,and $\Delta S = R \cdot intercept$. [26]

3. Materials, Work and Methods

This chapter explains briefly the principles and use of the FTIR spectrometer and the optical cryostat. Further, the preparations, methods, set-up and work are described in order to get from spectrometer optimization to the cryokinetic set-up.

3.1 Used equipment and materials

3.1.1 FTIR spectrometer: Tensor 27

As stated in paragraph 2.2.2, FTIR spectrometers, including the Tensor 27 [27], consist out of an (Michelson-) interferometer, laser, laser source (in this case MIR) and detector (in this case a Mercury Cadmium Telluride detector; MCT). Figure 3-1 shows a schematic overview of the Tensor 27.

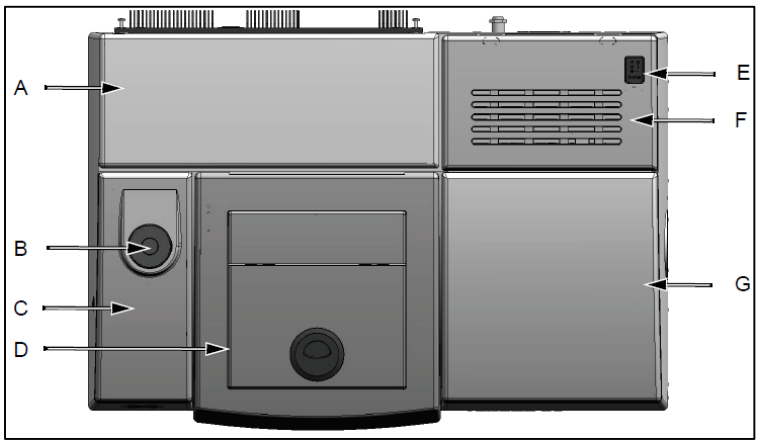

Figure 3-1: Schematic overview Tensor27. A) Electric compartment, B) filler inlet, C) Detector compartment, D) Sample compartment, E) spectrometer display, F) source/laser compartment, G) interferometer compartment. [27]

Since the essentials of FTIR spectroscopy are already discussed in paragraph 2.2.2 this section will only summarize the general steps for executing measurements. Other useful information, like troubleshoots and other schematics, are found in Appendix B.2.

First, turn on the Tensor 27 (switch on the back), this takes approximately 10 minutes (warm up). While waiting start the PC and open the Opus program, connect the nitrogen (gas) tubes with the purge in- & outlet on the back and pour liquid nitrogen into the detector (B). Nitrogen gas is used to purge the sample chamber, so water vapor and other air particles cannot interfere with the measurements. Since the MCT detector operates significantly below room temperature, liquid nitrogen is used to cool it. The MCT detector was chosen over a DLaGTS detector since it is relatively more sensitive, see Appendix B.3 for more information. The FTIR is operational 20 minutes after filling the liquid nitrogen with 3 to 5 funnels of (67±1) mm diameter and the STATUS LED is green on the spectrometer display (E).

Second, an optical sample holder is placed inside the sample chamber, without a sample (H fig. B.3, Appendix B.2). Use Opus to check the interferogram (optimal amplitude, with fully opened aperture, is ±32-33.000 counts [27] [-]). When the interferogram has a proper amplitude close the sample chamber, purge it down and scan the background with Opus. After scanning the background, place the sample in the sample holder, make minimal changes inside the chamber and purge again. Now the Tensor 27 is ready to measure a sample. Opus automatically subtracts the background scan from the sample scan. This way only the sample's IR spectrum is shown. Note that the Tensor 27 can be set on either number of scans taken per sample/background or minutes of scanning resulting in an *x* number of scans.

3.1.2 Optical Cryostat: Optistat DN-V

The Larsen lab uses an Optical Cryostat [28] to cool the protein samples (~150 K). The cryostat consists of a liquid nitrogen reservoir, heating coil (heat exchanger), inner and outer chamber. The outer chamber is pumped to a vacuum (10^{-6} mbar) for insulation. The inner chamber at atmospheric pressure is temperature controlled. The thermal link between heat exchanger and sample is made by exchange nitrogen gas, with a temperature stability of ± 0.1 K [28]. Figure 3-2 shows a schematic of the Optical Cryostat.

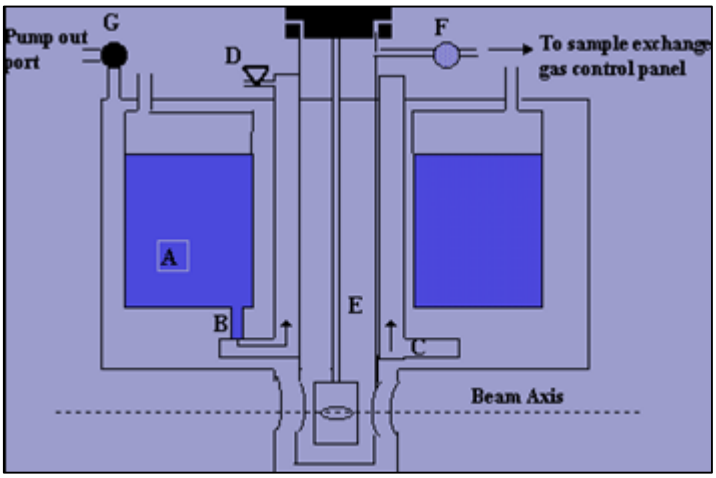

Figure 3-2: Schematic of Optical Cryostat, with A) liquid nitrogen reservoir, B) capillary tube, C) heat exchanger, D) needle valve, E) sample/ exchange gas space, F) pump-down/backfill valve and G) vacuum space pump-out valve (do not touch!). [28]

Liquid nitrogen flows from the reservoir (A) via a capillary tube (B) into the heat exchanger (C) to cool the interior gas and the sample. The resulting gas then travels up the annular space surrounding the sample volume and exits to atmosphere through the needle valve (D) which controls the flow. After loading the sample, the sample chamber (E) is evacuated and back filled with nitrogen gas through valve (F) to purge the sample space of CO_2 and water vapor which interfere with the IR signals. To maintain a vacuum in the outer chamber, pump-out valve (G) must not be opened.

Figure 3-2 also shows that the bottom of the cryostat consists an optical sample compartment. With a sample rod, the sample is top loaded into this compartment. Four CaF_2 windows surround the sample compartment, two (1“) in the inner and two (2“) in the outer chamber, so light can travel through the sample. CaF_2 is used due to its low absorbance in the infrared region of the electromagnetic spectrum.

For more information on operating the Cryostat and CaF_2 window choice see Appendix B.4 and A.6. Note that prior to the measurements, the vacuum in the outer chamber needs to be checked, the liquid nitrogen reservoir is full, and the needle valve (D) is slightly opened.

3.2 Set-ups

Since this thesis is set up to build towards the cryokinetic experiment by optimizing the FTIR spectrometer followed by room and Temperature dependent temperature measurements, this paragraph discusses the set-up of the last two and the cryokinetic measurements. The optimization experiments (see §3.3.1) are relatively small and do not require any set-up explanation. Therefore, only the general set-up, room temperature and Temperature dependent measurement set-ups are described in the paragraph below.

3.2.1 General set-up

The FTIR spectrometer, especially the sample compartment, needs to be purged before and during measuring. Figure 3-3 shows a schematic of the built liquid nitrogen (LN2) purging system. The LN2 purging system was handmade by the author of this thesis for the experiments and is the first liquid nitrogen purging system in the Larsen Lab. This system is set to use the blow-off gas from a LN2 tank, followed by a copper coil (to warm up gas to room temperature), desiccant column (ensure no water vapor travels into the spectrometer) and a flow meter. (*6A0107BV-NC, Dakota instruments* to check the gas flow).

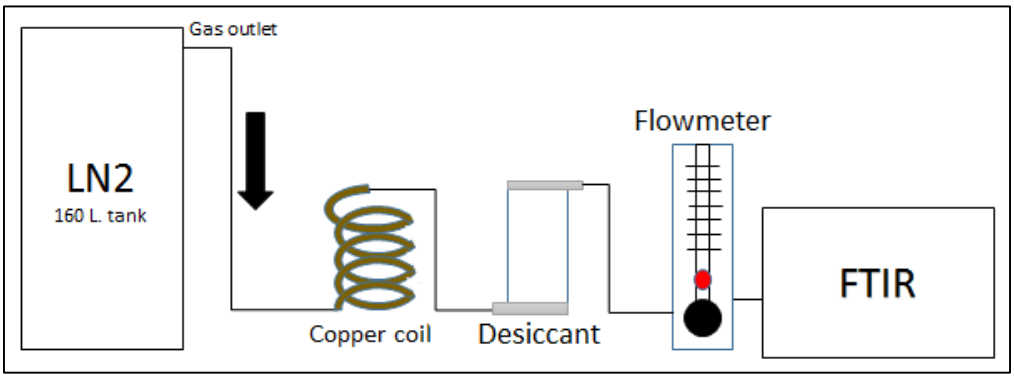

Figure 3-3: Schematic of the LN2 purging system, wherein a 160L LN2 tank is coupled to a copper coil followed by a desiccant column and flow meter before the gas enters the FTIR spectrometer.

During optimizing the spectrometer, it was discovered that the spectrometer needs at least an overnight (~12h) purge before measuring, see paragraph 4.1.4.

In addition, most experiments take a few hours (see §3.3.2) of measuring. Liquid nitrogen expands 645.3 [29] times when transitioning from liquid to gas (at room temperature). Therefore, a liquid nitrogen tank lasts days longer than a pressurized gas nitrogen tank of the same volume (160 L), which is 71 days against, respectively, 3 hours when set at 1 $L \cdot min^{-1}$.

The second part of the basic set-up is located inside the Tensor 27 sample compartment. Since the protein sample is illuminated to photo-convert between photostates, two diode lasers (connected to the dual output power supply) are installed inside the Tensor 27 on a lab platform. To maintain a constant environment inside the Tensor 27, the sample compartment should not be opened during the experiment. Due to space shortage and the lasers being unable to stand in the infrared beam pathway of the Tensor 27, a system of mirrors is installed inside the sample compartment. Figure 3-4 shows a schematic of the mirrors, laser diodes, beam pathways and cryostat (replaceable by other sample holders) inside the Tensor 27.

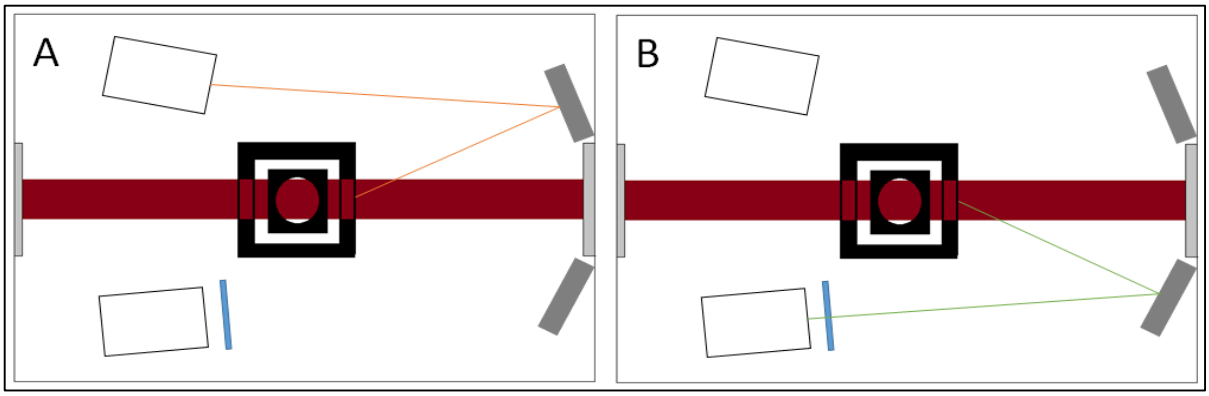

Figure 3-4: Schematic top view of FTIR sample compartment with beam pathways. Middle square is the Optical Cryostat, Large 'beam' represents the FTIR infrared light (in /out the sample compartment windows, from right to left), rectangles aside the Cryostat are the diode lasers (with or without a diffuser lens, small blue rectangle) and on the right two Ag mirrors (dark grey rectangles). Beam pathways shown are of the red (A) & green (B) diode laser.

3.2.1 Differences in set-up

In both room temperature and temperature dependent experiments, the cryostat in figure 3-4 is replaced by a Thorlabs mff 101 motorized flipper. In order to move the sample (the 1", respectively, 20 mm lens) in and out of the infrared beam, which will be explained in paragraph 4.1.2.

For the room temperature experiments, NpF2854g3 and Anacy 4718g3 are measured and compared with each other and other known data. The laser used for these experiments are the 650 and 532 nm, respectively, 730 and 590 nm lasers, see Appendix A.1 and B.1. Figure 3-5 shows a picture of the set-up inside the spectrometer's sample chamber.

For the temperature dependent experiment, a metal lens holder, mounted on the mff 101 flipper, is connected to the refrigerating circulator chiller, taking more space in the sample compartment. This does not matter for the set-up since the Cph1 protein in this experiment will not be illuminated. Only interest in this experiment is the temperature dependence of the protein in the dark ground state. Meaning, that the lasers (2 and 3 fig. 3-5) are removed from the set-up.

Appendix B.5 gives a visualization of the described set-ups

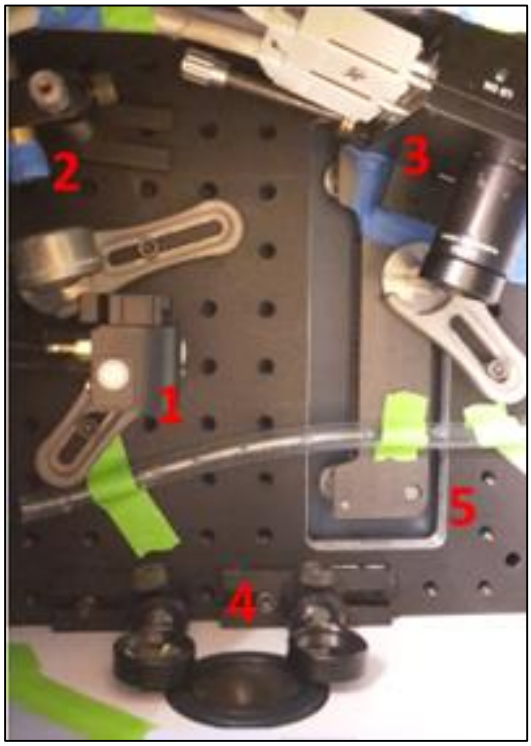

Figure 3-5: Photo of Anacy 4718g3 room temperature set-up inside the FTIR spectrometer sample compartment. With: 1) the motorized flipper, 2) 590 nm laser, 3) 730 nm laser, Ag mirrors and laser window, and 5) purge tube.

3.3 Measurement methods and procedures

3.3.1 Optimization and preparation measurements

To prepare the FTIR spectrometer, measurements are performed without usage of the cryostat (only a simple lens holder). In the following enumeration sub questions are depicted and measurements are briefly descripted. Set-up differences are noted below if otherwise.

1. **How long does the detector last before refilling the liquid nitrogen?**
   Ten times the detector is filled with five (67±1) mm funnels (50.8 mL total) of liquid nitrogen. The time after filling (start time) is noted. The spectrometer is monitored and the detector is considered not functional either when the spectrometer's STATUS LED is red or scans are out of the ordinary (jumping baseline or increase in noise, see Appendix C.1). The time is noted again when the above occurs. The averaged time is subtracted with one hour (minimum) to prevent detector corruption. The experiment's outcome gives an advised time between liquid nitrogen refills of the detector.

2. **What is the influence of the detector's 'drift'?**
   Since the detector is cooled with liquid nitrogen, it warms up over time. So, there is a possibility that the detector 'drifts' over time. After taking a background, scans are directly taken of the air inside the Tensor 27 every three minutes for one hour. From a neutral region (no influence of airborne particles) the deviation with the first scan (presumed flat line) is calculated with Matlab and presented in a graph. This gives an idea what the detector's drift is per minute.

3. **Is there a difference in scanner velocity, besides scanning speed?**
   The MCT detector within the spectrometer can be set on three scanner velocities [27]: 2.2, 10 and 20 kHz. For every scanner velocity, the time is measured three times for: 5, 10, 15, 20 and 25 scans. Water is used as sample in an unpurged sample chamber at a resolution of 1 and 4 cm^{-1}. Afterwards, the scans are compared in Matlab to see if there is a detectible difference. The experiment's outcome gives an idea which scanner velocity should be used for further measurements. For the FTIR cryokinetics, fast measurements are preferred since one needs to examine the fast kinetic traces during temperature changes and reaching thermal equilibrium. However, a compromise in scanning velocity is required when higher scanner velocities deform the signal.

4. **What purge flow is required to maintain minimum change in the FTIR?**
   By purging, the air is pushed out of the spectrometer. Therefore, it is important to know the flow [$L \cdot min^{-1}$] at which the changes in water vapor and CO_2 peaks are at a minimum. Since the spectrometer is slightly adjusted, it is unknown what flow is needed to keep water vapor and CO_2 out. The air in the chamber is scanned every three minutes and differences between two following scans are calculated. The data is checked to see at which flow the difference does not change more than 10^{-4} (Appendix C.2) in Transmittance *T* difference, in CO_2 and water vapor peaks, for at least one hour (after an overnight purge). Both purge time and flow are noted.

3.3.2 Room temperature and Temperature dependent experiment description

All experiments are performed in a dark environment to prevent the sample from interacting with unanticipated light. The FTIR spectrometer will be set on a resolution of 4 cm^{-1} [9] (§ 4.1.3), with an aperture of 4 mm [27] to measure the spectral range of 1800-1400 cm^{-1}, which is believed to be the region where the photoactivity of the protein takes place (Appendix A.4).

Room temperature experiment:
For this experiment the NpF2854g3 is placed in a motorized flipper (Thorlabs, mff 101) inside the FTIR spectrometer. The spectrometer is sealed and purged, on yet to be determined flow, for 12 hours in the dark (full dark state conversion of entire sample) prior to measuring.

Afterwards, the NpF2854g3 is illuminated for 10 minutes with 532 nm (green) light, followed by 20 background and 20 sample scans and repeated with 650 nm (red) light. The 20 scans are averaged and subtracted to obtain the Optical Difference. This experiment is repeated with the protein Anacy 4718g3, with far-red (730 nm) and yellow (590 nm) light.

The above described measurements will give the static optical difference spectrum of the two proteins' stable states, needed to work towards the cryokinetic measurements, since multiple similar spectra are taken at different temperatures and times.

Temperature dependent experiment:
The Cph1 sample is placed in a metal sample holder, which is mounted on the motorized flipper and connected to a refrigerating circulator chiller. After purging in the dark, at room temperature (298 K), the sample is scanned every three minutes. Starting from 5 °C the sample is heated every hour by 5° C, while scanning, till 40° C. From the measured spectra the optical difference, in correspondence to the first measured spectra, is calculated for every measured temperature and time. The results of this experiment show the temperature influence on Cph1. This will be compared with the known visible light data of the protein. The outcome of this experiment shows the temperature influence on the spectra of the photosensitive protein and sets another step towards the Cryokinetic measurement, since this is also executed with temperature differences between measurements.

4. FTIR Optimization and FTIR measurement results

In this chapter, the results of the previous mentioned set-ups and procedures are presented, processed and discussed. First, the results for the optimization of the FTIR spectrometer, concluded with a settings advice for following experiments. Second, the results and data processing of the room temperature and temperature dependent measurements. The chapter is concluded by summarizing how to build and perform the FTIR cryokinetic experiment.

4.1 Optimization of the FTIR spectrometer

4.1.1 Refill time of liquid nitrogen for the MCT detector

In table 4-1, the time after filling the detector with liquid nitrogen and getting corrupted (§3.3.1) are presented. From this data the time difference in minutes was taken and also represented in the table, as well as the date of the measurements. The average $\bar{X}$ and the standard deviation σ were calculated with formula 20 [30]. Where N is number of measurements with i^{th} measurement of x, in this case time. 3σ is taken for a 99.7% probability (three-sigma rule of thumb [30,31]).

$$\sigma = \sqrt{\frac{1}{N(N-1)}\sum_{i=1}^{N}(x_i - \bar{X})^2}, \quad where\ \bar{X} = \frac{1}{N}\sum_{i=1}^{N}(x_i) \qquad (20).$$

Using formula 20 for calculating the average and accuracy with the data of table 4-1, gives:

$$\bar{X} = \frac{456+460+439+444+434+434+431+438+431+437}{10} = 440.4$$

$$3\sigma = 3 \cdot \sqrt{\frac{(456-440.4)^2+(460-440.4)^2+(439-440.4)^2+(444-440.4)^2+(434-440.4)^2 \\ +(434-440.4)^2+(431-440.4)^2+(438-440.4)^2+(431-440.4)^2+(437-440.4)^2}{10\cdot(10-1)}} = 3 \cdot\ 3.19 = 9.58$$

Table 4-1: Data of start time when five funnels of liquid nitrogen were filled into the detector, end time when detector was found corrupted and the time in between with the average [min].

Day [m/d/y]	Start time [am]	End time [pm]	Time difference t [min]
03/15/16	9:25	5:01	456
03/16/16	9:20	5:05	460
03/17/16	9:05	4:24	439
03/18/16	9:10	4:34	444
03/21/16	9:23	4:37	434
03/22/16	8:55	4:09	434
03/23/16	9:01	4:22	431
03/24/16	9:14	4:32	438
03/29/16	10:14	5:25	431
03/30/16	9:18	4:35	437
Average ($\bar{X} \pm 3\sigma$)			440.4 ± 9.6

Since the average time between filling and corrupting is (7.3±0.2) hours it is advisable to refill the detector every 6 hours, 6.1 hours is minimum value minus the discussed one hour (§3.3.1), with five funnels of liquid nitrogen to prevent the detector from corrupting. One scan of five hours is shown in Appendix C.3, giving an idea of the detector's reaction on warming up. In addition, Appendix C.1 shows the detector's corruption when warmed up.

4.1.2 Detector drift of the MCT detector

For this experiment the sample compartment was closed without placing a sample inside, so only the air was measured. After taking a background scan, scans of the air were taken every three minutes for one hour. Three minutes is the maximum time between measurements that the Larsen lab takes for the UV-VIS cryokinetics experiment. Therefore, it is important to know how much the spectra changes within this time frame. Figure 4-1 shows one out of three measurements (only showing the measurements 10 minutes apart, clarifying the figure).

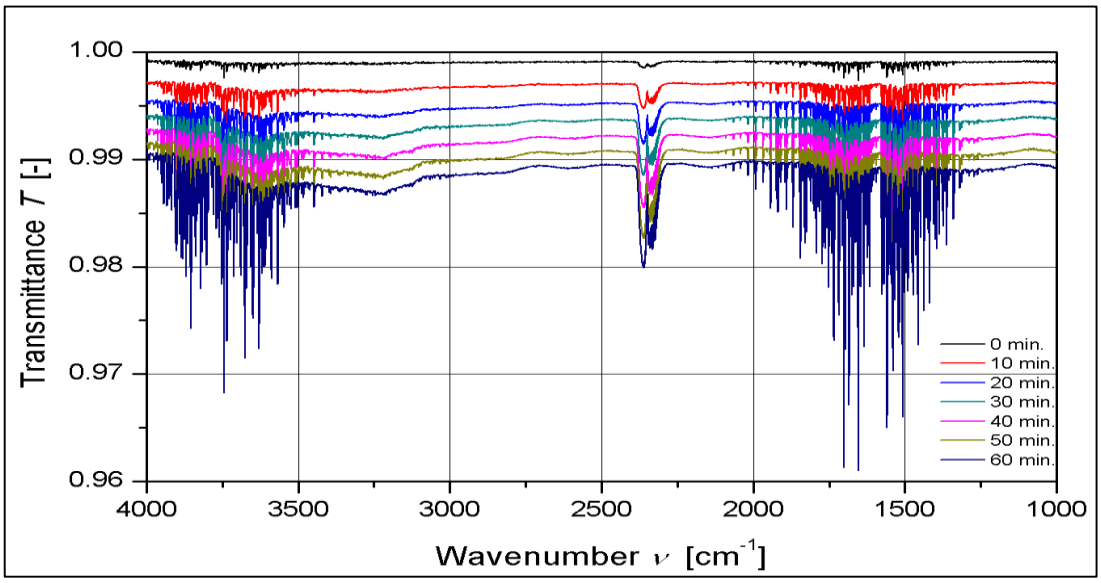

Figure 4-1: Detector drift of air in sample compartment with taking one background scan followed by sample scans, taken every three minutes for one hour. Here, only scans shown of every 10 minutes. At 2400 cm^{-1} CO_2 and at 4000-3500/2000-1500 cm^{-1} water vapor concentrations rises. Here transmittance *T* is plotted against wavenumber *ν*.

Figure 4-1 shows two issues to deal with: detector drift/deformation (baseline going down and small 'bumps' are growing) and the CO_2 and water vapor bands rise in time (more molecules means less transmission).

To calculate the drift difference *D*, the transmittance value of a scan at time *t* is subtracted from the first scan (*t* = 0 s) at 2550 cm^{-1} (no H_2O vapor/CO_2, see Appendix A.7). The calculated drifts are presented in figure 4-2. The average detector drift *D* is $(2.4\pm0.3)\cdot10^{-4}$ min^{-1} (Averaging trend lines and using Excel's LINEST for *σ*, see Appendix C.3).

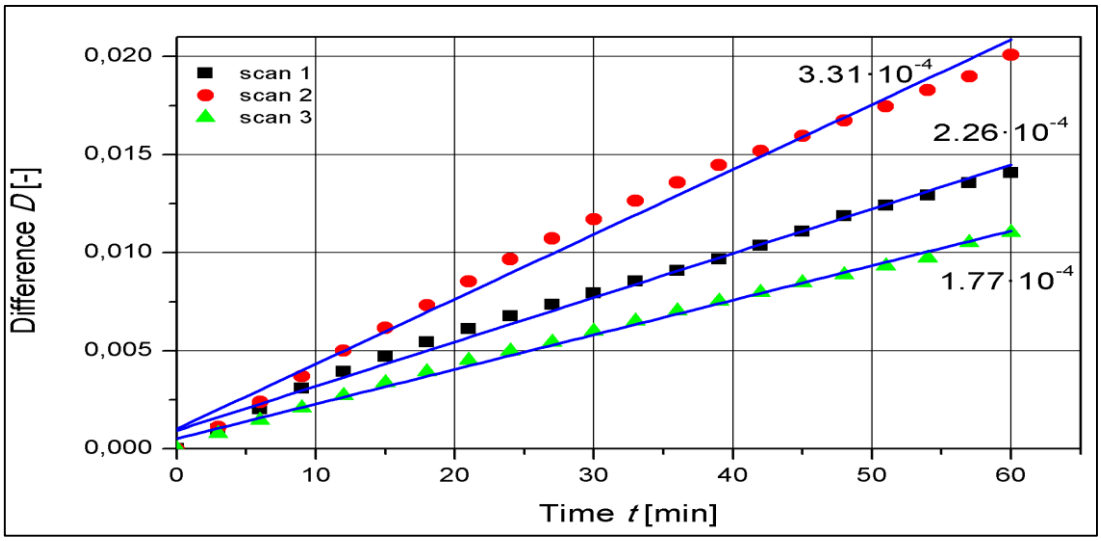

Figure 4-2: Plot of the difference *D* [-] against time *t* [min] of scan 1 (black squared), 2 (red circle) and 3 (green triangle), after one background, measured every three minutes for one hour. All scans are plotted with a trend line and slope.

Although the drift difference *D* is relatively small over a long period of time (FTIR Cryokinetics §4.4), the difference could add up to even larger differences than the calculated optical differences of the green/red state (Appendix C.2). In addition, the detector will also be refilled several times during the measurements thus changing the drift several times in either slope or symbol (+/-).

So, to compensate the drift use:

(1) manipulation of the data, or
(2) make a background scans, followed by sample scans, repeatedly.

The second option is preferred since there is no data manipulation involved, which prevents to (possibly) lose data. Therefore, the measurements above are repeated. This time background scans are taken between sample scans. The additional measurements confirm that by repeatedly taking a background scan before the sample scan, no drift is detected. All baselines stay around 1.00, see figure 4-3.

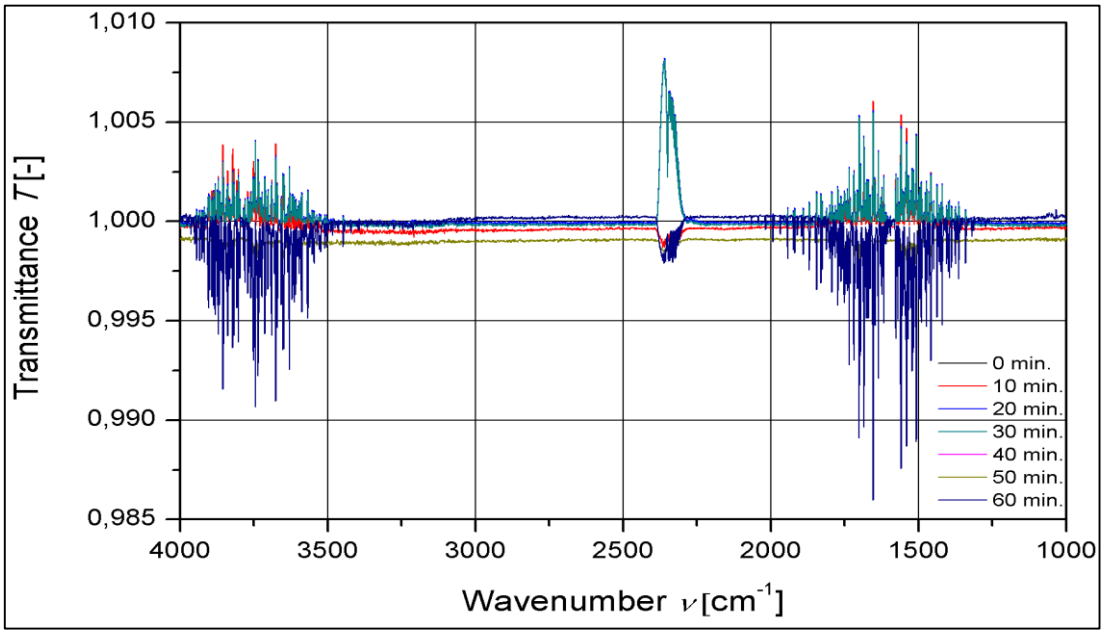

Figure 4-3: Detector drift of air in sample compartment with repeatedly taking background scans before sample scans every three minutes for one hour. At 2400 cm^{-1} CO_2 and at 4000-3500/2000-1500 cm^{-1} water vapor does not rise in concentrations.

When taking a new background scan, a new standard is set as maximum (1.00) transmission. If the background is only taken once, the maximum detected transmission lowers in time due to the detectors warm up, which causes the drift downwards, see figure 4-1.

This approach does not prevent the decrease or increase of CO_2 and water vapor inside the sample compartment, as shown in figure 4-3. When not purging the sample chamber sudden changes in the environment like: humidity, speed of fans in the lab, temperature or even breathing can change the number of detected air molecules (CO_2 and water vapor). This problem is discussed further in paragraph 4.1.4.

4.1.3 Difference in scanner velocity

No significant differences were found between the scanner velocities 10 and 20 kHz, see Appendix C.4. Since, multiple background and sample scans are taken within three minutes or even less, time is still a key role for performing cryokinetic measurements (§4.4). Therefore, the time was measured to see which scanner velocity meets the requirements. Table 4-2 shows the measured times *t* [s] for 10 and 20 kHz, each measured three times. Scanner velocity 2.2 kHz was dismissed, since it took an average of (1:22 ± 0:02) minutes to do 5 scans.

Table 4-2: Number of scans set out against measured times at 10 and 20 kHz scanner velocity. Time is measured three times for each setting, with calculated time average t_{av}.

Number of scans [-]	Time *t* at scanner velocity 10 kHz [s]			Average time t_{av} [s]	Time *t* at scanner velocity 20 kHz [s]			Average time t_{av} [s]
	Scan 1	*Scan 2*	*Scan 3*		*Scan 1*	*Scan 2*	*Scan 3*	
5	18.02	17.42	17.60	17.68	9.38	10.41	10.59	10.13
10	34.67	35.19	34.99	34.95	19.02	19.11	19.56	19.23
15	48.55	49.38	55.97	51.30	29.64	26.98	29.54	28.73
20	64.68	65.44	64.02	64.71	34.29	34.59	34.03	34.30
25	79.54	79.06	80.24	79.53	41.89	41.83	42.41	42.04

Furthermore, the average times of table 4-2 are divided by the corresponding number of scans and averaged once more. This was done by using formula 20 from paragraph 4.1.1, which results are presented in table 4-3.

Table 4-3: Calculated time per scan at scanner velocity 10 and 20 kHz, corresponding to the measurement taken with a set number of scans at 1 cm^{-1} resolution.

Number of scans [-]	1 cm^{-1} Corresponding time per scan [s]		4 cm^{-1} Corresponding time per scan [s]	
	For 10 kHz	For 20 kHz	For 10 kHz	For 20 kHz
5	3.54	2.02	1.14	0.51
10	3.50	1.92	1.08	0.58
15	3.42	1.92	1.03	0.52
20	3.24	1.72	1.04	0.53
25	3.18	1.68	1.02	0.51
Average ± accuracy	3.4 ± 0.1	1.9 ± 0.1	1.06± 0.02	0.53 ± 0.01

The above was also done for a resolution of 4 cm^{-1}. Scanner velocities 10 and 20 kHz needed an average of (1.06 ± 0.02) s and, respectively, (0.53 ± 0.01) s to measure 1 scan. See Appendix C.4 for additional results of the resolution 4 cm^{-1} and the difference between the resolutions.

The program OPUS scans a set number of scans before averaging those into one presentable scan, i.e. several scans are taken and represented and saved as one scan. It was chosen to take at least 10 scans 10 times to average it greatly, plus background scans taken before each scan. Resulting in 200 scans to take, which could be measured in 1:40 minutes for 20 kHz and 3:20 minutes for 10 kHz, when set on a resolution of 4 cm^{-1}.

Therefore, 20 kHz scanner velocity and resolution of 4 cm^{-1} gives the desired number of scans within the maximum of three minutes. Leaving about 1:20 minutes to push the buttons and get the protein sample in and out of the scanning beam.

4.1.4 Flow meter experiment results

In order to prevent CO_2 and water vapor entering the spectrometer (figure 4-1, §4.1.2), the sample compartment is purged by using nitrogen gas, see Appendix B.6.

As briefly explained in paragraph 3.2.1, a pure (99.98%) nitrogen tank does not suffice because the largest tank size provided in the Chemistry building is 160 L. The tank runs out of nitrogen during an overnight purge, resulting in a precarious tank switch. This switch could lead to water vapor and CO_2 re-entering the system, making an overnight purge unnecessary.

So, for this measurement a liquid nitrogen purge system (§3.2.1) was build and the FTIR was sealed with plastic and tape. Since the spectrometer is built with a lab platform, holding the laser diodes and mirrors, the conventional purging equipment of the spectrometer itself is blocked. Thus, a tube is inserted into the sample compartment from the top, preventing the top lid from closing. Once sealed, the purging system was set on a flow of 1 $L \cdot min^{-1}$ for an overnight purge. On the following day, the change in CO_2 and water vapor (Appendix A.7) was measured.

Every three minutes a scan was taken of the air inside the sample compartment while purging on different nitrogen flows. For this experiment only one background scan is needed no repetition, as stated in paragraph 4.1.2. Figure 4-4 shows the increasing CO_2 and water vapor peaks during the purge, in the first hour.

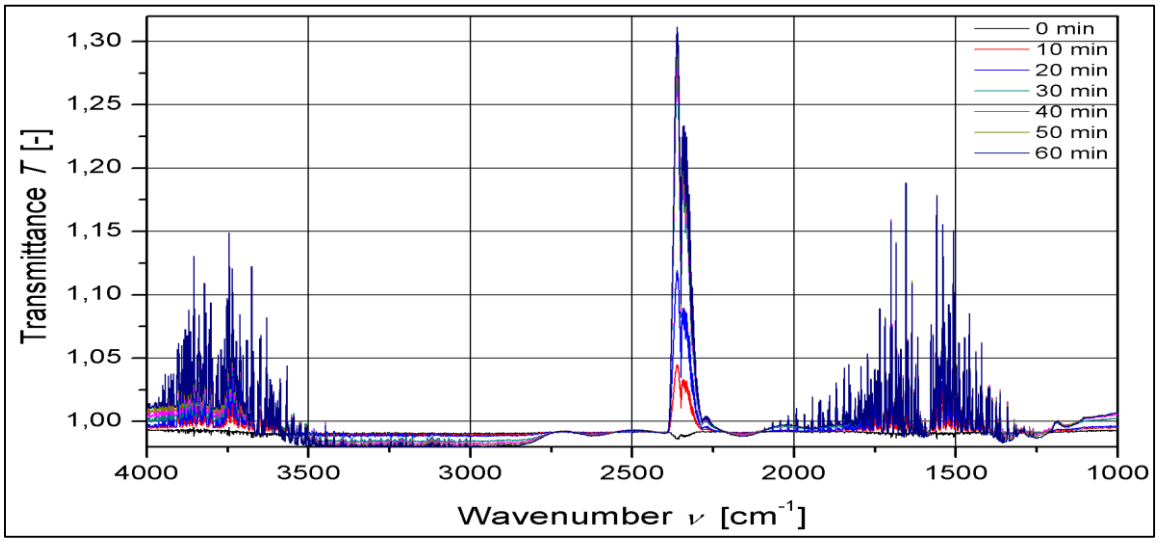

Figure 4-4: Plot of the first scans of the overnight purge. Showing a growth in the CO_2 and water vapor peaks, meaning a decrease in the amount of CO_2 and water vapor. Here transmittance *T* is plotted against wavenumber *ν*.

The figure above shows that the peaks grow above 100% transmittance (here 1); i.e. the amount of CO_2 and water vapor is less compared to the background scan. This is logical since these air particles are being pushed out the spectrometer by the nitrogen.

The difference between two following scans in the peaks 2365 cm^{-1} (CO_2) and 1635 cm^{-1} (water vapor) are calculated in Matlab, while compensated for the detector drift. The differences for the first 60 minutes are presented in figure 4-5.

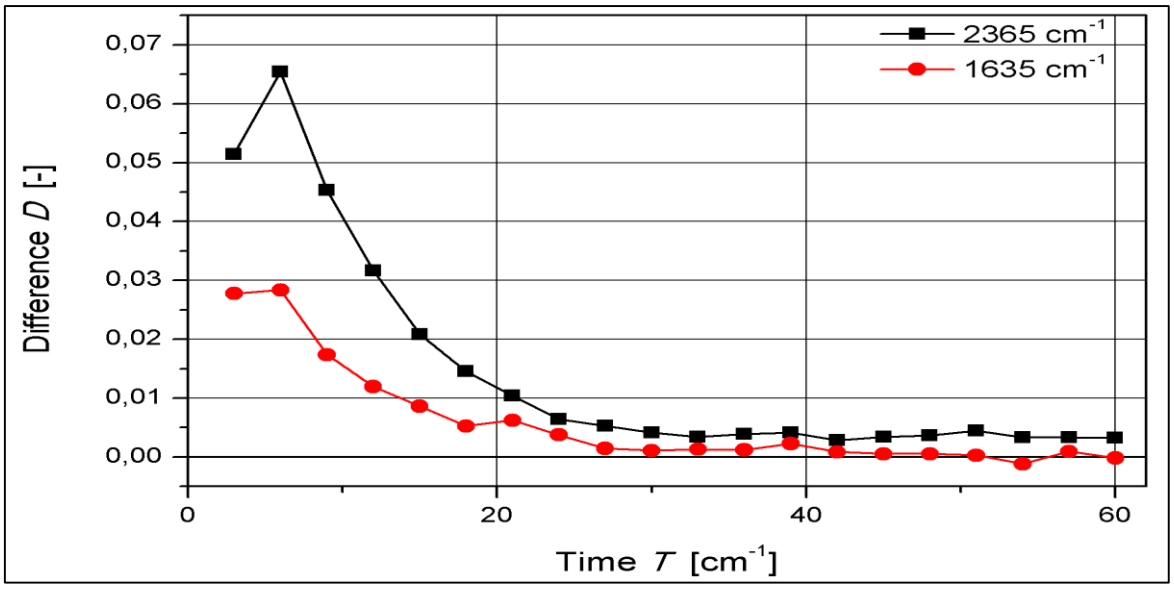

Figure 4-5: First three-hour scan of the nitrogen purge, where the difference between two successive scan in peak 1635 (red) and 2365 (green) cm^{-1} are calculated. Lines between data points are drawn to visualize the course.

Most air particles are pushed outside the spectrometer within 40 minutes. However, there are still differences in the 2365 cm^{-1} peak (green) of $3 \cdot 10^{-3}$, which is still more than 10^{-4} (§3.3.1).

After the overnight purge, similar measurements were taken for flows of 2, 3 and 4 $L \cdot min^{-1}$ (maximum advised flow [27]) purging for an hour. Before each measurement, the purge system was shut down for five minutes to allow air particles back into the system, so all flow rates are measured on the same grounds. The calculated results, depicted in figure 4-6, are compared to see which flow has the least changes between successive scans. Extra data on these measurements are found in Appendix C.5.

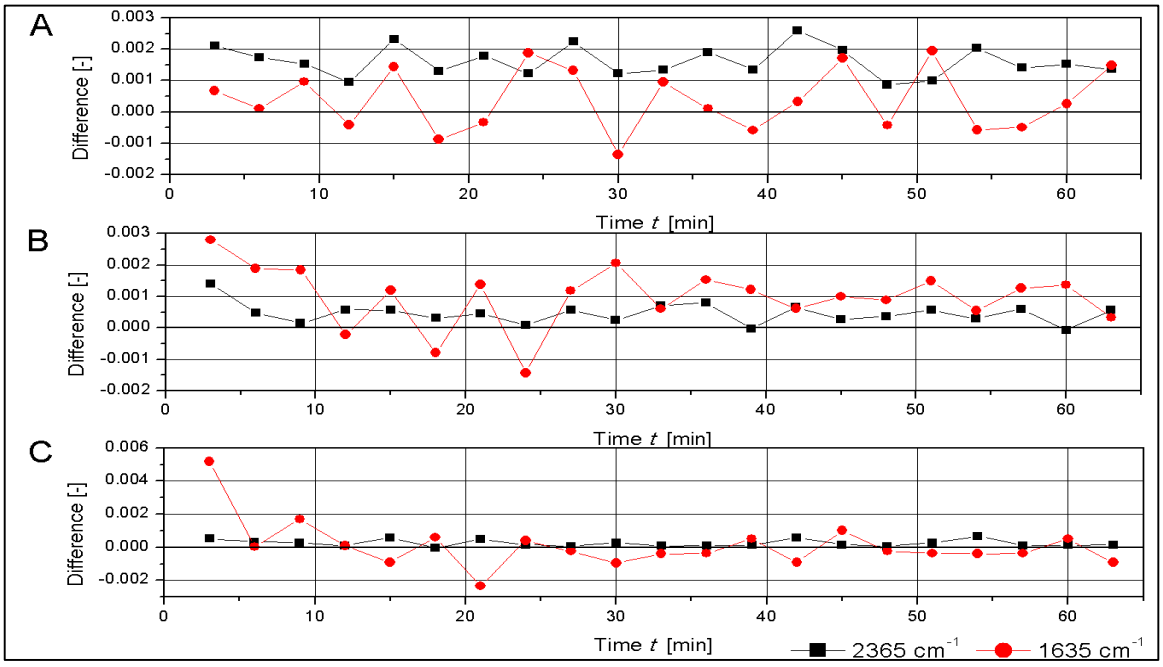

Figure 4-6: Graphs of transmittance changes during purge, at wavenumber 2365 cm^{-1} (black) and 1635 cm^{-1} (red), which are related to CO_2 and water vapor. In each graph the difference [-] is plotted against time *t* [min], measured for flows of 2 (A), 3 (B) and 4 (C) $L \cdot min^{-1}$. Lines between data points are drawn to visualize the course.

The figure above shows that the 4 L·min^{-1} setting (fig. 4-6.C) has the least fluctuations, seen in both the CO_2 and water vapor peak. For each flow F, in both CO_2 and water vapor, the average and standard deviation were calculated with formula 20, shown in paragraph 4.1.1.

Table 4-4: Calculated average differences between successive measurements. Calculations were done in the peak values of either CO_2 (2365 cm^{-1}) or water vapor (1635 cm^{-1}). Standard deviation (σ) was also calculated and presented below.

Flow F [L·min^{-1}]	Calculated in peak [cm^{-1}]	*Differences* 10^{-4} [-]	σ 10^{-4} [-]
2	2365	16.1	1
2	1635	3.9	2
3	2365	4.6	1
3	1635	9.9	2
4	2365	2.5	0.5
4	1635	0.8	3

Table 4-4 shows that almost all flow settings exhibit an average difference of 10^{-4} in both CO_2 and water vapor peaks. Due to many fluctuations between successive measurements the uncertainty is relatively high. However, this should not matter since the aim is to keep the changes within 10^{-4} difference, which is accomplished. 4 L·min^{-1} shows the least changes ($(2.5\pm0.5)\cdot10^{-4}$ and $(1\pm3)\cdot10^{-4}$). Thus using 4 L·min^{-1} as the purge flow for further measurements in this thesis.

4.1.5 Setting parameters for further measurements

Paragraphs 4.1.1-4.1.4 showed a few features, which help taking spectra in the FTIR room temperature and temperature dependent measurements. First, the detector runs out of liquid nitrogen (50.8 mL) within (7.3±0.2) hours and is therefore refilled every 6 hours.

The detector warms up during measuring, leading to a drift difference D of $(2.4\pm0.3)\cdot10^{-4}$ [-] per minute. However, by taking background scans and sample scans repeatedly the drift will not affect the sample measurement. This is accomplished by using a motorized flipper inside the sample chambers, moving the sample in and out of the detector beam. The detector will be set on a scanner velocity of 20 kHz to take fast scans ((0.53 ± 0.01) s per scan), which is preferred for the cryokinetics.

The LN2 purging system, after sealing the FTIR, will be set on 1 and 4 L·min^{-1} purge flow for an overnight purge and, respectively, during the experiment. The differences in air particles are still checked before measuring, since the humidity and temperature changes every day. To conclude, the spectrometer will also be set on an aperture of 4 mm [27] with a 4 cm^{-1} resolution (see Appendix C.4).

4.2 Room temperature experiment results

For this experiment a program was written, with AutoHotkey, to automatically move the motorized flipper, scan, and save 20 spectra (each containing 10 scans) for both green (532 nm) and red (650 nm) illuminated sample.

Before measuring, the protein sample NpF2854g3 was illuminated 10 minutes with either green or red light. The measurement took 30 minutes total, with 20 minutes of illumination for red and green light and 10 minutes (total) to scan, flip, and save. Transmission spectra were taken in the range 4,000-900 cm^{-1}, to keep track of water (vapor) and CO_2 during the experiment. See figure 4-7 for the transmission spectra.

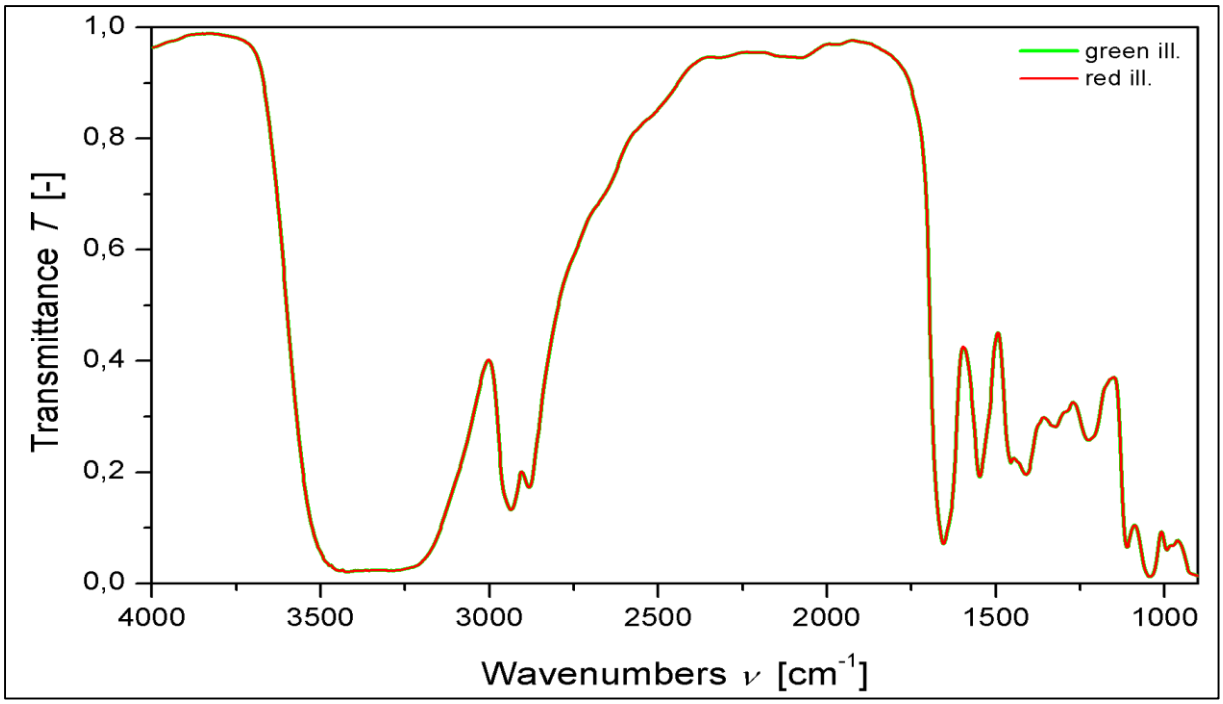

Figure 4-7: Transmittance spectra of one measurement of red illuminated NpF2854g3 (red) and one of the green illuminated (green). In this figure the transmittance value *T* [-], measured for each wavenumber, is plotted against wavenumber *ν* [cm^{-1}]. 3500-3000 and 1600 cm^{-1} are water peaks. The others (±2800 and 1600-1000 cm^{-1}) are the protein and buffer material.

The figure above shows two spectra (green and red illuminated) of NpF2854g3, which by the naked eye looks the same. Due to illumination the proteins structure changes (§2.1.2), which causes relatively small changes seen in the region 1800-1400 cm^{-1} on the order of 10^{-3}, shown in figure 4-8 by a zoom in of a peak at 1445 cm^{-1}.

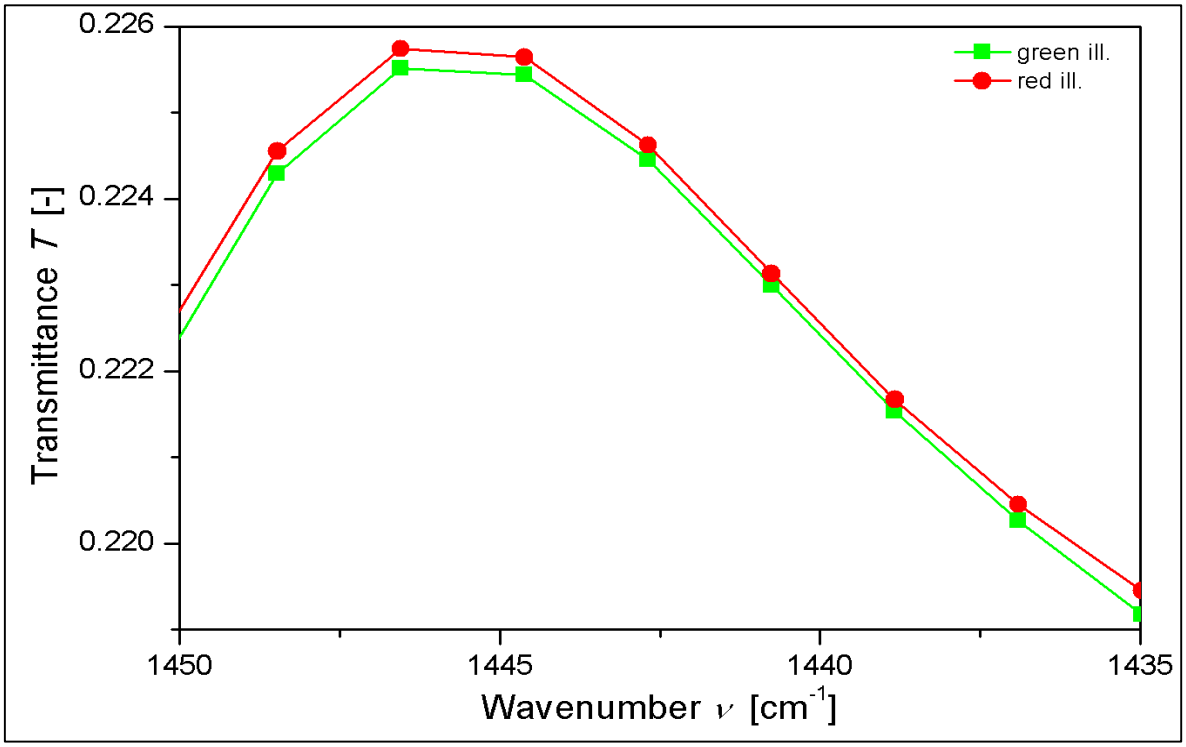

Figure 4-8: Zoom in on figure 4-7 a peak at 1445 cm^{-1}. The figure shows spectral differences between red and green illuminated protein sample NpF2854g3 in the order of 10^{-3}. In this figure the transmission value *T* [-], measured for each wavenumber, is plotted against wavenumber *ν* [cm^{-1}]. Lines between data points are drawn to visualize the course.

Since the interest is to find the absorbance difference ΔA [-] between the two illuminated states. Formula 11 (§2.2.2) was used to calculate the absorbance, followed by formula 21 to calculate the absorbance difference ΔA [-] in each wavenumber v at the same time t after illumination.

$$\Delta A(\nu, t) = A_{light}(\nu, t) - A_{dark}(\nu, t_0) \qquad (21).$$

The band at 1454 cm^{-1}, in figure 4-8, represents as example for the calculations below. Here the red illuminated protein represents the light state (P_g) and green the dark state (P_r).

$$-\log_{10}(0.2173) = 0.6629 = A_{light}$$
$$-\log_{10}(0.2169) = 0.6637 = A_{dark}$$

$$\Delta A(\nu, t) = 0.6629 - 0.6637 = -8.0 \cdot 10^{-4} \text{ [-]}.$$

These calculations were done at each wavenumber for all 20 measured spectra of both states using Matlab. After, the average was calculated using formula 20 (§4.1.1), the maxima and minima were identified and a graph was made. Figure 4-9 shows the absorbance differences ΔA, with peak identification for NpF2854g3 (red line) in the region 1800-1400 cm^{-1}.

The same measurement and analysis process was performed with Anacy 4718g3, which is a yellow/far-red protein. The only difference is that this protein is illuminated with yellow (590 nm) and far-red (730 nm) light for a half hour instead of 10 minutes, due to its relatively small response. For the calculations the yellow illuminated spectrum is considered as the dark state and far-red illuminated as the light state. The absorbance differences ΔA [mOD] (arbitrary units a.u.), with peak identification for Anacy 4718g3 (black line) in the region 1800-1400 cm^{-1} is shown in figure 4-9 as well.

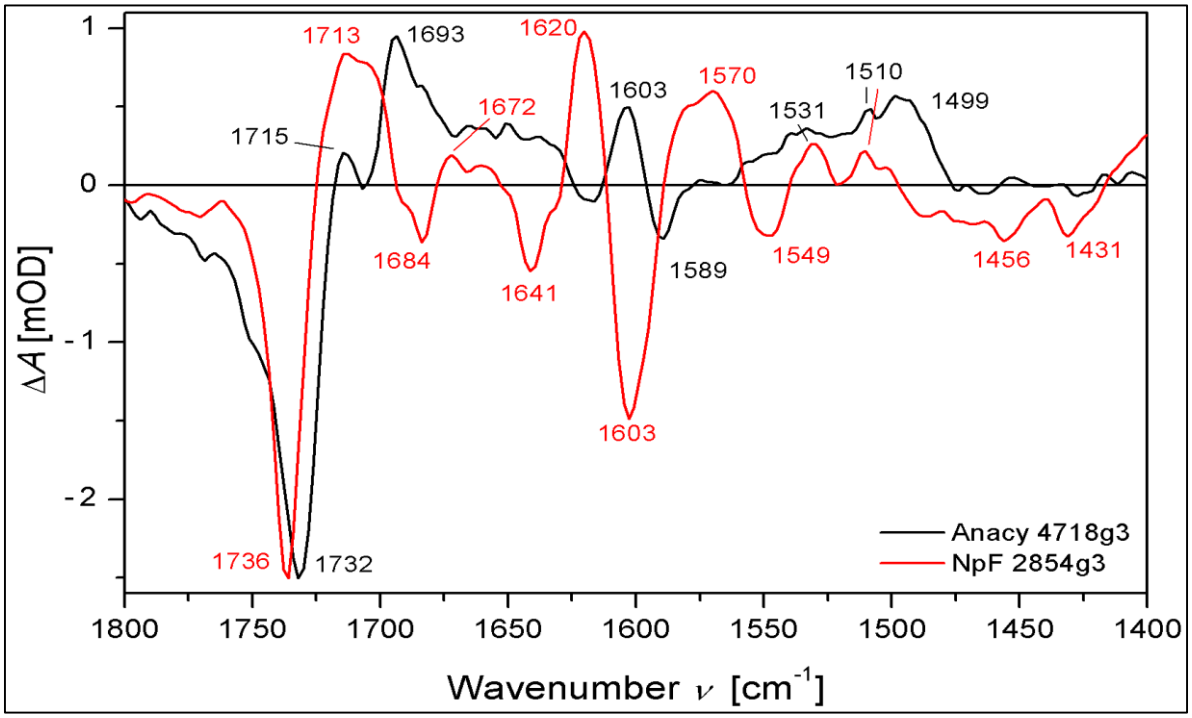

Figure 4-9: light-minus-dark Absorbance difference ΔA of NpF2854g3 (red) and Anacy 4718g3 (black), zoomed in the region 1800-1400 cm^{-1}, with peak identification. ΔA [mOD], in arbitrary units, was plotted against wavenumber v [cm^{-1}].

The figure shows the averaged light-minus-dark spectra of the mentioned proteins. Anacy 4718g3 is scaled to NpF2854g3 at 1736 / 1732 cm^{-1} (multiplied by 1.64) to get a better view on the difference in peak position and to see if the peaks are positive or negative.

For comparing photosensitive proteins, the overall amplitude of the signal it is not important as it varies between experiments.

To get the absorbance difference ΔA under the same circumstances is difficult, since this depends on multiple factors: the concentrations of both protein and its buffer material, the chance of photo-conversion, the laser power and the environment during the measurement. The interest is in the relative differences in amplitude, which indicate changing concentrations of intermediates and the identity of those intermediates by the vibration structure.

The identified peaks could be related to molecular vibrations using one of three methods:

1. Measure the same protein multiple times, wherein each measurement limited changes are made. These changes include substitution of atoms by isotopes or removing parts of the molecule. Change in mass will shift the peaks to the right or left on the x-axis.
2. Using quantum mechanical equations to calculate the atomic bonds. These equations are an extension of the previous method and usage of multiple different type of experiments, like NMR.
3. Using reference papers where one of the above has already been executed on similar proteins.

Method 1 and 2 are time consuming considering that multiple proteins should be made and sent to the lab. This process can take several weeks to make such proteins with different isotopes, measure, interpret the data and request another protein for further measuring.

Since time is limited for the research done in this thesis, method 3 of the above was chosen to correlate the identified peaks to known atomic bonds. In the individual light-minus-dark spectra, the peaks were also identified and used to average and calculate the standard deviation. Appendix C.6 contains extra data on the identified peaks.

Table 4-5 below contains the identified peak values of both proteins along with assignments to which atomic bonds and states these peaks belong ($P_{r/y}$ (-) is dark and $P_{g/fr}$ (+) is light).

Table 4-5: Found peaks of both measured NpF2854g3 (red/green) and Anacy 4817g3 (yellow/far-red) of the light-minus-dark spectra, with atomic bonds assignments corresponding to the peaks. | in the middle means two possibilities here.

NpF 2854g3		*Anacy 4718g3*		*Assignment*	*Ref.*
P_g (+) [cm^{-1}]	P_r (-) [cm^{-1}]	P_{fr} (+) [cm^{-1}]	P_y (-) [cm^{-1}]		
	1736 ± 1		1732 ± 1	Ring A carbonyl stretch C_1=O	32,36,34,37
1713 ± 2		1715 ± 1		D ring carbonyl stretch C_{19}=O	33,32,34
		1693 ± 1		Amide I (loop/turn) | propionate PCB	33,34,35,38, 41 | 37
	1684 ± 1			Amide I (loop/turn) | propionate PCB	33,34,35 | 37
1672 ± 1		1670 ± 1		Amide I turns & bends | Methine bridge A-B stretch	35,38,41 | 36
1661 ± 2		1655 ± 1		α helical Amide I | Amide I	34,41,38,39,40 | 37,38
	1641 ± 1			C-D methine bridge str. | uncorded	36 | 41
1620 ± 1			1616 ± 1	β-sheet amide I band | methine bridge B-C stretch	35,39,41 | 36,39
	1603 ± 1	1603 ± 1		methine bridge B-C stretch | amide I, β structure	37 | 34,39,40
			1589 ± 1	N-H Mode C D ring | C=C A-B stretch	34
1570 ± 1				Amide II | methine bridge A-B	36,39,40
	1549 ± 2			Amide II band shift	34,39,40
1531 ± 1		1533 ± 1		chromophore *î*(C=C) + *ä*(N-H) **or** *Î*(C-N) + *ä* (N-H)	34
1510 ± 1		1508 ± 1		chromophore *î*(C=C) + *ä*(N-H) **or** *î*(C-N) + *ä*(N-H)	34
		1499 ± 1		Trp, *î*(C-N) + *ä*(C-H) + *ä*(N-H) chromophore *î*(C-N)	34
	1456 ± 1			-	-
	1431 ± 2			-	-

The data in table 4-5 showed to be inconsistent. Since this field of study is still developing, there are some unresolved issues.

To illustrate the positions of the assignments and atomic bonds, figure 4-10 shows a schematic overview of the chromophore. Here, all the rings (A, B, C & D), NH, propionates (O^--C=O) and carbonyl bonds (C=O) are represented.

Figure 4-11 shows a schematic of the position of the chromophore inside an (example) protein. See Appendix A.4 for more information on Amide's vibrational bands and *α*-helices / *β*-sheets.

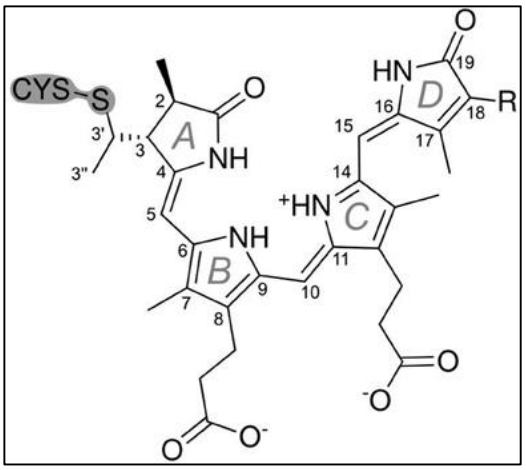

Figure 4-10: Schematic overview of the Chromophore to show the known rings and atomic bonds. [5]

It can be seen in figure 4-11 [42] that the chromophore (detailed left bottom) is attached to the rest of the protein by a sulfur linkage to Cys. The protein consists several structures: α-helices (green coils), β-sheets (green arrows) and loops (thin lines).

Recent X-ray studies on the phytochrome DrBphP [43] and NMR studies on CBCRs NpF2163g3 and TePixJ [44] suggest that during photo-conversion not only the chromophore undergoes structural changes. These studies revealed that the protein also experiences secondary structural changes, suggesting that the α-helix partially transforms in a β-sheet [44] or a total β-sheet-to-α-helix conversion [43].

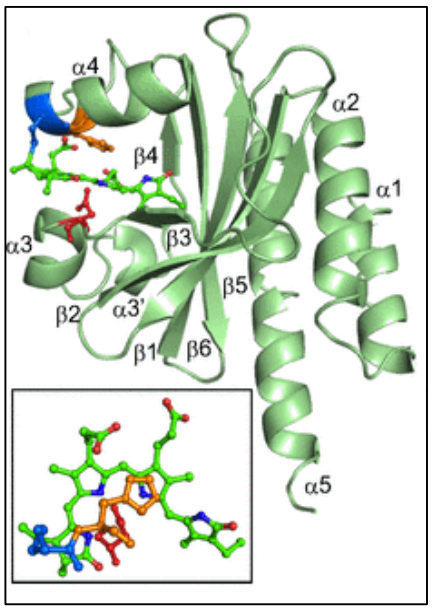

Figure 4-11: Tertiary schematic of an example protein containing α-helix, β-sheets, loops and chromophore (left bottom). [42]

From the data shown in figure 4-9 and table 4-5 it is interesting to look at the region of 1625-1550 cm^{-1} (fig. 4-12). At 1620 cm^{-1} NpF2854g3 shows an increase in the β-sheet P_g light state structure coupled to a decrease in the β-sheet structure in the P_r dark state at 1603 cm^{-1}. There is also an increase in the Amide II band at 1570 cm^{-1}. Anacy 4718g3 shows almost the same results as NpF2854g3. The P_{fr} light state shows an increase in β-sheet structure and the P_y dark state decreases in β-sheet structure. These changes are not unexpected as X-ray studies suggested B sheet transformations during photoconversion.

Anacy also shows to lost NH band (1589±1) cm^{-1} (-) in the C and D ring.

It is still difficult to understand the photo-conversion process from the measured FTIR data. However, the data from figure 4-12 shows signs of secondary structural changes in both Anacy 4718g3 and NpF2854g3, which are slightly different from each other. To confirm this, more measurements are needed. Mostly repeated, reproducibility and atom substitution experiments are needed to filter out the exact structural changes.

Due to shortage of time it was not possible to perform more of these measurements.

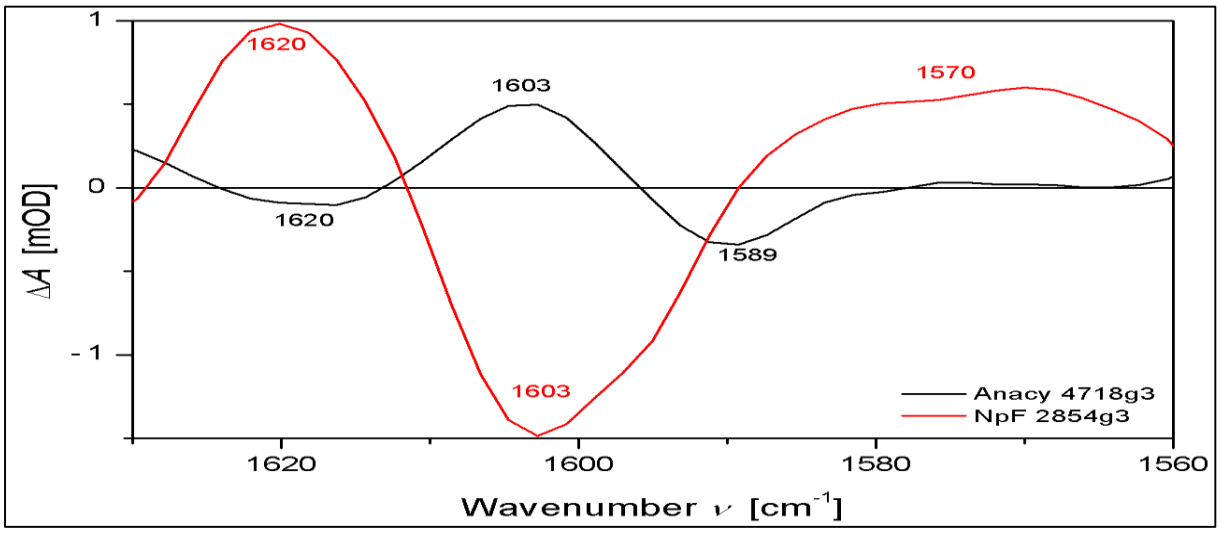

Figure 4-12: Zoom in on region 1625-1560 cm^{-1} of figure 4-9 of the scaled Anacy 4718g3 (black) and NpF2854g3 (red). Here the absorbance difference Δ*A* [mOD] (arbitrary units) is plotted against wavenumber *v* [cm^{-1}].

The data in figure 4-9 and table 4-5 also showed that both NpF2854g3 and Anacy 4718g3 lost vibrational energy in the C_1=O band and the A-ring (1732/1736 cm^{-1}) during photo-conversion.

Both also exhibit gains in the C_{19}=O band, on the D-ring even though the Anacy peak at 1715 cm^{-1} is less than the NpF (1713 cm^{-1}). These changes may prove to be significant in the photocycle of CBCRs as the isomerization occurs on the D-ring which shows increases vibrational energy.

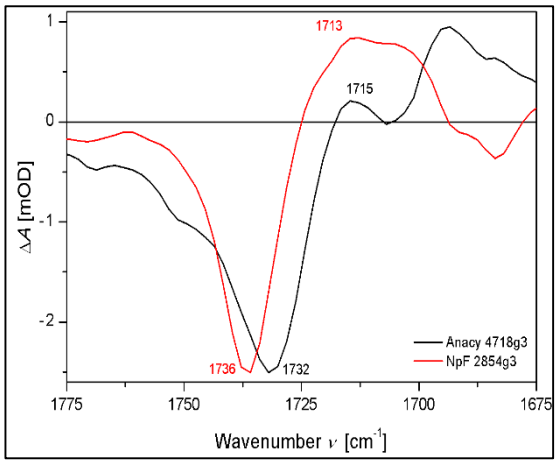

Figure 4-13: Zoom-in of figure 4-9 at 1775-1675 cm^{-1}.

Figure 4-14 shows a comparison between Anacy 4718g3, NpF2854g3 and Cph1 [34], where the data is scaled at wavenumber 1510 cm^{-1} of NpF2854g3.

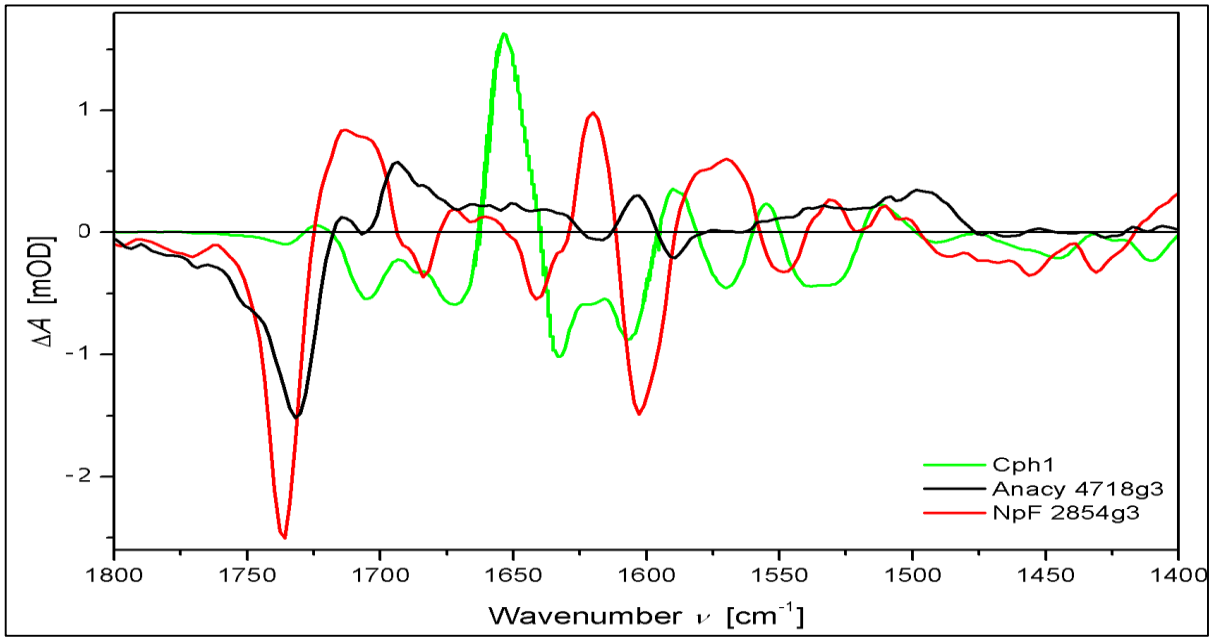

Figure 4-14: Comparison of Anacy 4718g3, NpF2854g3 and Cph1 [34] in the region of 1800-1400 cm^{-1}. Here the Δ*A* is plotted against wavenumber *ν* [cm^{-1}]. All graphs are scaled in point 1510 cm^{-1}.

The figure above shows that the cyanobacterial phytochrome Cph1 has an almost no change in the C_1=O and C_{19}=O band of the chromophore's A-ring and D-ring. Both CBCRs (Anacy and NpF) have more activity in the C_1=O band in contrast to Cph1. This result would suggest that during photo-conversion (dark to light) CBCRs tend to loosen more in the C_1=O band than cyanobacterial phytochromes. This might be in the form of a hydrogen bonding break.

Other available CBCR data on NpR6012g4 [45] and NpR5113g2 [45], shown in figure 4-15, support this suggestion. FTIR studies on the bacteriophytochrome BphPs [33] (graph not available) also show lack of C_1=O and C_{19}=O activity, making the suggestion even more acceptable.

In this field of study there are still discussions going on about where the chromophore's isomerization takes place. Most studies confirm that it takes place in the D-ring ($C_{15}/_{16}$ double, §2.1.2), while a few suggest it takes place the A-ring instead or simultaneously [46]. The Ames Lab (collaborating lab at UC Davis), discovered with NMR data that activity in the CBCR's C_3 atom of the A-ring was showing (in preparation).

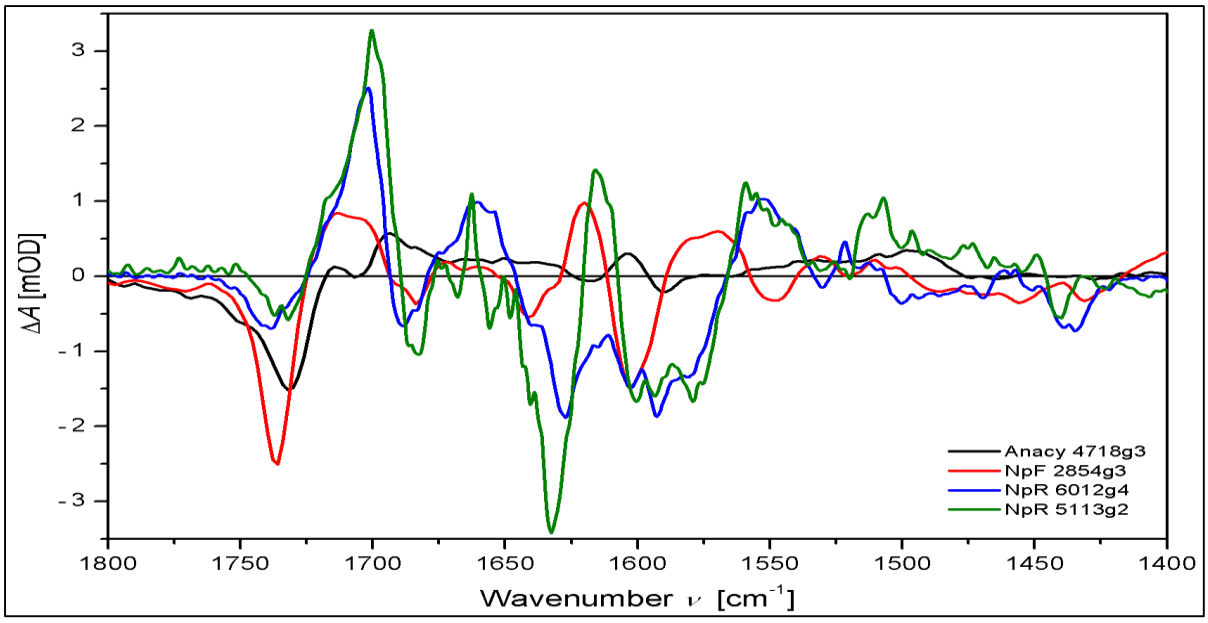

Figure 4-15: Comparison of Anacy 4718g3, NpF2854g3, NpR6012g4, and NpR5113g2 [45] in the region of 1800-1400 cm^{-1}. Here the Δ*A* is plotted against wavenumber *ν* [cm^{-1}]. All graphs are scaled in point 1603 cm^{-1} of NpF2854g3.

The figure shows that there is definitely a distinct difference in the A-ring of CBCRs in contrast to cyanobacterial phytochromes (Cph1), which could lead to more activity in the A-ring. Just like the region of 1625-1550 cm^{-1}, the vibrational energy in the C_1=O and C_{19}=O band need more measurements to confirm this. Mostly repeated, reproducibility and atom substitution experiments are needed to filter out the exact structural changes.

This experiment has proven to be useful for the cryokinetic measurement set-up. The AutoHotkey program, FTIR settings and use of the motorized flipper gave no problems in collecting the data as discussed above. The calculated uncertainties in table 4-5 (±1 and ±2 cm^{-1}) prove that taking 20 background scans, flips and sample scans repeatedly give an accurate peak position. Therefore, showing that this system can handle quick scans needed for following measurements.

4.3 Temperature dependent measurement results

For this experiment the set-up used in the room temperature measurements was slightly adjusted. Now the motorized flipper moves a sample holder that is connected to a chiller. The chiller pumps temperature controlled water through the metal casing of the sample holder.

A similar program was written with AutoHotkey that controls the flipper and FTIR automatically, see Appendix B.5, to take 10 scans every minute for the entire experiment (a requirement and next step to the FTIR cryokinetics). This is done while each hour the chiller is set on a different temperature, starting from 5° C up to 40° C, in 5° C increments. This experiment was done in a dark environment, therefore, only the dark state of the protein Cph1 is examined on its temperature behavior.

Figure 4-16 shows the averaged spectra in the range of 4000-900 cm^{-1}, after the sample reached thermal equilibrium. This is done for each set temperature.

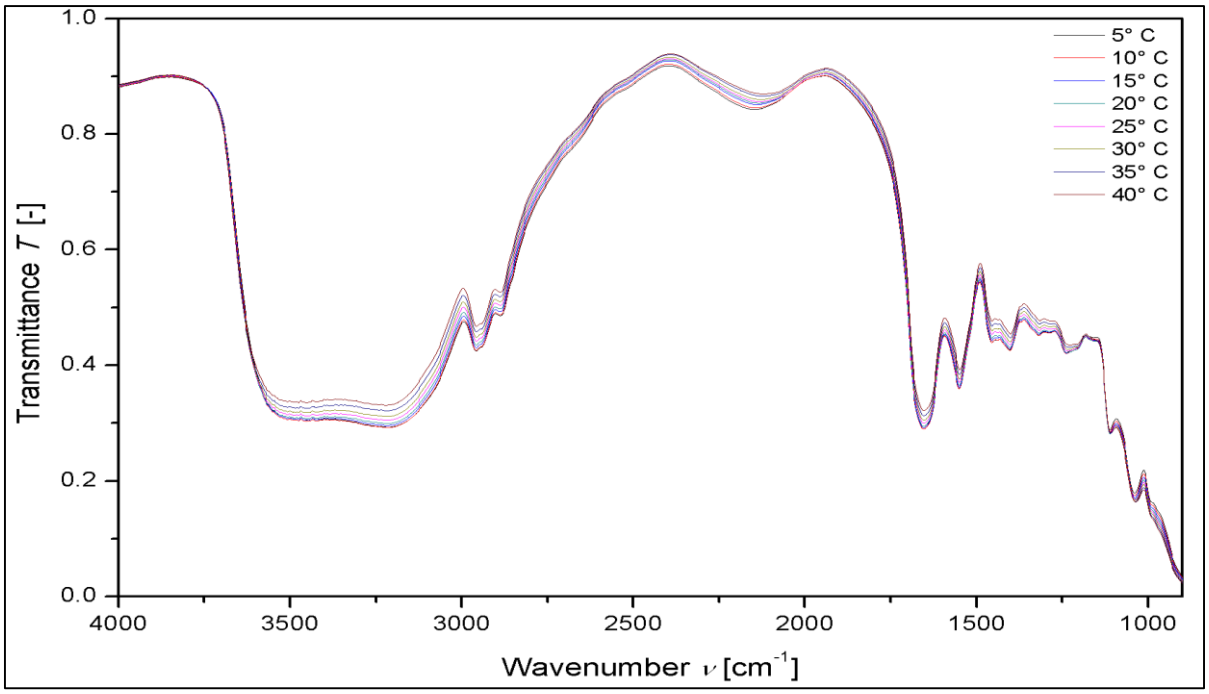

Figure 4-16: Averaged transmittance spectra of Cph1 for temperatures 5° C up to 40° C, in 5° C increments. Here tranmittance *T* is plotted against wavenumber *ν* [cm^{-1}]. Features of water can be seen in 3600-2800, 2200 and 1600 cm^{-1}, while Cph1 features are seen between 1800 and 1000 cm^{-1}. The graphs going down at 1200-900 cm^{-1} is due to the CaF_2.

It can be seen that there are differences between the spectra during temperature changes. Figure 4-17 below shows two zoom-ins of the spectra above in the region of 3700-2600 cm^{-1} and 1800-1500 cm^{-1}.

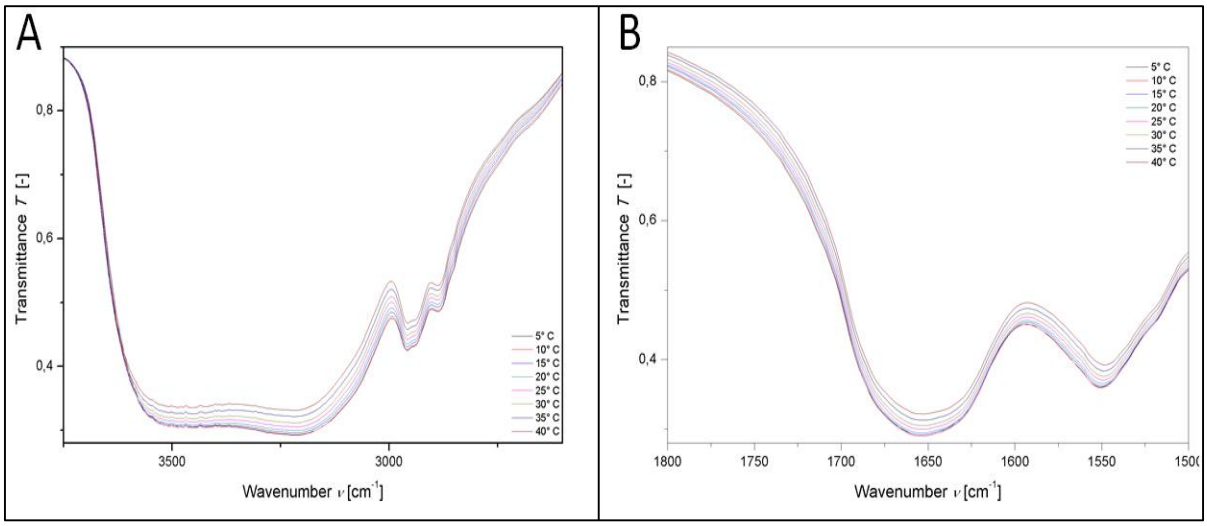

Figure 4-17: two zoom-ins of figure 4-16 for the regions 3700-2600 cm^{-1} (A) and 1800-1500 cm^{-1} (B).

To calculate the transmittance difference ΔT between the first measured spectra (5° C) and other consecutive spectra, formula 22 is used in the same way as formula 21 from paragraph 4.2. Here, t_5 is the measured spectra at 5° C at every measured wavenumber ν and t_{temp} the spectra of any consecutive temperature.

$$\Delta T(\nu, t_{5-temp}) = T(\nu, t_5) - T(\nu, t_{temp}) \qquad (22).$$

These calculations where performed to see the 'growth' of the Cph1 characteristic peaks as the temperature rises. The results are shown in figure 4-18.

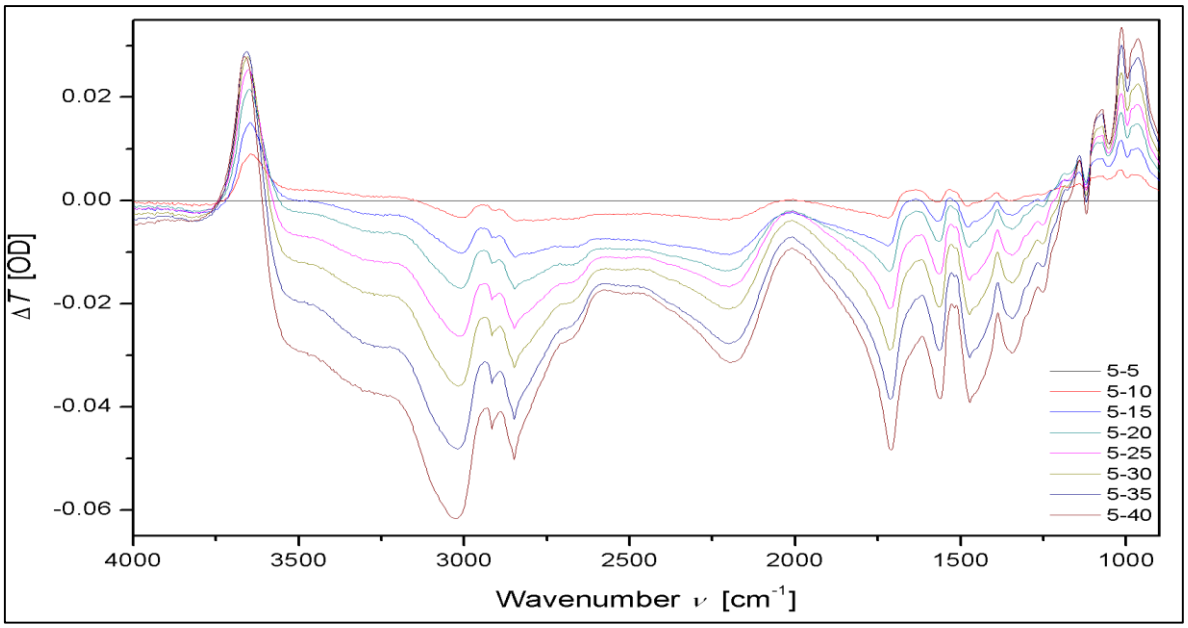

Figure 4-18: Transmittance difference Δ*T* between 5° C and other following measured spectra at temperature 10-40° C. Here Δ*T* is plotted against wavenumber *ν* [cm^{-1}] between 4000-900 cm^{-1}.

The figure shows that there is growth in a few peaks. However, it was not expected to see a 'wobble' in the data. The expectation was to see positive and negative peaks around a baseline at zero, as in paragraph 4.2, while increasing or decreasing at certain points.

The new hypothesis from this data is that water, in the protein's buffer material, might have temperature dependent characteristics. Since the OH stretching peak (3600-3000 cm^{-1}) also changes with temperature, it is expected that this causes the 'wobble' over the entire Cph1 spectrum. Research on the infrared spectra of water [47] shows that the OH stretching peak becomes narrower with increasing temperature, as seen in figures 4-16 and 4-17. Which was concluded to be caused by librations (sham vibrations) of the water molecules.

Therefore, it is chosen to do the temperature dependent experiment over with only water. The averaged spectra and difference spectra are shown below in figure 4-19 and 4-20.

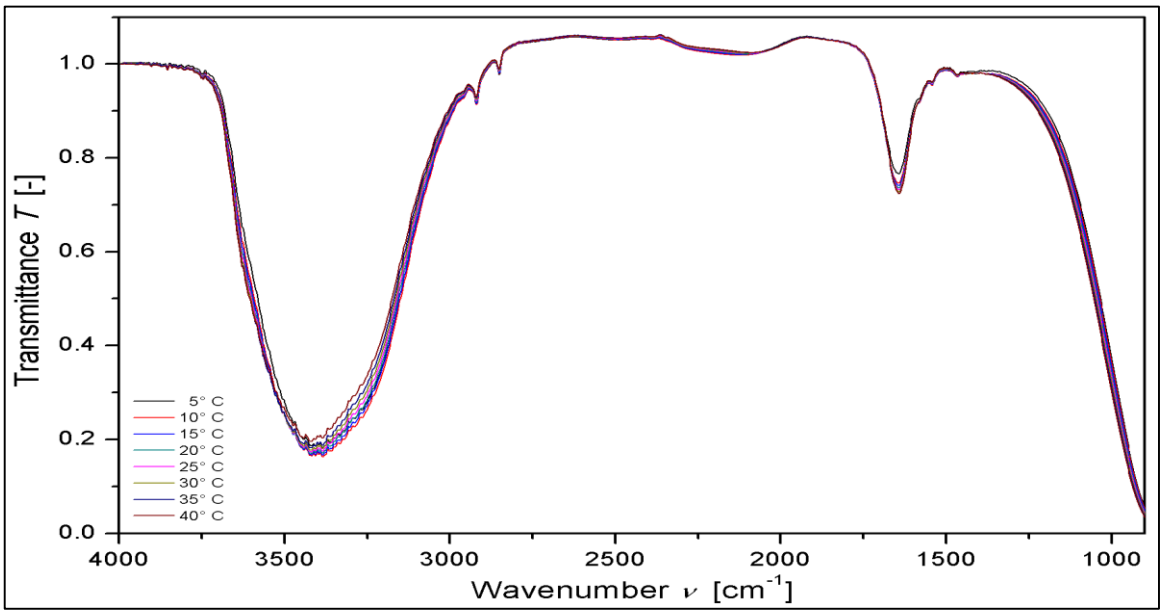

Figure 4-19: Averaged transmittance spectra of water for temperatures 5° C up to 40° C, in 5° C increments. Here tranmittance *T* [-] is plotted against wavenumber *ν* [cm^{-1}]. Features of water can be seen in 3600-2800, 2200 and 1600 cm^{-1}. The down going graph at 1200-900 cm^{-1} is due to the CaF_2.

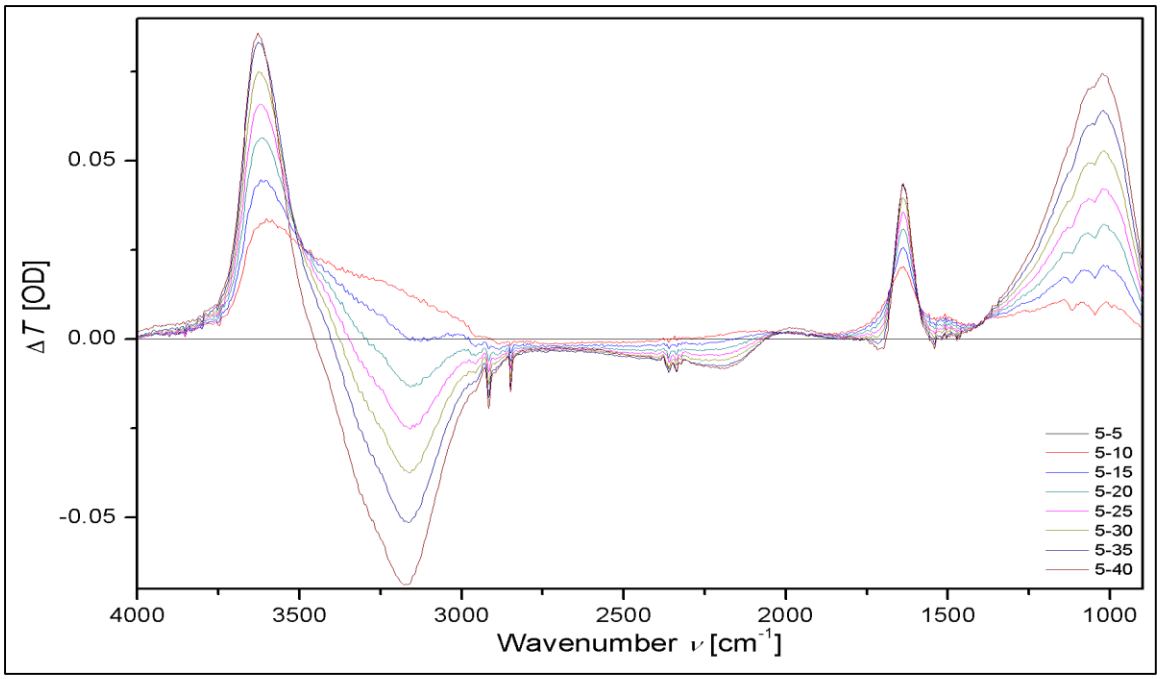

Figure 4-20: Transmittance difference Δ*T* of water between 5° C and other following measured spectra at temperature 10 to 40° C. Here Δ*T* is plotted against wavenumber *ν* [cm^{-1}] between 4000-900 cm^{-1}.

Both figures 4-19 as 4-20 show to have the same features as seen in figures 4-16, respectively, 4-18. The peaks at 3600 and 3200 cm^{-1} are due to water band narrowing, 1600 cm^{-1} due to the increasing H-O-H bending mode and in between is a decreasing combined peak. The peak at 1100 cm^{-1} is due to the CaF_2 windows (two 2 mm thick windows, see Appendix A.6).

After scaling the transmittance Δ*T* of water to Cph1, the water difference was subtracted from the Cph1 difference data (Figure 4-21).

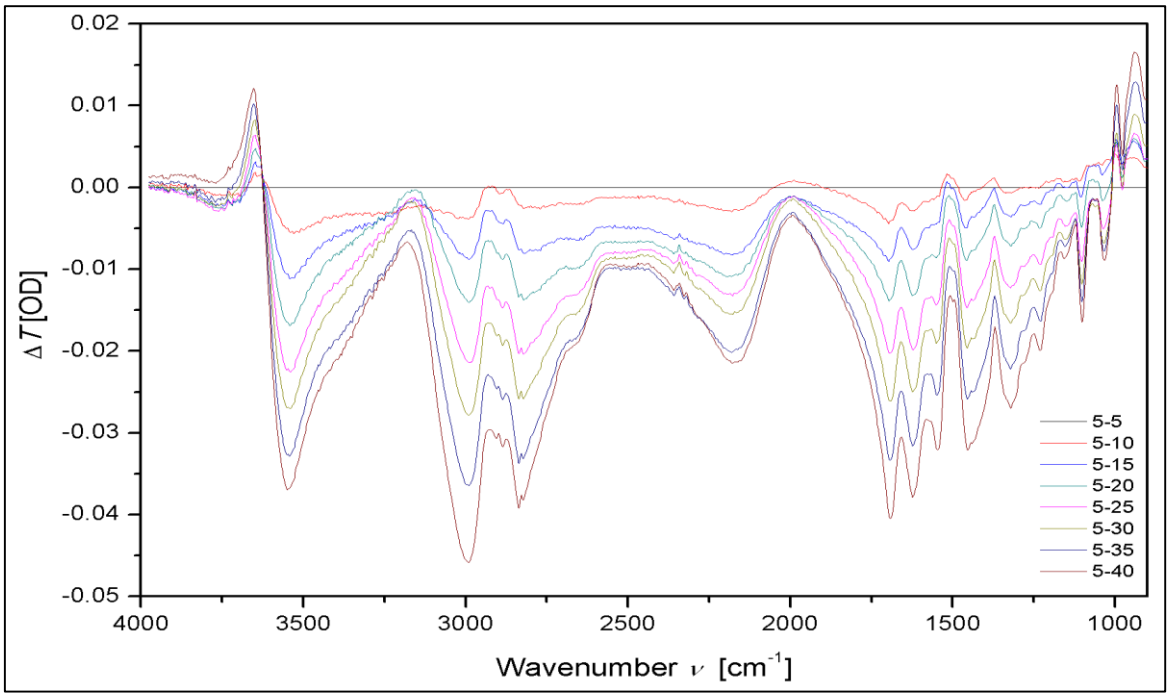

Figure 4-21: Transmittance difference Δ*T* of Cph1-minus-water (scaled in 3585 cm^{-1}) between 5° C and other following measured spectra at temperature 10-40° C. Here Δ*T* is plotted against wavenumber *ν* [cm^{-1}] between 4000-900 cm^{-1}.

Scaling and subtracting did not help, most of the data did not change appreciably or had an un-satisfying effect. Therefore, a new approach is needed.

The water temperature dependence data shows that there is influence of water in the FTIR spectral data. However, a new hypothesis is that the rest of the buffer material gives temperature dependent FTIR spectra as well. To overcome this problem, a new set-up is required.

Figure 4-22 shows a schematic of the used (A) and new proposed (B) set-up for this experiment.

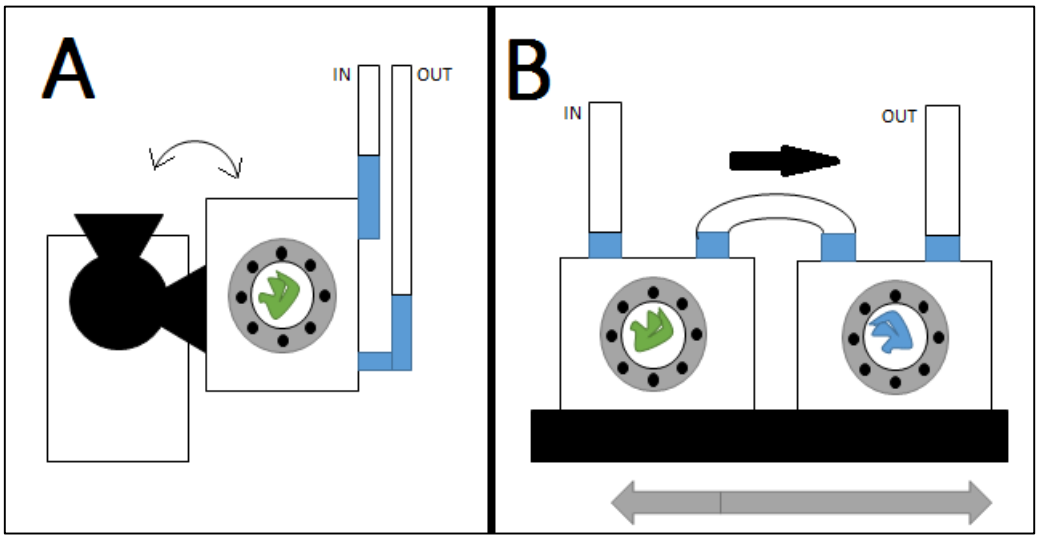

Figure 4-22: Schematic of the used motorized flipper set-up (A) and the new proposed set-up (B) for the temperature dependent measurement. Here the motorized flipper has a circular motion, while in B the motion is sideways. IN and OUT stands for the temperature controlled water flow going through the metal casing of the sample holder. The sample holders are sketched with either the sample (green) or buffer (blue) in the window of the sample holder.

Due to the fact that the sample holder has a wide base it was not possible to put a second one on the motorized flipper. Since it was not expected that the water in the buffer material or the buffer itself had temperature dependent aspects, it was chosen to leave the second sample holder out.

For the new set-up (B) there are two sample holders, connected together by tubes, placed on a movable stage. Since the coolant input and output tubes are connected, both sample holders will have the same temperature during the measurement. One sample holder contains the buffer material and the other the Cph1 protein. By using a Newport mover (LTA-HS) either the Cph1 or buffer is placed in the beam pathway of the spectrometer. Doing so, a background and sample scan is made repeatedly back-to-back.

In addition, the CaF_2 will be switched to BaF_2. Since the BaF_2 windows have less influence on the spectral region of 1100-900 cm^{-1}, see Appendix A.6.

Due to shortage of time and a two-week delivery time on the buffer material and new protein, it was not possible to perform this experiment with the new set-up.

4.4 Putting the FTIR cryokinetic experiment together

Throughout this thesis many experiments and discoveries contributed to build the cryokinetic set-up. In this paragraph is a simple description and summary for carrying out the experiment.

1. Settings of the FTIR spectrometer

Resolution:	4 cm^{-1}	Scanner velocity:	20 kHz
Aperture:	4 mm	Scanning range:	4000-900 kHz
Type of scanning:	repeated scans, 10 scans (of 10 measurements) no wait time.		

2. Set-up

In the final set-up, the Optical Cryostat is top loaded into the FTIR spectrometer (Tensor 27). The NpR6012g4 protein sample is used for this experiment due to its relatively high response on illumination. The sample is held with a sample rod and placed into the inner chamber of the cryostat.

Due to results in paragraph 4.3 the end of the rod will hold a double window system (not made yet). This system will have a plate, which can hold two ½" BaF_2 windows.

The rod is connected to a Newport mover (LTA-HS and ESP300), to move the sample up and down the cryostat. This mover is the replacement of the motorized flipper, because the flipper travels in two dimensions (Z and X). The cryostat does not have room inside the inner chamber to do so, only the Z-axis is available.

At the bottom of the cryostat are two CaF_2 (2") windows (outer windows) and two ZnS (1") windows (inner windows) to allow (IR) light to travel through the sample. An intelligent temperature controller (ITC 601) is connected to the Optical Cryostat to control the temperature in the inner chamber. The temperature controller, mover and Tensor 27 are connected to two PCs. A photo of the set-up is found in figure 4-23.

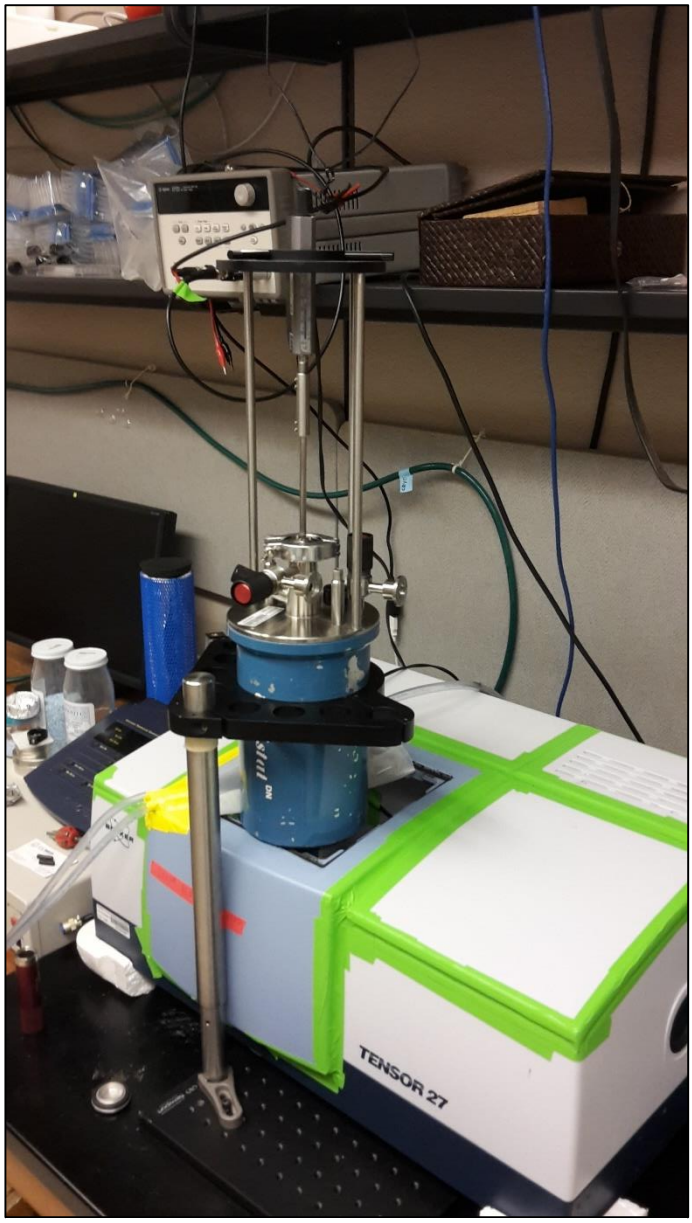

Figure 4-23: Photo of the cryokinetic set-up, where the cryostat dark blue cylinder is top loaded into the FTIR spectrometer (Tensor 27). Above the cryostat are rods connected to hold the Newport mover, which moves the sample rod in and out the scanning beam of the spectrometer.

Figure 4-24 (next page) shows a schematic overview of all components for the cryokinetic measurements.

Here computer 2 has the OPUS program, which controls the FTIR's settings and starts scans. Computer 1 simultaneously controls the Newport mover and computer 2 (using remote desktop connection over the network). This way everything is controlled by a single computer. For this experiment a program was written, with AutoHotkey, to operate the

Termite program which automatically moves the Newport mover and sets the desired temperature. The same program also scans and saves the spectra of the sample within the cryostat. The Autohotkey program was successfully tested in the room temperature and temperature dependent measurements.

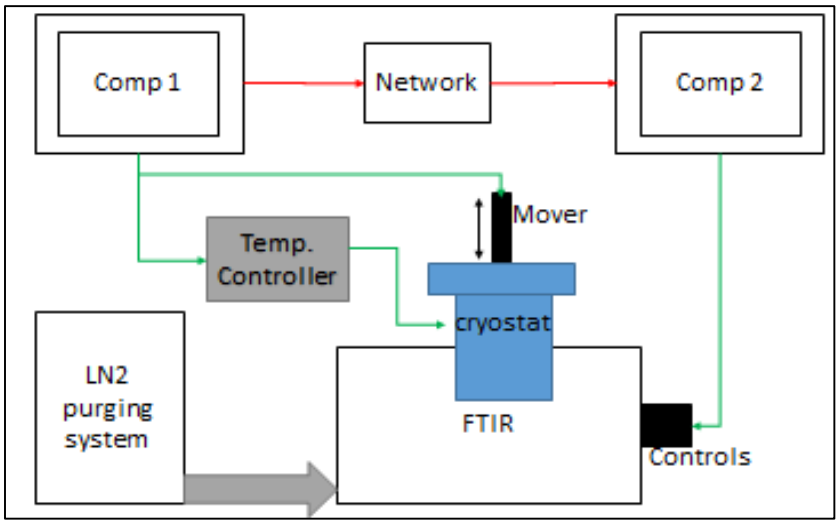

Figure 4-24: Schematic overview of the controlling connection for the cryokinetic measurement. Here computer 1 and 2 (comp) are either connected to the temperature controller and mover or the FTIR controls. Both computers are linked to each other through the network. The LN2 purge system is manually controlled.

The purge system is only controlled prior to the experiments. Once the purge flow is set on 4 $L \cdot min^{-1}$ it should not be changed. Note that a tank of nitrogen gas is connected to the Cryostat to purge the inner chamber before loading the sample rod, while the spectrometer is purged by the LN2 purging system. This is done because only the inner chamber is in contact with the atmosphere when it is open, while the rest is sealed. Once the sample is loaded and the inner chamber is closed, the inner environment does not change any more.

3. FTIR Cryokinetic experiment procedure:

The Forward reaction FTIR cryokinetic measurement

Prior to the experiment, the sample NpR6012g4 is maintained in a dark environment at room temperature (298 K) for 12 hours to ensure full conversion to the dark state of the entire sample. Afterwards, the absorption spectra are measured at different temperatures from 290 to 150 K in 10 K decrements. The sample is then reheated back to 290 K in the same 10 K increments. Absorption spectra are measured, every minute, for each temperature point for one hour, after which the sample was cooled or heated to the next temperature. At 150 K the sample is illuminated for an hour with 650 nm (red) light (forward reaction, §2.1.2) before heating it again.

The Reverse reaction FTIR cryokinetic measurement

After another 12-hour purge in the dark, a similar measurement is performed. Except now, prior to the measurement the sample is illuminated with 650 nm (red) light and at 150 K with 532 (green) light.

During the cooling or heating periods, to achieve a desired temperature, the sample chamber of the cryostat typically needs 15 to 20 minutes to reach consistency in temperature after the monitor claimed the desired temperature. Additional data on both described measurements are found in Appendix B.7. All difference spectra will be obtained according to:

$$\Delta A(\lambda, t, T) = A(\lambda, t, T) - A_{ref}(\lambda, t_0, T) \qquad (\S2.3.1, \text{formula } 14\ [8])$$

Prior to the cryokinetic experiment a lot of issues occurred. The purging system consumed most of the time for ordering the parts and building the system by hand from scratch. Ordering protein sample, which were made elsewhere on UC Davis, also consumed time to be prepared.

However, when it was time to do the experiment, the cryostat broke down. To use the cryostat, the windows of the inner and outer chamber needed to be replaced. At first the cryostat only contained quartz windows, which would absorb IR illumination. Thus, the windows were replaced by CaF_2, but during test with the cryo temperatures the windows cracked. When contacting the company Oxford instruments it turned that these windows were not supposed to be used for cryostatic experiments due its large thermal expansion coefficient ($18.85 \cdot 10^{-6}$/°C) [48].

So, the windows of the inner chamber were replaced again, with ZnS windows. ZnS was recommended by the Oxford instruments company to use in IR experiments, since ZnS windows have a thermal expansion coefficient of ($6.6 \cdot 10^{-6}$/°C) [48].

Although this should work now a new problem occurred. The seal surrounding the windows never properly closed for unknown reasons. After many attempts to re-seal it and testing it with a Helium sniffer, the vacuum between the chambers could not be maintained, therefore having no insulation.

The cryostat had to be taken back to the shop for inspection and reparations. Due to this and a shortage of time the cryokinetic experiments above never got to be performed for this thesis.

5. Conclusion, Discussion and Future works

5.1 Recap, conclusion and discussion

The research work done in this thesis was to build the Larsen Lab's first FTIR cryokinetics set-up. In the past, Larsen Lab conducted multiple cryokinetic experiments with a UV-VIS spectrometer to obtain visible spectra on different proteins and needed to extend this for IR spectra. FTIR spectroscopy techniques were chosen, since measurements of samples could be relatively quickly performed.

To work towards the FTIR cryokinetic set-up, the work was performed in three stages: preparation of the FTIR spectrometer, conducting static room temperature measurements, followed by temperature dependent measurements. Doing so the basics of the cryokinetic measurement (static spectra and varying temperatures) were covered to take static measurements within three minutes while the temperature in the used cryostat changes during the experiment.

During the preparation of the FTIR spectrometer, it was discovered that the MCT detector needed to be refilled with liquid nitrogen (50.8 mL) every (7.3±0.2) hours. To prevent the detector from running out of liquid nitrogen is was chosen to refilled it every 6 hours.

When performing measurements, the detector warms up, leading to a drift difference D of $(2.4\pm0.3)\cdot10^{-4}$ [-] per minute. By taking background scans and sample scans repeatedly back-to-back the drift will not occur. This was accomplished by using a motorized flipper inside the sample chambers (moving sample in/out the detector's beam pathway) for the following experiments.

In addition, the detector is set on a scanner velocity of 20 kHz to take scans (0.53 ± 0.01) s per scan, while the spectrometer is set on an aperture of 4 mm with 4 cm^{-1} resolution.

To purge the spectrometer a LN2 purging system was built by the author. After sealing the FTIR, the LN2 purge system is set on 1 and 4 $L\cdot min^{-1}$ purge flow for an overnight purge and, respectively, during the experiment.

After the preparations, the spectrometer was set for room temperature measurements. Here, the dark ground state and light absorbing photostate of the yellow/far-red Anacy 4718g3 and red/green NpF2854g3 were measured. The absorbance difference ΔA revealed that the two CBCRs are distinctively different from each other, but share a resemblance.

Signs were found in the region of 1625-1550 cm^{-1} that both NpF2854g3 and Anacy 4718g3 undergo secondary structural changes during photo-conversion. NpF2854g3 showed to have gained β-sheet structure in the P_g and lost β-sheet in the P_r state.

Anacy 4718g3 showed almost the same results as NpF2854g3 for this region with β-sheet structure gains in the light state and decreases in the dark state. Anacy also shows to lost NH band (1589±1) cm^{-1} (-) in the C and D ring.

When comparing both Anacy 4718g3 and NpF2854g3 with known Cph1 data, it was discovered that cyanobacterial phytochrome have an almost non existing change in the (1715±2) / (1713±1) cm^{-1} and (1736±1) / (1732±1) cm^{-1} bands. These were linked to C_1=O and C_{19}=O atomic band of the chromophore's A and, respectively, D ring.

Together with other available CBCR data of NpR6012g4 and NpR5113g2 and bacteriophytochrome BphPs, it is suggested that during photo-conversion (dark to light) CBCRs tend to loosen more in the C_1=O band and tighten more in C_{19}=O band than cyanobacterial phytochromes.

During the temperature dependent measurements, it was discovered that the water inside the protein sample also had temperature dependence. This caused to 'drag' the Cph1's protein peaks in FTIR spectrum down, which was not expected. To eliminate this problem, the set-up needed to be changed to clamp two sample holders. One sample holder contains only buffer material for backgrounds scans, while the other holds the Cph1 sample. Due to time shortage this experiment could not be executed in this thesis.

During the research, it was concluded that a liquid nitrogen purging system is needed for an FTIR cryokinetic experiment. This experiment also needs a moving rod to move either protein sample or buffer material in and out of the detector's beam pathway. By doing so a temperature dependent background scan is taken repeatedly to eliminate the detector's drift and airborne particles. Along with the settings found in during the preparations and an automated system, provided by an AutoHotkey program, 10 scans are made every minute to keep track of the kinetic traces of the protein during cryo-cooling.

5.2 Future works

It is recommended to build more mechanical parts for the FTIR spectrometer. For instance, a new top lid where the purging tube is pulled through a sealed hole. This way, possible errors in sealing the FTIR spectrometer for purging are reduced. Another suggestion is to extend this top lid by inserting another wider tube from the top down the spectrometer. The samples are then loaded into this tube and the rest of the spectrometer is always sealed. This will shorten the wait time of purging the sample chamber.

Additional measurements with the room temperature experiment need to be performed. The proteins need to be measured with isotopic differences, to check if there still is a distinct difference between CBCRs and bacterial phytochromes.

For the temperature dependent measurements, the set-up needs to be changed to move two sample holders of the same temperature. One sample holder contains the protein sample, while the other one only has the buffer material. By moving back and forth between these two, a better background scan is made and the temperature dependence of the protein itself will be measured instead of the protein and buffer material.

For the FTIR cryokinetic measurements, a double window system, of ½"windows, at the end of the measuring rod needs to be made. After this and the return of the cryostat from the shop, measurement can be performed.

To complement the FTIR cryokinetic measurements, it would be an idea to extend the IR spectroscopic measurements to a Raman cryokinetic set-up. This will have multiple benefits: comparing with FTIR data, elimination of large water bands in the spectra and less problems with putting windows in the cryostat, since quartz could be used in these experiments.

6. References

1. SISGR: cyanobacterial photoreceptor systems for regulation and optimization of energy harvesting, *J. Clark Lagarias, James B. Ames and Delmar S. Larsen, University of California, Davis*, 2015.
2. E. Schafer & C. Bowler, '*Phytochrome-mediated photoperception and signal transduction in higher plants*', Universitat Freiburg, (10/01/02).
3. Raven, '*Biology*', Eighth Edition, unknown binding, (09/08).
4. www.bio.miami.edu/dana (02/17/16).
5. F.J.V. Escobar, '*Vibrational spectroscopy of phytochromes and phytochrome-related photoreceptors*', Dissertation paper, TU Berlin, (3/18/15)
6. Larsenlab archive on Cyanobacteriochromes and Phytochromes (2/17/16)
7. *'Femtosecond Photodynamics of the Red/Green Cyanobacteriochrome NpR6012g4 from Nostoc punctiforme: 1. Forward Dynamics*', Peter W. Kim, L.H. Freer, N.C. Rockwell, S.S. Martin, J. C. Lagarias, and D. S. Larsen, *Biochemistry*, 51, 608−618 (2012).
8. *'Secondary Transient and Cryokinetics of the Forward Reaction Dynamics of the Red/Green Cyanobacteriochrome NpR6012g4 from Nostoc punctiforme'*, Che-Wei Chang, D. Madsen, S.M. Gottlieb, S. S. Martin, N.C. Rockwell, J. C. Lagarias, and D.S. Larsen, Biochemistry, 2015
9. De Loos-Vollebregt, '*Spectrometrische Analysetechnieken'*, Syntax Media, Arnhem, 2009.
10. F.L. Pedrotti, '*Introduciton to optics*', second edition, Prentice-Hall International inc., USA NJ,1993
11. https://commons.wikimedia.org/wiki/File:Morse-potential.png (04/11/16).
12. http://www.kurabo.co.jp/el/world/en/room/infrare/page1_2.html (04/11/16)
13. NIST Chemistry webbook (04/06/16).
14. Chemwiki, (non)linear molecules (04/08/16).
15. "*Introduction to Fourier Transform Infrared Spectroscopy*", Thermo Nicolet co, 2001.
16. N. Birkner & Q. Wang, "*How an FTIR spectrometer operates*", Chemwiki, UC Davis, (03/31/2015).
17. http://felix.physics.sunysb.edu/~allen/252/PHY251_Michelson.html (2/16/2016).
18. B.C. Smith, '*fundamentals of Fourier Transform Infrared Spectrometry*', Wiley, New York, 1996.
19. van Stokkum, L.H.M., Larsen, D.S., and van Grondelle, R. (2004) Global and target analysis of time-resolved spectra, biochimica et biophysica acta-bioenergetics 1657, 82-104.
20. Holzwarth, A.R., '*Data analysis of Time-Resolved Measurements, Inn biophysical techniques in photosynthesis*' (Amesz, J., and Hoff, A.J., Eds.), pp 75-92, Springer, Netherlands, (1996).
21. P.W. Kim, Photoactivities of Phytochrome-related Photoreceptor Proteins Dissertation, UC Davis, 2012.
22. C.W.Chang, Photoactivities of Phytochrome-related Photoreceptor Proteins Dissertation, UC Davis, 2015.
23. J.F. Nagle, '*Solving complex photocycle kinetics'*, Biophys. J. 59 ('91) 476–487.
24. R.H. Lozier, A. Xie, J. Hofrichter, G.M. Clore, '*Reversible steps in the bacteriorhodopsin photocycle*', Proc. Nat. Acad. Sci. U. S. A. 89 (1992) 3610 – 3614.
25. W.H. Wisman, H.C. Meijer, '*Inleiding Thermodynamica*', 5e druk, P. van der Meeren, 2012.
26. bilbo.chm.uri.edu/CHM112/lectures/lecture31.htm (04/20/16)
27. Tensor User Manual I 22200, 6th updated edition, Bruker Optics, Ettelingen, DE, (4/11)
28. Larsen Lab archive on Cryostatic measurements and equipment.
29. Cryogenic cooling of (N_2/CO_2), installation guide of G1565A, Agilent Technologies, USA DE, 2010.
30. '*Formuleblad Onnauwkeurigheidsanalyse*', TN Blackboard, The Hague University, Delft, 2015.
31. P.F.H.M. van den Eijnde, '*Meettechniek en meetsystemen: fysische meettechniek voor HTO*', 3th edition, HB *uitgevers*, Baarn, 2005.
32. Foerstendorf, H.; Benda, C.; Gartner, W.; Storf, M.; Scheer, H.; Siebert, F. *Biochem.* 2001, *40*, 14952.
33. Stojkovic E.A., '*FTIR Spectroscopy Revealing Light-Dependent Refolding of the Conserved Tongue Region of Bacteriophytochrome'*, VU University, Amsterdam, The Netherlands, 2014.
34. van Thor, J. J., '*Assignments of the Pfr−Pr FTIR Difference Spectrum of Cyanobacterial Phytochrome Cph1 Using 15N and 13C Isotopically Labeled Phycocyanobilin Chromophore*', J. Phys. Chem. B 2005, 109, 20597−20604.
35. Gallagher W., '*FTIR Analysis of Protein Structure'*, Chemistry department, University of Wisconsin-Eau Claire, WI, US, 2008.
36. F.J.V. Escobar, '*Photoconversion Mechanism of the Second GAF Domain of Cyanobacteriochrome AnPixJ and the Cofactor Structure of Its Green-Absorbing State*', TU Berlin, (06/28/13)
37. Fukushima Y., '*Photoconversion Mechanism of a Green/Red Photosensory Cyanobacteriochrome AnPixJ: Time-Resolved Optical Spectroscopyand FTIR Analysis of the AnPixJ-GAF2 Domain*', Nagoya University, Japan, 2011
38. Heberle J., '*Fourier-transform infrared spectroscopy applied to proteins*', mol. biophysics, FU Berlin, 2014

39. Siebert, F.; Grimm, R.; Rudiger, W.; Schmidt, G.; Scheer, H. *Eur. J. Biochem.* 1990, *194*, 921.
40. Foerstendorf, H.; Mummert, E.; Schafer, E.; Scheer, H.; Siebert,F. *Biochemistry* 1996, *35*, 10793
41. A. Jabs, '*Determination of Secondary Structure in Proteins by Fourier Transform Infrared Spectroscopy (FTIR)*', Jena Library of biological macromolecules. (05/26/16)
42. Narikawa R.; et al., '*Structures of cyanobacteriochromes from phototaxis regulators AnPixJ and TePixJ reveal general and specific photoconversion mechanism*', 918–923, doi: 10.1073/pnas.1212098110, 11-19-2012
43. Takala, H.; et al., '*Signal amplification and transduction in phytochrome photosensors*' Nature 2014, 509, 245−248
44. Lim S.; et al., '*Photoconversion changes bilin chromophore conjugation and protein secondary structure in the violet/orange cyanobacteriochrome NpF2163g3*', Photochem. Photobiol. Sci., 2014, 13, 951–962
45. Archive Larsen Lab on CBCRs and other photosensitive proteins (05/16/16).
46. Cornilescu C.C. '*Dynamic Structural Changes Underpin Photoconversion of a Blue/Green Cyanobacteriochrome between Its Dark and Photoactivated States*', J Biol Chem. 2014 Jan 31; 289(5): 3055–3065.
47. Maréchal, Y. '*Infrared spectra of water*', J. Mol. Struct. 1994, 322, 105
48. Crystan ltd., Broom Road Business Park, Poole BH12 4PA, UK.
49. http://classroom.sdmesa.edu/eschmid/Lecture21-Microbio.htm (03/14/16).
50. *'Red/green cyanobacteriochromes: sensors of color & power*', *Rockwell NC, Martin SS, Lagarias JC.*
51. PIKE technologies, '*Choice of window materials for transmission sampling of liquids in the Mid-IR Spectral Region*', Application Note-0602.
52. E.F. von Rei*s, 'Synthesis and characterization of poly (vinyl alcohol) hydrogels and hybrids for rMPB70 protein adsorption',* departamento de medicina veterinaria preventiva, Brasil, (06-2006).
53. Hangzhou Shalom Electro-optics Technology Co., Ltd.
54. Thermo fisher scientific, *'High-Sensitivity Detectors in the Mid-IR spectroscopy*', application note-50730.

Appendix A: Additional information

A.1: Properties of the proteins: NpF2854g3, Anacy 4718g3 and Cph1

Name: *NpF2854g3* [50]
Class: *Cyanobacteriochrome*
Family: *Red/Green*
Origin: *Nostoc punctiforme*
Chromophore: *PCB*

As shown in figure A-1, NpF2854g3 is a red/green CBCR and photo-converted by 550 and 653 nm light. NpF2854g3 is used in the room temperature experiment explained in paragraphs 3.3.2 and 4.2.

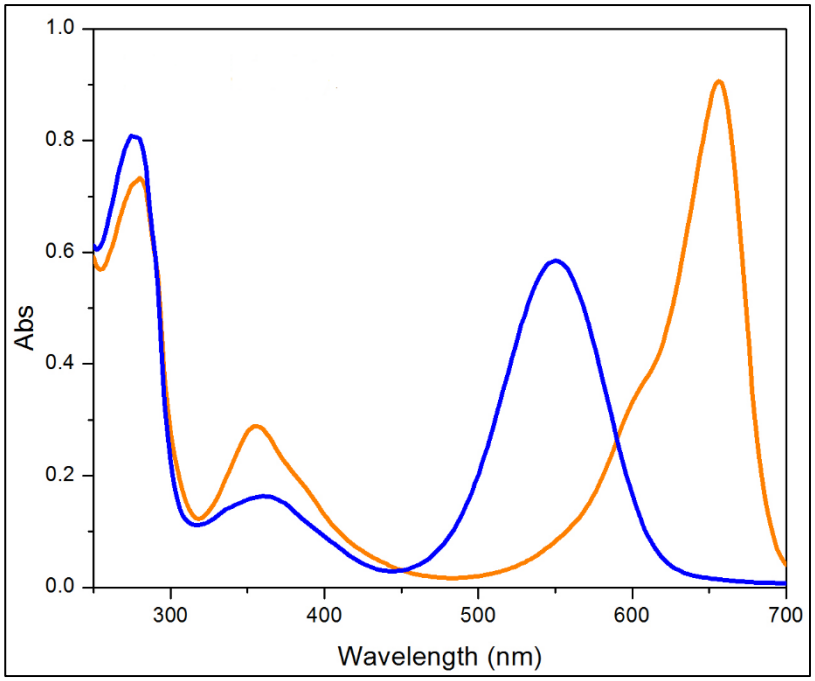

Figure A-1: Absorption spectra of NpF2854g3 are shown in the 15Z (orange) and 15E (blue) photostates. Peak wavelengths at 550 nm and 653 nm. [45]

Name: *Anacy 4718g3* [50]
Class: *Cyanobacteriochrome*
Family: *Far-red/ Yellow*
Origin: *Anabaena cylindrica PCC 7122*
Chromophore: *PCB*

Anabaena is a genus of filamentous cyanobacteria that exists as plankton. Just like *N. punctiforme* (§2.1.2), it has nitrogen fixing abilities, and forms symbiotic relationships with certain plants, such as the mosquito fern.

Anacy is a far-red/yellow (730/590 nm) switchable protein and it is advised to illuminate it for a long time (3x longer than NpF2854g3) due to its relatively small response.

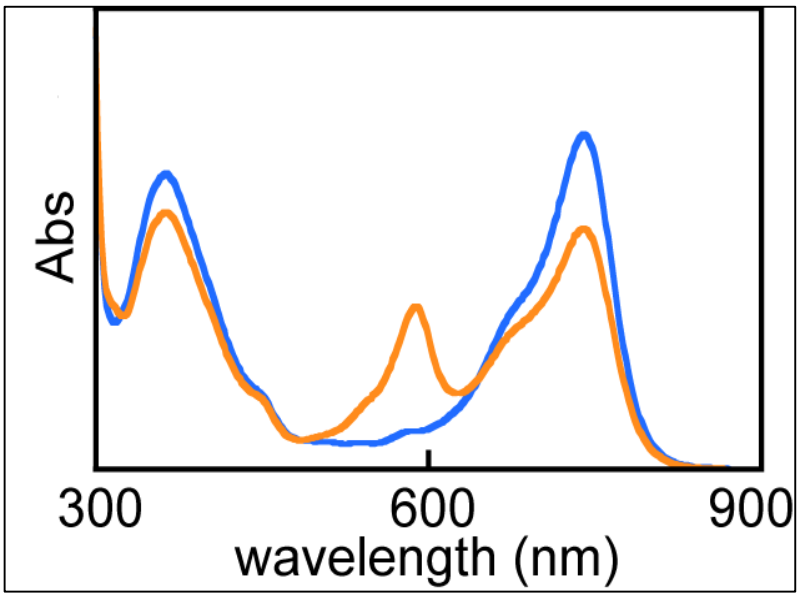

Figure A-2: Absorption spectra of Anacy 4718g3 are shown in the 15Z (blue) and 15E (orange) photostates. Peak wavelengths at 760 nm and 590 nm. [45]

Name: *Cph1* [45]
Class: *Cyanobacterio-phytochrome*
Family: *Red/Far-red*
Origin: *Synechocystis*
Chromophore: *PCB*

Red illumination of the dark adapted 15Z P_r state of Cph1 (Fig. A-3, red) initiates forward photo-conversion (P_r -P_{fr}), generating the primary isomerized Lumi-R_f intermediate. Lumi-R_f thermally evolves via several intermediates to generate the 15E P_{fr} photoproduct (dark red, fig. A-3). The dark-stable P_r state could be regenerated from 15E P_{fr} either rapidly by far-red light or via spontaneous dark reversion on a very slow (>24 h) timescale.

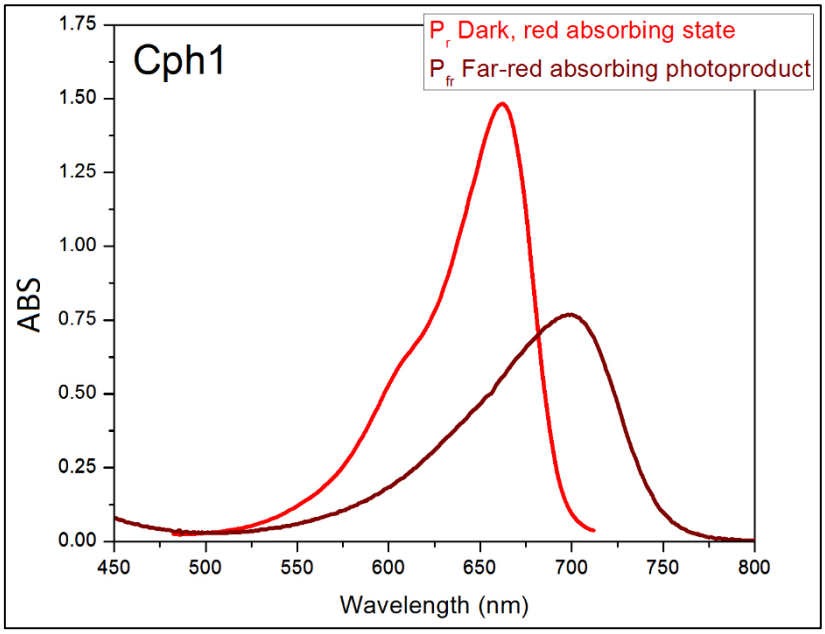

Figure A-3: Absorption spectra of Cph1 are shown in the 15Z (red) and 15E (dark red) photostates. Peak wavelengths at 650 nm and 710 nm. [45]

A.2: Information on Carbon and Nitrogen fixation

This section shows a figure that provide a better understanding of Carbon and Nitrogen fixation as stated in paragraph 2.1.1.

As seen in figure A-4, the bacteria form nitrogen for the plants growth. During this process the bacteria also produce hydrogen (H_2), which could be used as energy product.

The figure also shows how the plant uses carbon dioxide to produce Glucose, photosynthesis, to convert inorganic carbon (CO_2) into organic compounds (Glucose). Although the figure shows this process inside the plant the same process appears in some bacteria as well.

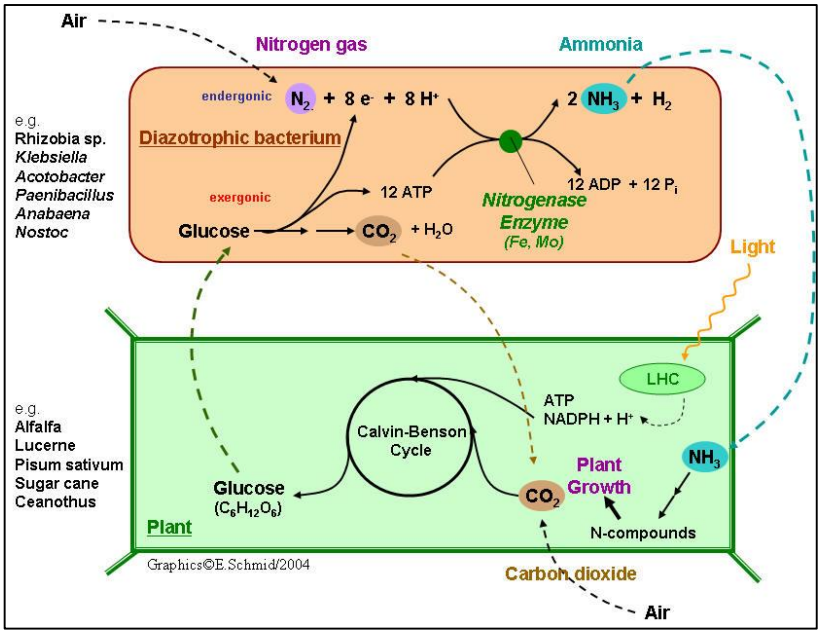

Figure A-4: Schematic of Nitrogen cycle within a symbiosis of plants and bacteria, in this example Diazotorphic bacterium, in soil. Bacteria take nitrogen from the air/soil to make components for the plants growth. This process also produces hydrogen (H_2). The figure also shows the plants photosynthesis by using carbon dioxide, light and water to produce Glucose. [49]

A.3: Derivation of vibrational frequency

In molecules, atoms always move relatively from or towards each other. During these vibrations, potential energy is constantly converted into kinetic energy and vice versa. The potential energy E_P of a molecule A-B as function of distance R between atoms A and B has a minimum at an equilibrium distance R_e, see also figure 2-6 in paragraph 2.2.1, and is calculated with formula A.3.1 [9]:

$$E_P = \frac{1}{2} k_{AB}(R - R_e)^2 - C\text{on} \qquad \text{(A.3.1).}$$

The constant *Con* is equal to the dissociation energy of the atomic bond. The back driving force at a certain distance from the equilibrium distance R_e is proportional to the deflection (Hooke's law). k_{AB} is a force constant, determined by the strength of the atomic bond, and the factor ½ is used because $dE_P/dR = k_{AB}$. The vibrations that can be described with a quadratic potential energy function are harmonic oscillator, like [10]:

$$x = U_m \sin(2\pi\nu t). \qquad \text{(A.3.2).}$$

Wherein x is the deflection from the equilibrium at time t, U_m the maximum deflection. During the vibration the center of gravity remains in place.

Since, Newton's law tells:

$$F = m\frac{d^2x}{dt^2} \qquad \text{(A.3.3)}$$

And, Hooke's law tells:

$$F = -k_{AB}x \qquad \text{(A.3.4).}$$

With F, the force [N], m the mass [kg] and time t [s]. Combining the two formulas gives:

$$m\frac{d^2x}{dt^2} = -k_{AB}x$$
$$\frac{d^2x}{dt^2} = \frac{-k_{AB}x}{m}$$

Substituting formula A.3.2 gives:

$$\frac{d^2U_m \sin(2\pi\nu t)}{dt^2} = \frac{-k_{AB}U_m \sin(2\pi\nu t)}{m}$$
$$-U_m\, 4\pi^2\nu^2 \sin(2\pi\nu t) = \frac{-k_{AB}U_m \sin(2\pi\nu t)}{m}$$
$$4\pi^2\nu^2 = \frac{k_{AB}}{m}$$
$$\nu^2 = \frac{k_{AB}}{4\pi^2 m}$$

$$\nu = \sqrt{\frac{k_{AB}}{4\pi^2 m}} = \frac{1}{2\pi}\sqrt{\frac{k_{AB}}{m}}$$

So, the frequency ν is calculated by:

$$\nu = \frac{1}{2\pi}\sqrt{\frac{k_{AB}}{\mu_{AB}}}, \qquad \text{with: } \frac{1}{\mu_{AB}} = \frac{1}{m_A} + \frac{1}{m_B} \qquad \text{(2).}$$

μ_{AB} is the reduced mass of system AB, masses m_A and m_B.

A.4: Characteristic vibrations

Molecular vibrational motions [9,14] are divided into two groups: stretching and bending.
In stretching motions the molecules vibrate in a horizontal motion, while in bending the molecules vibrate by making angular motion. These two groups can be divided into other motions, like: (a)symmetric stretching, twisting, rocking, wagging and scissoring. These motions are shown below in figure A-5 using H_2O as example:

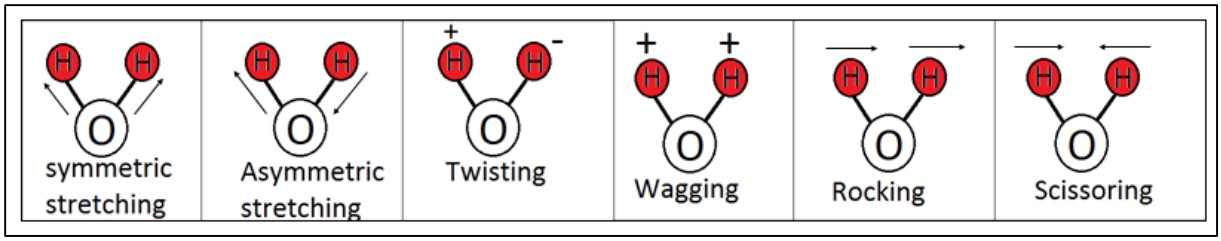

Figure A-5: Basic known molecular vibrational motions. Starting from left to right: symmetric and a symmetric, bending motions: twisting (opposite direction in/out paper), wagging (same direction in/out paper), rocking (moving towards same direction in x-axes) and scissoring (opposite direction in x-axes)

Most 'basic' stretching and bending motion are collected in the past decades. Most of these collections contain stretching and bending modes of different combination of basic elements, such as carbon, oxygen and hydrogen. Table A-1 shows a small collection of these basic combinations and vibrational motions corresponding to wavenumbers.

Table A-1: Basic known bonds, name for type of compound and according wavenumbers. [9]

Bond		type of compound	wavenumber
–C–H	(stretch)	alkanes	2800–3000
=C–H	(stretch)	alkenes, aromatics	3000–3100
≡C–H	(stretch)	alkynes	3300
–O–H	(stretch)	alcohols, phenols	3600–3650 (free) 3200–3500 (H-bonded) (broad)
–O–H	(stretch)	carboxylic acids	2500–3300
–N–H	(stretch)	amines	3300–3500 (doublet for NH_2)
–C(=O)–H	(stretch)	aldehydes	2720 and 2820
–C=C–	(stretch)	alkenes	1600–1680
–C=C–	(stretch)	aromatics	1500–1600
–C≡C–H	(stretch)	alkynes	2100–2270
–C(=O)–	(stretch)	aldehyde, ketones, carboxylic acids	1680–1740
–C≡N	(stretch)	nitriles	2220–2260
C–N	(stretch)	amines	1180–1360
–C–H	(bending)	alkanes	1375 (methyl)
–C–H	(bending)	alkanes	1460 (methyl and methylene)
–C–H	(bending)	alkanes	1370 and 1385 (isopropyl split)

Figure A-6 below, shows a FTIR example spectrum of pure MPB70 recombinant protein [52]. This protein does not take part in the research done in this thesis. However, the figure shows in which regions Amide bands might be found (1600-1300 cm^{-1}). Amides are organic functional groups consisting carbon, (double bonded) oxygen, nitrogen which is connected to either hydrogen or other functional groups as alkynes, for example. This organic group is often found in protein, meaning that this is the region of interest for the research. This and information in table A-1 (C=C, C-N/H), makes the region 2000-900 cm^{-1} an interesting region to investigate.

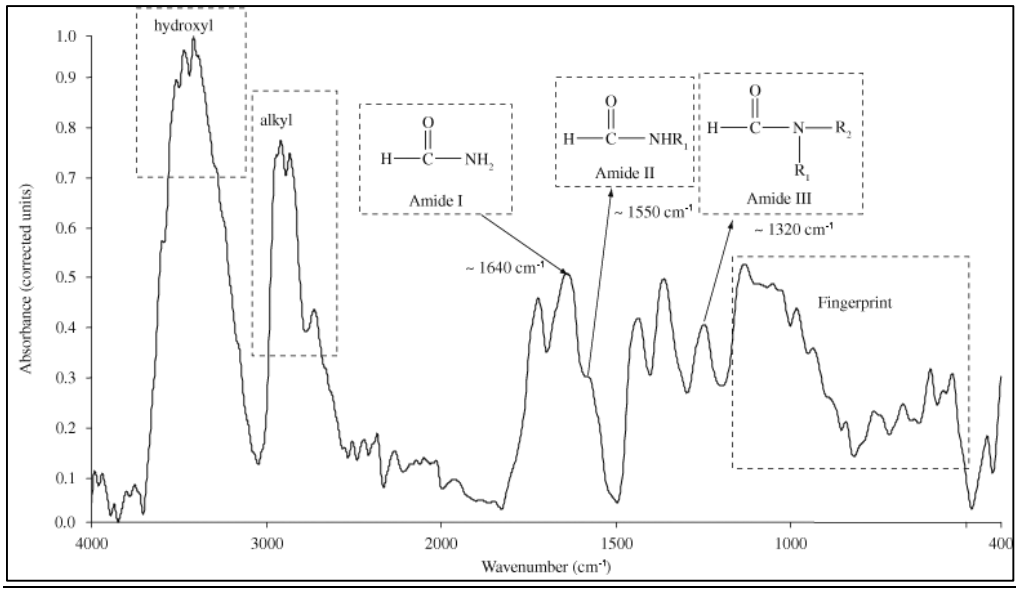

Figure A-6: FTIR spectrum of pure MPB70 recombinant protein, produced and characterized. Serving as example. [52]

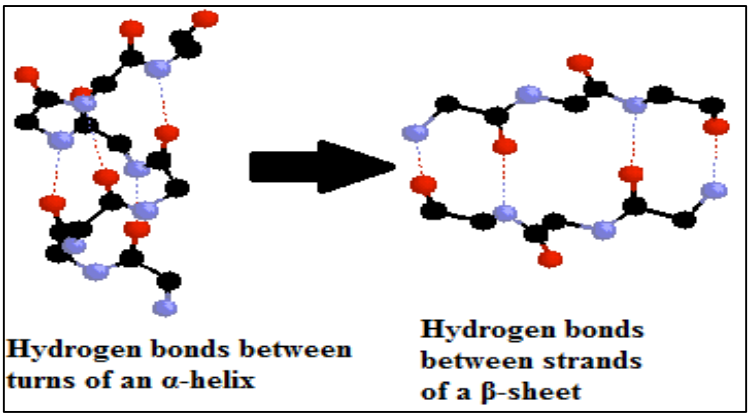

Figure A-7: Structural change of an α-helix to β-sheet. [35]

Figure A-7 above shows the structural change of an α-helix into a β-sheet [35]. Both structures are build out of amino acids, which is consist of Amide and acid groups. The difference between the two structures is defined by type of hydrogen bonding within/between the molecule. When molecules form hydrogen bond between parallel molecules, it forms a β-sheet. The α-helix is formed hydrogen bonds between the oxygen of C=O on the top of the helix and the hydrogen of N-H on the bottom of the helix.

A.5: Derivation of Beer's law

Beer's law [9] describes the degree of attenuation due to light absorbance when passing through a cuvette filled with a sample solution, which is described below.

$$-\frac{dI_x}{dx} = kCI_x \qquad \text{(A.5.1).}$$

Wherein dI_x is the lessening of the intensity I_x [W], measured in position x over distance dx. C is the concentration [mol·L^{-1}] of the absorbing monster and k is a constant [L·mol^{-1}·cm^{-1}]. Integrating the formula above gives:

$$\int_{I_0}^{I_t} \frac{dI_x}{I_x} = -kC \int_0^b dx \qquad \text{(A.5.2)}$$

Wherein I_t stance for the transmitted intensity, I_0 initial intensity and b [m] of the path length inside the cuvette. Solving formula A.5.2, gives:

$$ln\left(\frac{I_0}{I_t}\right) = kcb \qquad \text{(A.5.3).}$$

Transmission T [-] (<1 & >0), is the ratio I_t/ I_0 and represent the amount of transmitted and detected intensity, i.e. the remaining intensity of the initial bundle of light.
The extinction Ex [-] is calculated from transmittance T, whereby ε is the extinction coefficient [L·mol^{-1}·cm^{-1}], with the following formula:

$$E_x = \log_{10}\frac{I_0}{I_t} = -\log_{10} T = \varepsilon cb \qquad \text{(5).}$$

A.6: Properties of IR windows and window choice explanation

Table A-2 gives information on different types of optical IR windows, with quartz (SiO_2 or infrasil) and CaF_2. Since the interest is in the region of 3000-800/900 cm^{-1} quartz and AMTIR do not suffice. Out of the remaining window materials CaF_2 has the lowest refractive index, which is desirable so minimal deflections in the beam pathway would occur when IR beams is not 100% perpendicular on the window.
For 20 mm diameter and 2 mm thick windows CaF_2 is $40 per window, while BaF_2 or ZnS are $53 respectively $45 (for example). This makes CaF_2 the cheapest choice as IR window material. [48,51,53]

Table A-2: Properties of materials for MID-IR spectroscopy [51], with SWL-shortest wavelength for transmission, LWL-longest wavelength for transmission, RI-refractive index [-], Solubility [g/100 mL], Hardness [-], MP-melting point [K] & pH range [-].

Material	Comments	SWL, cm-1	LWL, cm-1	RI	Solu-bility	Hard-ness	MP	pH Range
AMTIR	SeAsGe glass, brittle	1100	593	2.5	0	170	370	1-9
BaF_2	Barium Fluoride	66600	691	1.45	0.17	82	1280	5-8
CaF_2	Calcium Fluoride	79500	896	1.4	0.0017	158	1360	5-8
CsI	Cesium Iodide, very hygro-scopic, somewhat toxic	42000	172	1.73	44	20	621	NA
Ge	Germanium, brittle, becomes opaque at elevated temperature	5500	432	4.0	0	780	936	1-14
Infrasil	Silicon Dioxide (fused silica)	50000	2315	1.53	0	460	1713	1-14
KBr	Potassium Bromide, most widely used for mid-IR applica-tions	48800	345	1.52	53	6	730	NA
KCl	Potassium Chloride	55600	385	1.45	35	7	776	NA
KRS-5	Thallium Bromide / Thallium Iodide, extremely toxic!	17900	204	2.37	0.05	40	414	5-8
NaCl	Sodium Chloride	52600	457	1.49	36	18	801	NA
SiO_2	Silicon Dioxide, strong IR ab-sorbance at 3675 cm-1	50000	3735, 2315	1.53	0	460	1713	1-14
Si	Silicon, strong IR absorbance between 624-590 cm-1	8900	624, 30	3.41	0	1150	1420	1-12
ZnS	Zinc Sulfide	17000	690	2.2	0	240	1830	5-9

The following figures A-8 and A-9 show transmission spectra of Barium Fluoride, respectively, Calcium Fluoride. These are shown to give perspective in the transmission values of the two materials. BaF_2 will transmit more IR radiation than CaF_2, however (as said before) BaF_2 is more expansive.

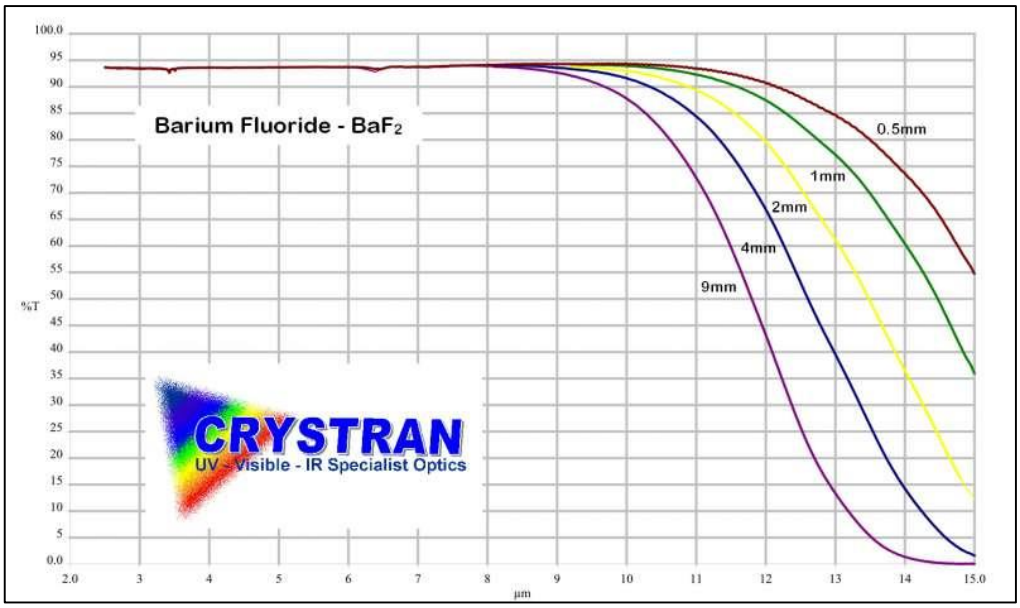

Figure A-8: Transmission graph of Barium Fluoride (BaF_2) for multiple thicknesses. [48]

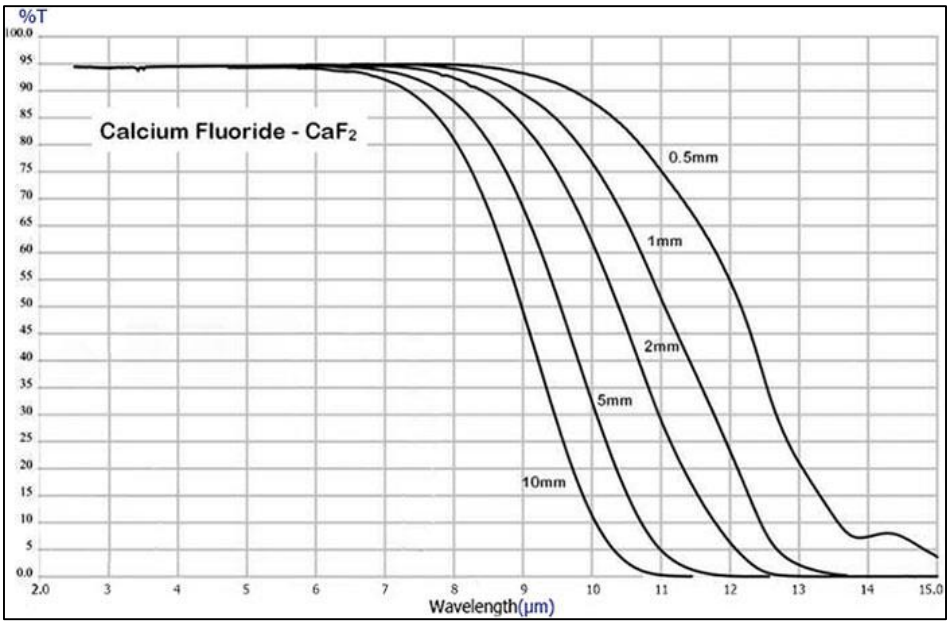

Figure A-9: Transmission graph of Calcium Fluoride (CaF_2) for multiple thicknesses. [53]

A.7: IR spectrum of CO_2 and water vapor

Figures A-10 and A-11 show the IR spectrum of CO_2, respectively, water vapor. It shows that CO_2 is less complex than water vapor. Since CO_2 is a linear molecule it has vibrations that are seen as one vibration. Water vapor is more complex due to its OHO bending. The water molecule has a very small moment of inertia on rotation resulting in a combined vibrational-rotational spectrum in the vapor giving millions of absorption lines. In the liquid form, the rotations tend to be restricted by hydrogen bonds and the spectral lines are broader causing overlap of many of the absorption peaks.

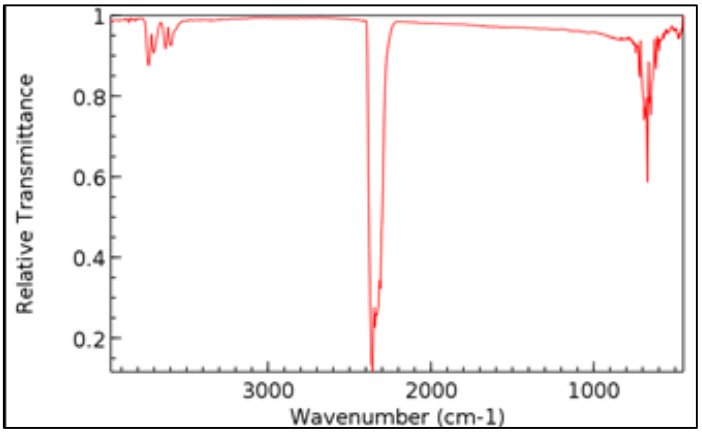

Figure A-10: Schematic of CO_2 IR spectrum, where relative transmittance is plotted against wavenumbers. CO_2 shows two peaks (main characteristics) around 2300 cm^{-1}, smaller peaks at 3800 and 700 cm^{-1}. [13]

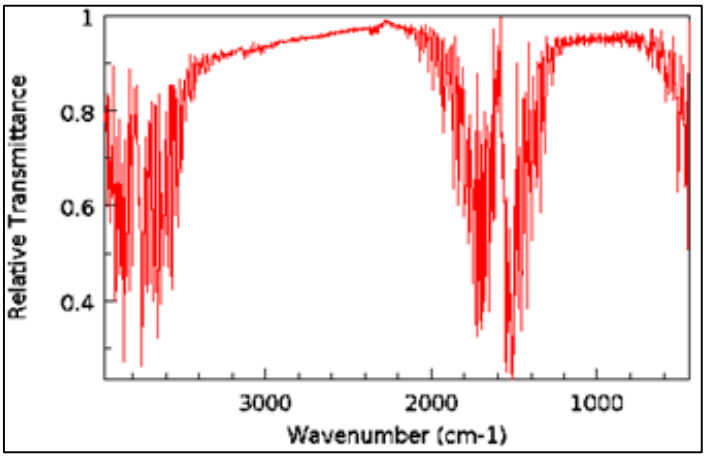

Figure A-11: Schematic of water vapor IR spectrum, where relative transmittance is plotted against wavenumbers. Water vapor shows to have many peaks and noise around 3500 cm^{-1} and 1800-1500 cm^{-1}. The complex spectrum is due to the OHO binding. [13]

Appendix B: Additional set-up information

B.1: General list of used equipment & materials

Measure equipment:

- Sample lens holder and CaF_2 windows (1", 20 mm and ½"):
- FTIR spectrometer (Bruker Optik, Tensor 27)
- Static gas Cryostat (Oxford instruments, OptistatDN-V) + sample rod

Electronics:

- Fisher Scientific 9105 Refrigerating Circulator Chiller
- Intelligent temperature controller (Oxford instruments, ITC 601)
- Agilent E3646A dual output DC Power supply (0-8V,3A/0-20,1.5A) +2 coax cables
- CW laser 3.20V diode (Roithner Laser), set at 650 nm (red)
- CW laser 3.00V diode (Roithner Laser), set at 590 nm (yellow)
- CW laser 2.15V diode (Roithner Laser), set at 532 nm (green)
- Thorlabs TCLDM9 cool mount and Laser, set at 730 nm (far-red)
- Thorlabs TED200c temperature controller
- Thorlabs LDC205c laser diode controller
- Newport mover (LTA-HS) + control box (Newport, ESP 300)
- Thorlabs mff 101 motorized flipper
- PC, installed with: Opus, Matlab, AutoHotkey, Termite, Thorlabs APT, Origin, Lab- & Carpetview

Optical instruments:

- Lab platform (Thorlabs, 23.8x25.5 cm)
- 2x mirrors (Ag) with mirror mount (Newport)
- 4x Clamping Forks (Thorlabs cF125)
- 4x 1" posts (Thorlabs RS4,3) & 4x Pedestal Base (Thorlabs BE1)
- 1x Diffuser (Fused Silica, FS, coating Plano-convex lens)
- Crystal diffuser

Other:

- Liquid and gas nitrogen (with Dewar flask respectively gas tubes)
- flow meter (Dakota instruments, 6A0107BV-NC)
- Protein samples NpF2854g3, Anacy 4718g3 and Cph1

B.2: Extra information on Tensor 27

Figure B-1 shows a picture of the back of the Tensor 27 [27]. Figure B-2 an overview of the internal components and figure B-3 on overview on the beam path inside.

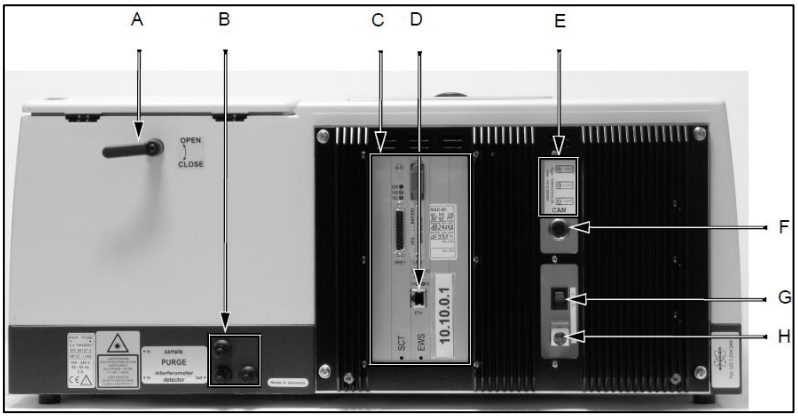

Figure B-1: Photo of the back of Tensor27. A) Handle for (un)locking the interferometer compartment, B) purge gas in/outlet, C) Electronics (connector sockets/LEDs), D) ethernet port, E) Voltage status, F) CAN bus port, G) on/off switch, H) low-voltage socket. [27]

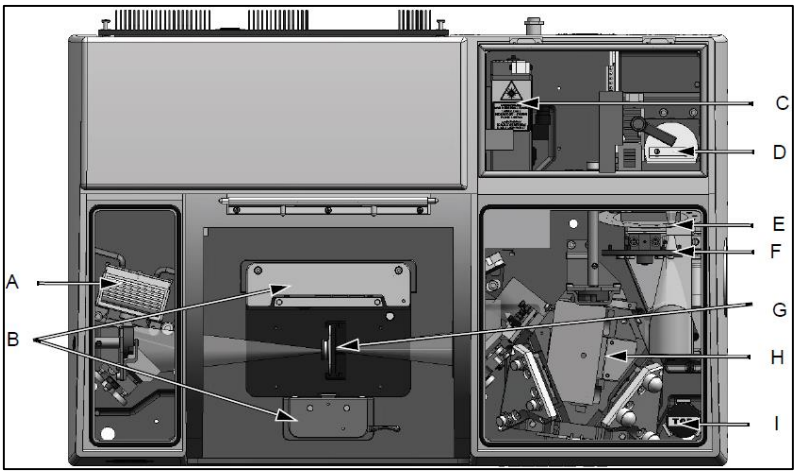

Figure B-2: Internal components Tensor27. A) Detector, B) Quick lock, C) Laser, D) MIR Source, E) Aperture wheel, F) filter wheel, G) sample holder, H) interferometer, I) Desiccant cartridge. [27]

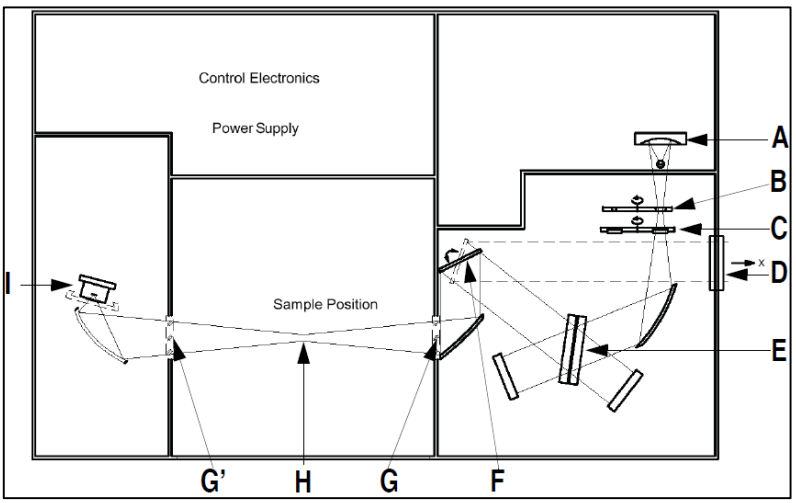

Figure B-3: Beam path in Tensor27. A) IR source, B) Aperture wheel, C) Filter wheel, D) IR beam outlet, E) Beam splitter, F) switch mirror, G &G') sample compartment window, H) Sample, I) Detector. [27]

Humidity indicator
- Red- water vapor concentration too high
- Off- water vapor concentration is OK

Laser indicator
- Yellow-Laser is operating
- Off- Laser power supply is interrupted

Status indicator
- Green- Spectrometer is in proper operating condition
- Red- a spectrometer problem or still initializing phase.

Figure B-4: Spectrometer display on Tensor 27. Respectively Humidity, laser and status indicators. [27]

Figure B-4 shows a close-up of the spectrometer display on top of the Tensor 27. On the right is a short explanation of the display indicators.

B.3: MCT versus DGTS detector

Most experiments done in (mid) IR measurements are performed using a conventional DLaGTS (deuterated L-alanine doped triglysine sulfate) detector [54]. These detectors are known to be used at room temperature, highly sensitive and excellent linearity. However, when one wants to take measurements at high speed it is advisable to use a MCT (mercury cadmium telluride) detector [27]. MCT detectors maintain a constant IR response while scanning at high velocities. Figure B-5 shows the results of rapids scans for a MCT and DLaGTS detector.

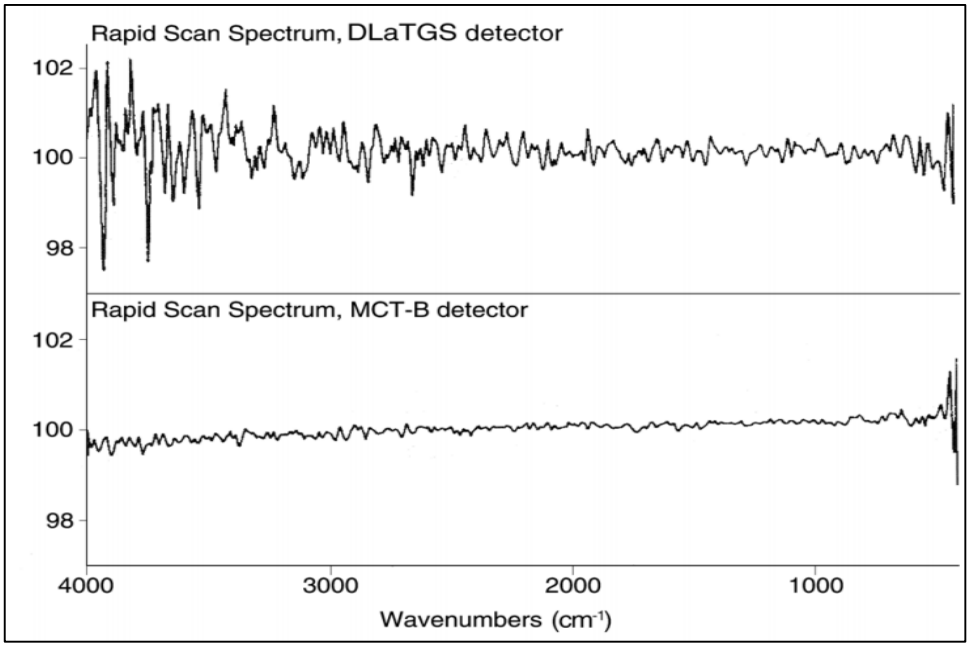

Figure B-5: rapid scan comparison between MCT and DLaGTS detector. Transmission is plotted against wavenumber [54].

It can be seen that the MCT detector has less noise than the DLaGTS when taking scans rapidly after each other. In addition, most MCT detector are about 10 times more sensitive. [54] This is preferred to do Cryokinetic measurements, to follow the kinetic traces when the protein reaches thermal equilibrium after temperature changes. Therefore, it is chosen to use the MCT detector for all experiments done in this thesis, in order to maintain equality between different experiments.

B.4: Cryostat Start-Up Procedure [28]

- The sample holder is at the end of the long insert (rod) that goes into the cryostat. Remove the metal cover that holds sample in place, insert sample and put metal holder back in place.


- Before inserting the sample into the sample chamber purge the chamber with nitrogen gas to displace water and other things that can potentially cause problems. Insert the nitrogen tube into the sample chamber, turn on the nitrogen and purge until all air is displaced. How long depends on flow. Insert the sample insert into the chamber while removing the nitrogen tube. It has to be done immediately so no air exchange happens.



- Place the two clamps to hold in the insert, hand tight.

- Attach the control unit to the cryostat. The correct plug is the one closest to the valve.



- Fill up the Dewar. It doesn't matter which one of the black tubes that is used for filling, just make sure the input has a funnel in it. The Dewar is full when liquid (not just steam) comes out the other hose/funnel. Wear goggles while doing this!


- The cooling of the chamber is controlled by a valve. If the valve is completely closed no cooling occurs. Open up the valve (by turning it counter clock-wise) will allow liquid nitrogen to enter the chamber and cool it down.

- Heating can either be manual or automatic. The set temperature is selected by pressing the button "set point" and while holding it down rotating the dial to the desired temperature.


A computer program is also provided at the lab to automatic change the temperature at set times and degrees Kelvin [K].

B.5: Schematic visualization of set-up connections:

Figure B-6 shows a schematic overview of all components used for the room temperature and Temperature dependent measurement. Here computer 2 has the OPUS program, which controls the FTIR's settings and starts scans.
Computer 1 simultaneously controls the flipper (mff 101) and computer 2 (via the network using remote desktop connection). This way everything is controlled by a single computer.
An Autohotkey program was written on computer 1 to automatically control the flipper and computer 2. By doing so, a loop is created to flip, scan and save the protein of interest.

The purge system is only controlled prior to the experiments manually. Once set the purge flow won't be changed.
The chiller is also manually controlled by setting the temperature of the water that flows through the sample holder.

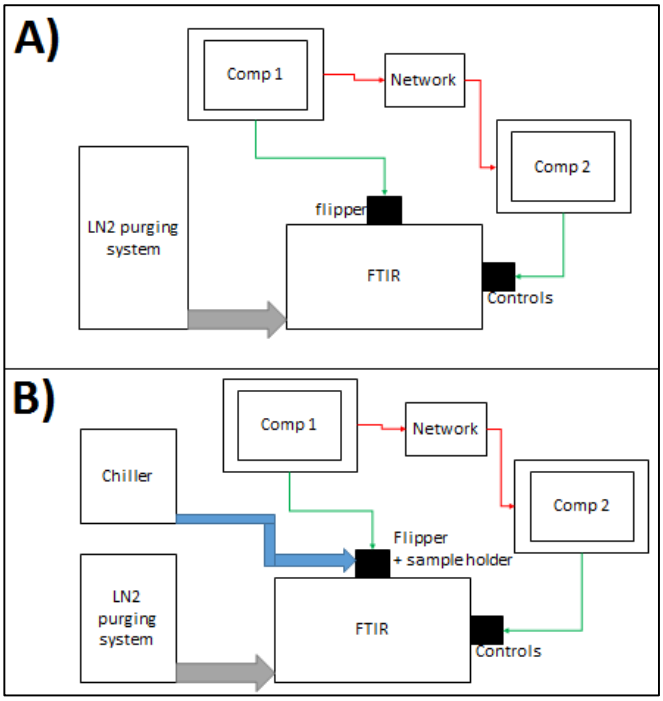

Figure B-6: Schematic overview of the controlling connection for the room temperature (A) and Temperature dependent (B) measurement. Here computer 1 and 2 (comp) are either connected to the flipper or FTIR controls. Both computers are linked to each other through the network. The chiller and LN2 purge system are manually controlled.

B.6: Choice of nitrogen gas as purge gas

As stated in section 3.1 nitrogen gas is used to purge the sample chamber of the FTIR spectrometer and optical cryostat. Nitrogen gas is commonly used in laboratories to control the atmosphere for highly sensitive equipment and procedures. The gas is applied to control oxygen levels, humidity, and temperature in lab equipment.

To observe a molecular vibration in the IR there must be a dipole moment change accompanying the vibration [9]. This is a selection rule for IR spectroscopy. For homonuclear diatomic molecules, A_2, the stretch, ↔A-A↔, is silent in the IR because the molecules have no dipole. For instance, H_2, N_2, O_2, F_2 (etc.), therefore no IR spectrum of nitrogen gas. The other gasses would suffice for purging, however O_2 and H_2 are flammable substances a risk in the lab. F_2 is highly toxic, Cl_2, S2 and P2 is highly reactive and C_2 is very unstable, therefore all are rejected as purge gas (advice inside the lab).
Another way would be the use of noble gasses. Since these gasses are more expensive than pure nitrogen gas, one 140 cm tank of helium ('cheapest' of noble gasses) is $120 against $70 for pure nitrogen (in stockroom of the Chemistry Department of UC Davis), nitrogen is chosen as purge gas.

B.7: Measuring schemes of crykinetic experiments:

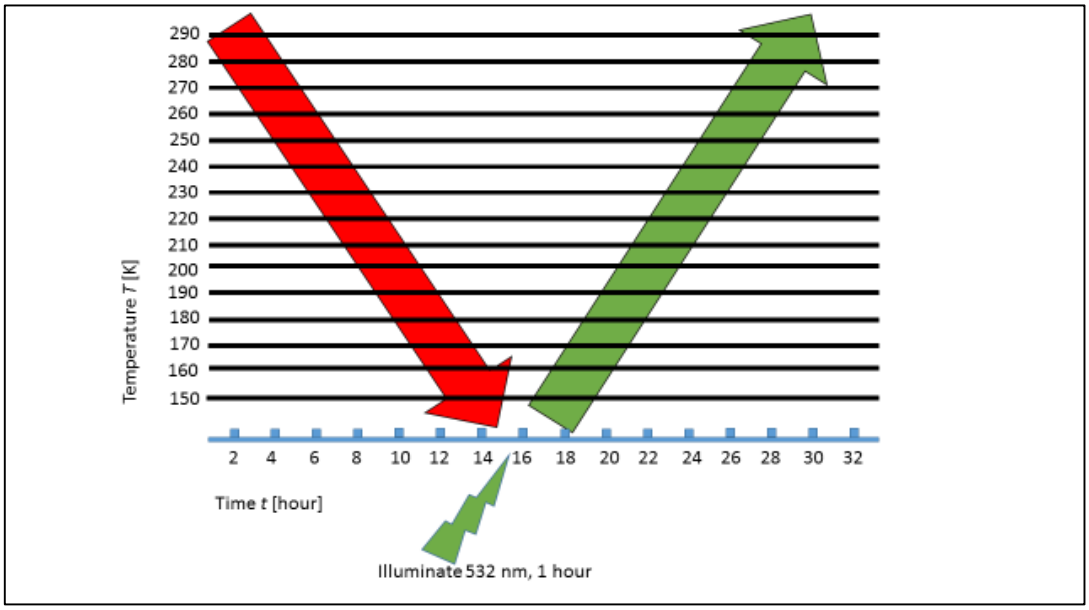

Figure B-7, Forward reaction, 12 hours in the dark, start measurement at 290 K decrease temperature every hour 10 K, at 150 K illuminate with 532 nm for 1 hour and then increase temperature 10 K every hour till 290 K.

Measurement itself takes about: 29 hours, followed by another 12-hour purge in the dark.

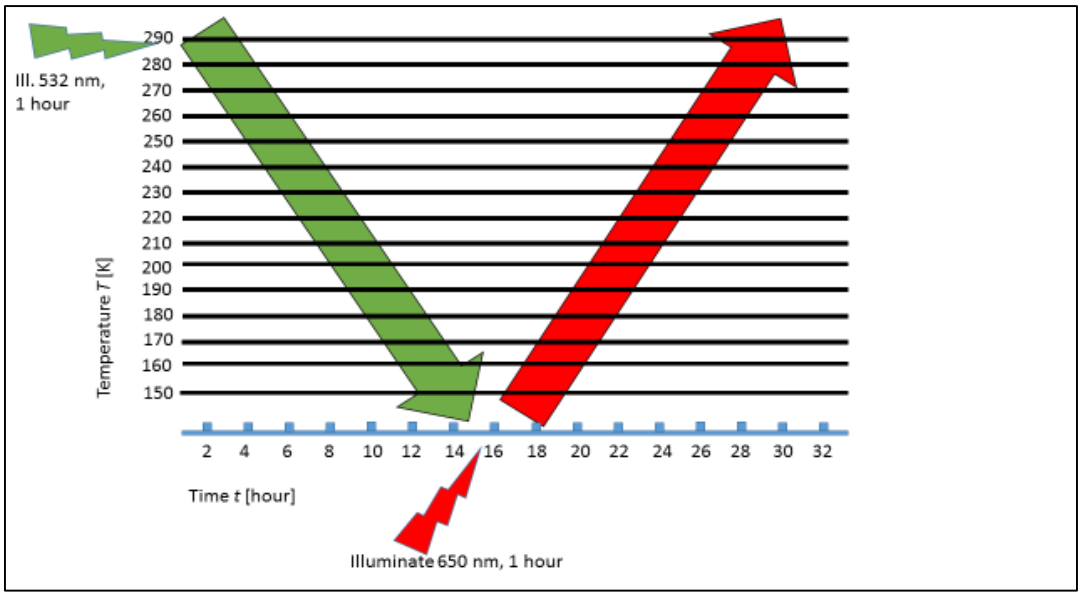

Figure B-8, Reverse reaction, sample is illuminated for 1 hour with 532nm, start measuring at 290 K every hour 10 K lower, at 150 K illuminate with 532 nm for 1 hour and then increase temperature 10 K every hour till 290 K.

This measurement also takes about 29 hours. Thus, in total the entire cryokinetic experiment will take 82 hours, i.e. 3 days and 10 hours.

B.8: Sample preparation

The given sample, made in the Department of Molecular Cellular Biology at UCD, consist protein and water. Since the FTIR is sensitive to vibrational spectra of molecules, the water can disturb the measurements on the protein. Therefore, it is preferred to have just enough water for the protein, but not too much to dry the protein completely out.

To make the sample FTIR experiment ready, drop one drop of the given sample on a window (for instance a CaF_2 window) and blow dry, gently, nitrogen gas (N_2) over it. The sample should look slimy and not liquidly. Dry the sample right before it begins to peel off and stops 'being sticky'.
Since it is hard to tell when the peeling begins it is advised to do several dry and drops (use water to rehydrate the sample). When it looks slimy enough by the naked eye add another window on top and put petroleum jelly around the edges to prevent the sample from drying or dripping out.

After preparation, an UV-VIS spectrometer is used to check the samples absorption spectrum in the visible region of the electromagnetic spectrum. In the case of NpR6012g4, red light is used to push the protein forward and green to push it back. Scan the spectra between illuminations; the absorption spectrum of the protein should shift from a 650 nm peak to 540 nm peak. If this does not occur the protein probably does not work anymore and a new sample should be picked up. The UV-VIS spectrometer is also used to check the height of the absorption peaks. The minimal absorption would be 0.6, when this is not the case more sample should be added and the process, described above, starts over.

Appendix C: Additional experimental data

C.1: Detector corruption data

The signal output of the detector [27] is relatively small and is overshadowed by noise generated internally at room temperatures. Since this noise within a semiconductor is partly proportional to the temperature, the detector operates at cryogenic temperatures for noise minimization. Therefore, the detector is relatively sensitive [54] and picks up a lot of noise when not cooled down. Resulting in, not getting the 'baseline' of background and sample scan at the same level (first stage). Next, the noise increases rapidly (± 20,000x) and thereby exceeding the sample data and is declared corrupted.

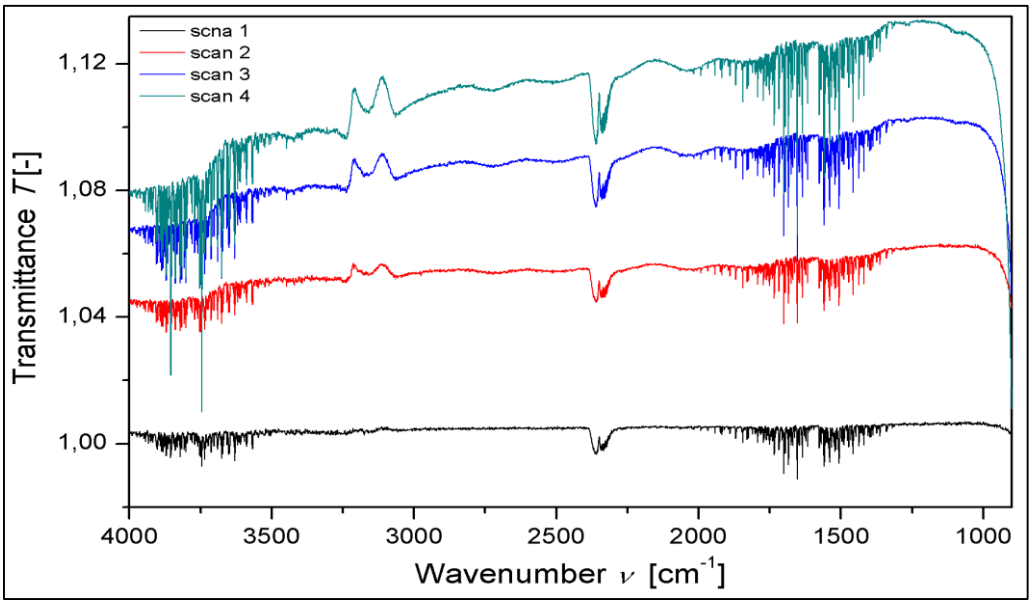

Figure C-1: Start of detector data corruption. 3 scans were taken 3 minutes after each other. Instead of a drift going down it drifts up with almost 0.07 transmittance per minute, which is faster than the 'normal drift'.

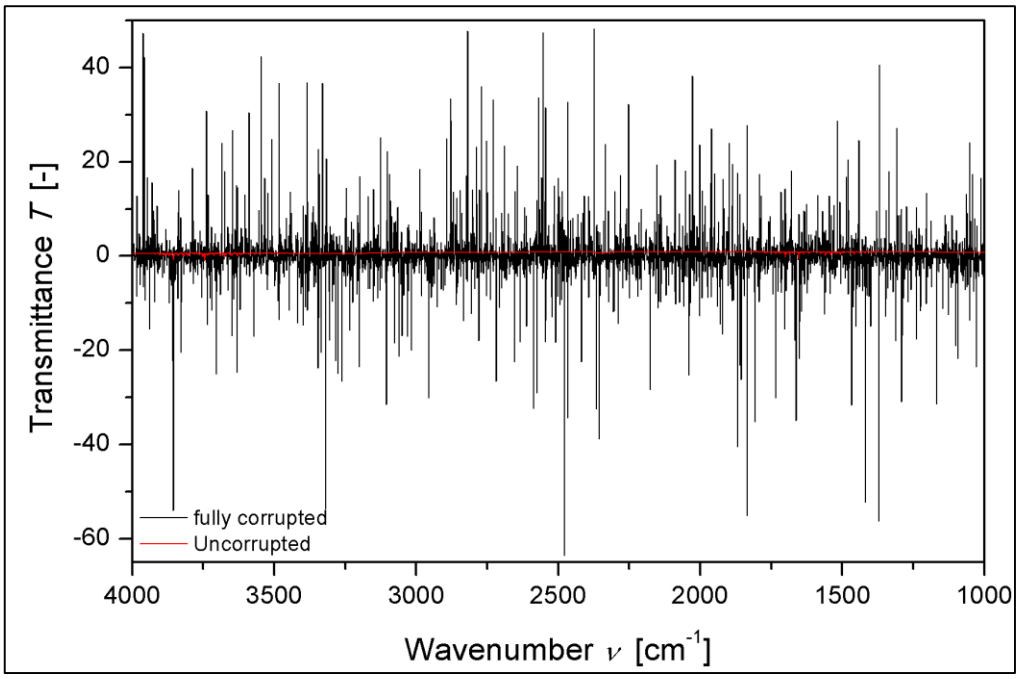

Figure C-2: Detector data corruption. The noise in the signal increases rapidly (±20000x (40 and 0.002)). Red line is scan 3 from figure C-1 above. Black is the scan 3 minutes after scan 3 and is the moment the detector is totally corrupted and noise exceeds data.

C.2: Old measurement of NpR6012g4 by D. Madsen

Figure C-3 shows one of the old measurements of D. Madsen, who worked on the FTIR before the author of this thesis. The plot gives a good indication what the differences in water vapor and CO_2 should be, explained in paragraph 4.1.4. The transmittance difference during the purge should be 10^{-4} per 3 minutes, since the data is in mOD.

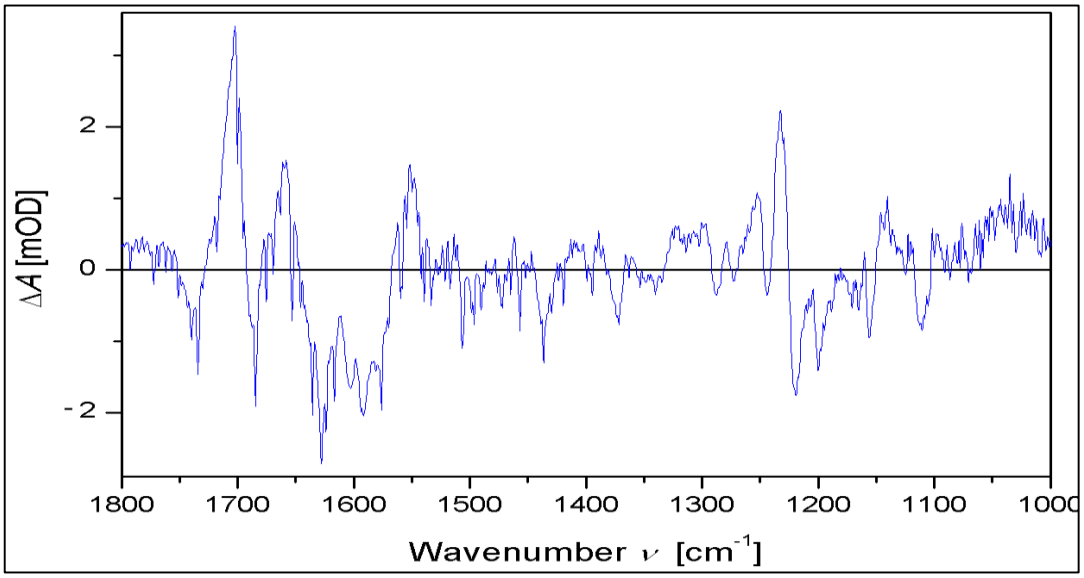

Figure C-3: Plot of old measurement of D. Madsen, showing the Δ*A* [mOD] between green and red illuminated NpR6012g4 sample. Wherein Δ*A* is plotted against wavenumber *ν*.

C.3: Detector drift additional data

Figure C-4 shows one scan of the detector warming up in 5 hours (309 min), and only one background scan was taken. Calculations, for the difference, were done as described in paragraph 4.1.2.

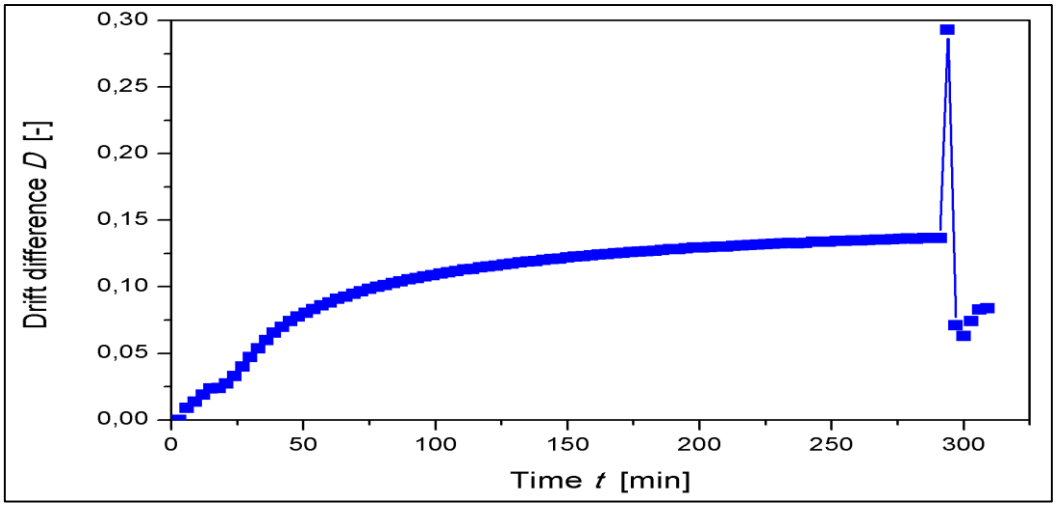

Figure C-4: One five-hour scan of detector drift. At 292 minutes, the detector is corrupted and needed to be refilled. Note that this is as scatter plot with lines to illustrate the corruption during tests. Difference *D* is plotted against time *t* [min].

Found σ of trend lines for the three detector drift measurements with LINEST are:

$3.82 \cdot 10^{-6}$, $5.14 \cdot 10^{-6}$ and $2.53 \cdot 10^{-6}$.

These values are added up and multiplied by three [30] to get the uncertainty in the detector drift:

$$3 \cdot (3.82 \cdot 10^{-6} + 5.14 \cdot 10^{-6} + 2.53 \cdot 10^{-6}) = 3.44 \cdot 10^{-5}$$

C.4: Scanner velocity measurements set at 10 and 20 kHz & resolution

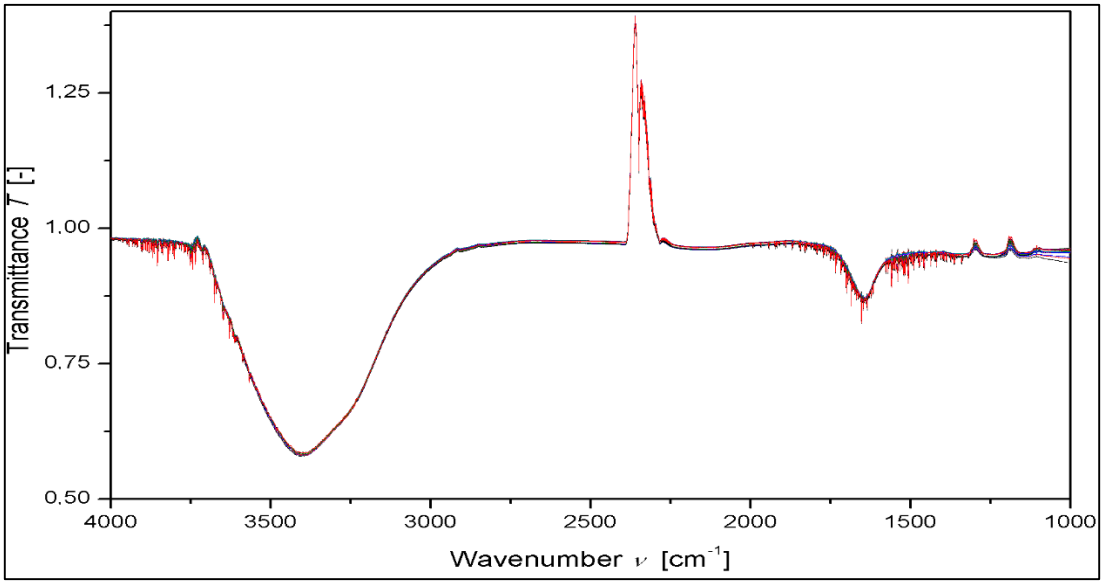

Figure C-5: Plot of all measured water scans, unpurged, of the 10 and 20 kHz, wherein transmission *T* is plotted against wavenumber *v*. It shows water peaks at 3400 and 1600 cm^{-1}, CO_2 influence at ±2300 and ±1300 cm^{-1} (less CO_2 then background) and water vapor 3500+ cm^{-1} and 2100-1400 cm^{-1}. No legend due to multiplication of the same data.

The maximum and minimum value in each data point (for 10 and 20 kHz) were taken and subtracted from each other, giving the largest differences between all the measurements. The difference is shown in figure C-6 below.

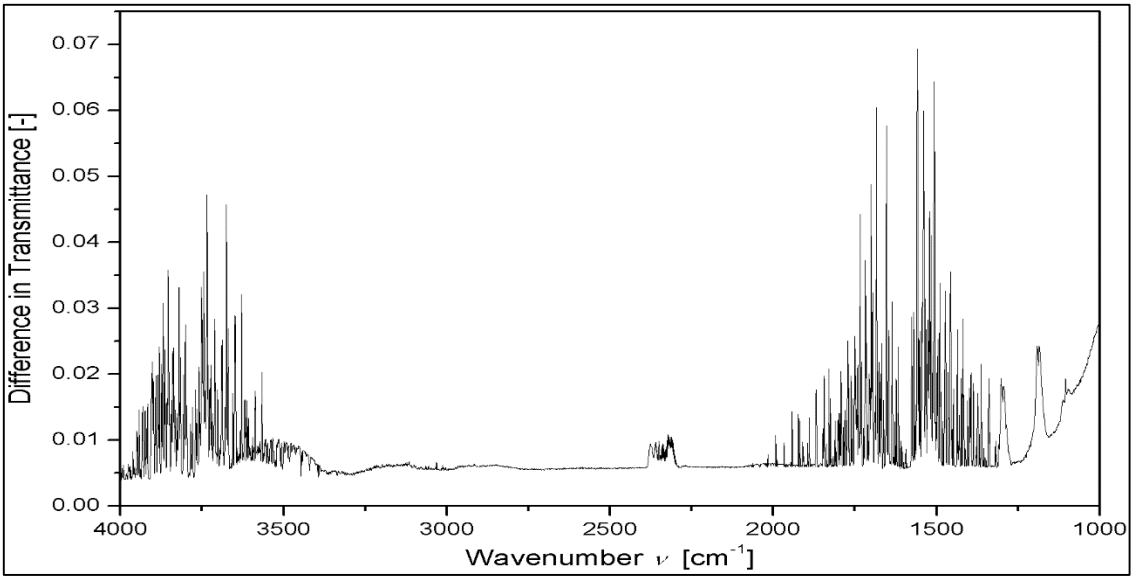

Figure C-6: Plot of the differences between maximum and minimum value in each data point of all the measurements from figure C-5, wherein transmittance *T* is plotted against wavenumber *v*. The most noticeable difference is the CO_2 at ±2300 and ±1300 cm^{-1}, water vapor at 3500+ cm^{-1} and 2100-1400 cm^{-1} and the specific detectivity of the detector at ± 1000 cm^{-1}.

The most noticeable differences are of CO_2 at ±2300 and ±1300 cm^{-1}, water vapor at 3500+ and 2100-1400 cm^{-1} and the cut-off influence of the CaF_2 windows at ± 1000 cm^{-1}. Since the system was not purged during these measurements, water vapor and CO_2 could freely get in and out of the sample chamber, i.e. decrease or increase of the absorption bands, which explains the differences. In the other regions (3000-2400 cm^{-1} & 2200-2000 cm^{-1}) similar to the baseline of the scan, the transmission difference is significantly lower: 0.005.

Figure C-7 contains a zoom-in of figure C-5, showing the non-changing position of the absorption bands and a small difference between scanner velocity of 10 and 20 kHz. 20 kHz tends to have higher transmissions values than 10 kHz. It can be seen that the two scanner velocities show no other significant differences. Since the interest goes to the difference between the dark state and photostate, it does not matter which scanner velocity is used. As long as it does not change during the experiment. Especially when the detector drift is compensated by repeatedly taking background scans, as described in paragraph 4.1.2.

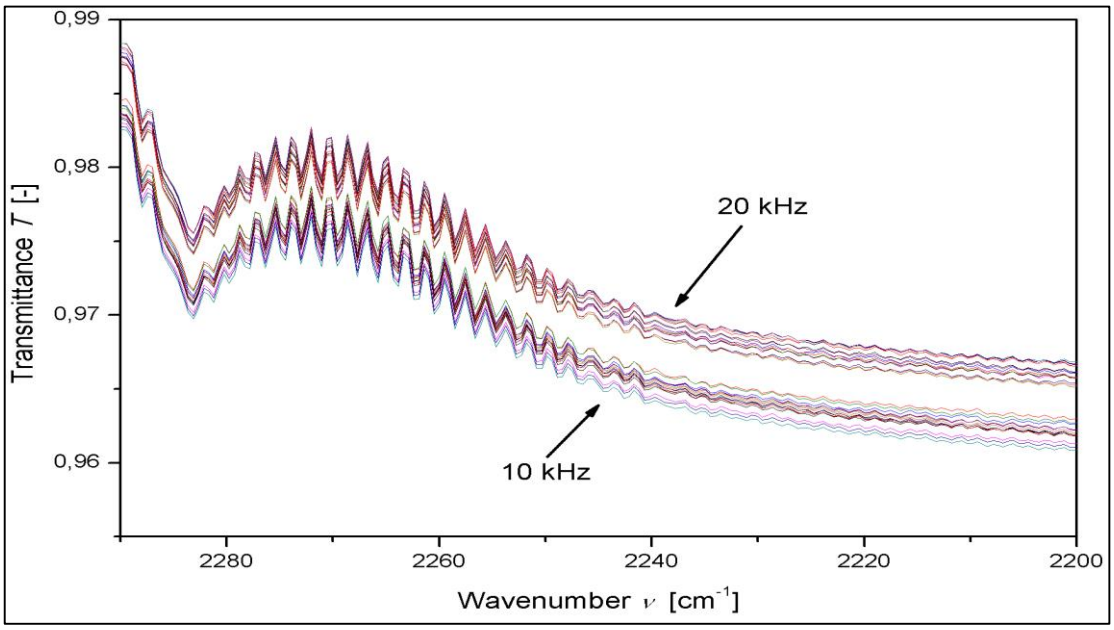

Figure C-7: Differences shown between 20 and 10 kHz, wherein transmittance *T* [-] is plotted against wavenumber *ν* [cm^{-1}]. Scanner velocity of 20 kHz is slightly (0.005) higher than 10 kHz. It shows also the detector drift during the measurements. However, the absorption peaks stay at the same position (2270 cm^{-1}).

The table C-1 below shows the additional results of the 4 cm^{-1} scanner velocity test.

Table C-1: Number of scans set out against measured times at 10 and 20 kHz scanner velocity. Time is measured three times for each setting, with calculated time average t_{av}.

Number of scans [-]	Time *t* at scanner velocity 10 kHz [s]			Average time t_{av} [s]	Time *t* at scanner velocity 20 kHz [s]			Average time t_{av} [s]
	Scan 1	*Scan 2*	*Scan 3*		*Scan 1*	*Scan 2*	*Scan 3*	
5	5.23	5.89	6.01	5.71	2.96	2.52	2.11	2.53
10	10.57	11.66	10.09	10.77	5.72	6.12	5.66	5.83
15	14.87	15.22	16.16	15.42	7.56	7.24	8.44	7.75
20	21.55	20.42	20.58	20.85	11.12	9.89	10.63	10.55
25	25.44	25.86	25.34	25.55	12.12	12.73	13.41	12.75

Figure C-8 shows a zoom-in of the region 1540-1450 cm^{-1} of three scans of water in an unpurged chamber. The three scans are taken with the resolution 1, 2 and 4 cm^{-1} (all other settings the same as measurements above). It can be seen that all scans have the same course, however resolutions 1 and 2 cm^{-1} show water vapor peaks, which is not wanted.

Appendix A.4 shows that the amide and protein bands are relatively wide, thus setting the resolution to 4 cm^{-1} only effects the water vapor [13] and amplitude (figure C-8). Since the interest goes to the difference between two spectra, the amplitude would not play a role when both spectra are measured at the same resolution and settings.

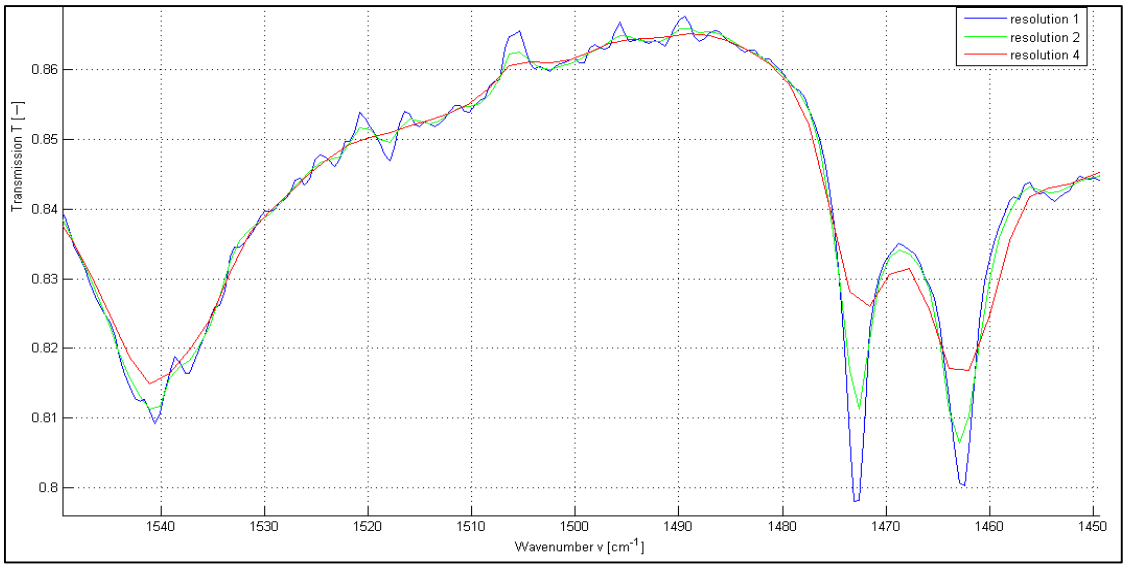

Figure C-8: Zoom-in of taken water spectrum (1540-1450 cm^{-1}) showing the differences between the resolution 1 (blue), 2 (green) and 4 (green) cm^{-1}. Here transmittance *T* [-] is plotted against wavenumber *ν* [cm^{-1}].

C.5: Flow meter test results

Table C-2: All calculated data from the flow meter experiment. Here the calculated differences between successive measurements for the flows 2, 3 and 4 L·min^{-1} of CO_2 (c) and water vapor (h) at time *t*. The average and standard deviation *σ* are found in the last row.

	Calculated difference at reference time *t* for flow (2,3,4) and peak (c/h)					
Time *t* [min]	2c [10^{-3}]	2h [10^{-4}]	3c [10^{-4}]	3h [10^{-4}]	4c [10^{-4}]	4h [10^{-4}]
3	2.099	6.720	$1.394 \cdot 10^{-5}$	$2.803 \cdot 10^{-5}$	5.213	$5.179 \cdot 10^{-5}$
6	1.739	1.058	4.771	$1.892 \cdot 10^{-5}$	3.367	0.384
9	1.532	9.696	1.547	$1.848 \cdot 10^{-5}$	2.758	$1.691 \cdot 10^{-5}$
12	0.948	-4.138	5.778	-2.140	1.060	0.957
15	2.321	$1.443 \cdot 10^{-5}$	5.632	$1.195 \cdot 10^{-5}$	5.895	-9.084
18	1.301	-8.728	3.138	-7.927	-0.494	6.010
21	1.786	-3.250	4.559	$1.386 \cdot 10^{-5}$	4.945	$-2.334 \cdot 10^{-5}$
24	1.221	$1.875 \cdot 10^{-5}$	0.765	$-1.440 \cdot 10^{-5}$	1.518	4.101
27	2.246	$1.324 \cdot 10^{-5}$	5.812	$1.179 \cdot 10^{-5}$	0.727	-2.390
30	1.229	$-1.355 \cdot 10^{-5}$	2.412	$2.061 \cdot 10^{-5}$	2.727	-9.635
33	1.337	9.560	7.140	6.048	0.885	-3.901
36	1.897	1.140	8.051	$1.532 \cdot 10^{-5}$	1.093	-3.663
39	1.354	-5.774	-0.315	$1.220 \cdot 10^{-5}$	1.289	5.099
42	2.592	3.249	6.609	6.131	5.895	-9.084
45	1.965	$1.710 \cdot 10^{-5}$	2.645	9.953	1.518	$1.010 \cdot 10^{-5}$
48	0.868	-4.184	3.684	8.829	0.727	-2.390
51	0.995	$1.946 \cdot 10^{-5}$	5.690	$1.500 \cdot 10^{-5}$	2.727	-3.635
54	2.042	-5.664	2.946	5.447	6.885	-3.896
57	1.406	-4.859	6.045	$1.269 \cdot 10^{-5}$	1.090	-3.663
60	1.529	2.574	-0.805	$1.370 \cdot 10^{-5}$	1.289	5.099
63	1.359	$1.488 \cdot 10^{-5}$	5.744	3.316	1.518	-9.084
Average	16.08	3.891	4.560	9.893	2.510	0.804
σ	1.043	2.157	0.707	2.099	0.453	3.136

C.6: Additional room temperature data

Table C-3: All individual found peak data used for calculating the uncertainty/accuracy of Anacy 4718g3.

Found peaks at corresponding average [cm^{-1}] (measurement 1-10)										
Average	1	2	3	4	5	6	7	8	9	10
1732	1731.995	1730.066	1730.066	1731.995	1731.995	1730.066	1731.995	1731.995	1730.066	1733.924
1715	1714.637	1714.637	1710.779	1712.708	1714.637	1714.637	1710.779	1714.637	1716.565	1712.708
1693	1693.421	1691.492	1691.491	1693.421	1691.492	1695.343	1693.421	1695.349	1695.349	1691.492
1670	1670.276	1670.276	1670.276	1672.205	1672.205	1672.205	1668.347	1674.133	1670.276	1668.347
1616	1616.272	1618.2	1616.272	1616.272	1616.272	1616.272	1616.272	1620.129	1616.272	1620.129
1603	1602.771	1604.699	1602.771	1608.557	1600.842	1602.771	1604.699	1600.842	1606.628	1600.842
1589	1587.341	1593.127	1585.412	1589.269	1587.341	1591.198	1589.269	1587.341	1591.198	1589.269
1533	1529.55	1535.408	1533.336	1533.336	1529.479	1531.408	1531.408	1535.265	1529.479	1529.479
1508	1510.192	1506.598	1510.192	1508.263	1508.263	1510.192	1510.192	1510.192	1508.263	1508.263
1499	1498.619	1494.762	1494.762	1498.619	1502.477	1500.548	1500.584	1496.691	1496.691	1496.691

Found peaks at corresponding average [cm^{-1}] (measurement 11-20)										
Average	11	12	13	14	15	16	17	18	19	20
1732	1731.995	1731.995	1730.066	1731.995	1731.995	1731.995	1735.853	1735.853	1731.995	1731.995
1715	1717.637	1710.779	1718.494	1716.565	1714.637	1712.708	1714.637	1714.637	1712.708	1714.637
1693	1695.349	1693.421	1693.421	1695.349	1689.563	1695.349	1693.421	1695.349	1693.421	1693.421
1670	1668.347	1670.276	1670.276	1668.347	1674.134	1670.276	1668.347	1674.133	1674.133	1674.133
1616	1618.2	1618.2	1618.2	1616.272	1616.272	1616.272	1616.272	1614.343	1618.2	1620.129
1603	1602.771	1602.771	1604.699	1602.771	1606.628	1604.699	1602.771	1602.771	1600.842	1604.699
1589	1591.198	1589.269	1589.957	1589.269	1589.269	1587.341	1591.198	1589.269	1591.198	1591.198
1533	1529.479	1533.336	1529.55	1533.336	1533.336	1529.479	1529.479	1535.265	1531.408	1531.408
1508	1508.263	1510.192	1512.12	1510.192	1506.481	1508.263	1510.192	1507.907	1510.192	1506.334
1499	1498.619	1498.619	1498.905	1500.769	1500.548	1498.619	1500.548	1498.619	1498.619	1500.235

Table C-4: All individual found peak data used for calculating the uncertainty/accuracy of NpF2854g3.

Found peaks at corresponding average [cm^{-1}] (measurement 1-10)										
Average	1	2	3	4	5	6	7	8	9	10
1736	1735.853	1735.853	1735.853	1737.781	1735.853	1737.781	1735.853	1735.853	1735.853	1735.853
1713	1716.565	1714.637	1710.779	1714.637	1710.779	1714.637	1714.637	1710.779	1714.637	1716.565
1684	1683.777	1683.777	1681.848	1683.777	1682.777	1685.706	1681.848	1683.777	1683.777	1683.777
1672	1670.276	1672.597	1673.062	1672.205	1674.133	1674.133	1670.276	1672.205	1674.133	1670.275
1641	1641.345	1641.345	1641.345	1639.416	1641.345	1639.416	1639.416	1641.345	1641.345	1641.345
1620	1620.129	1618.2	1618.2	1620.129	1618.2	1620.129	1620.129	1620.129	1620.129	1620.129
1603	1602.771	1602.771	1602.771	1602.771	1602.771	1602.771	1602.771	1600.842	1600.842	1602.771
1570	1568.054	1569.982	1573.84	1569.982	1568.054	1569.982	1568.054	1569.982	1568.054	1569.982
1549	1548.766	1550.695	1548.766	1554.552	1552.624	1548.766	1548.766	1550.695	1548.766	1548.766
1531	1531.408	1529.479	1531.408	1531.408	1531.408	1531.408	1531.408	1529.479	1527.55	1529.479
1510	1512.12	1512.12	1512.12	1512.122	1512.12	1512.12	1512.12	1510.192	1510.192	1512.12
1456	1456.187	1456.187	1456.187	1456.187	1452.33	1456.187	1454.259	1457.116	1458.116	1456.187
1431	1434.971	1429.185	1431.114	1431.114	1431.114	1431.114	1423.399	1433.043	1431.114	1431.114

Found peaks at corresponding average [cm^{-1}] (measurement 11-20)										
Average	11	12	13	14	15	16	17	18	19	20
1736	1735.853	1735.825	1735.853	1735.853	1735.853	1735.853	1737.781	1737.781	1737.781	1735.853
1713	1712.708	1712.708	1712.708	1717.494	1712.708	1710.779	1714.637	1716.176	1710.779	1716.565
1684	1683.777	1683.777	1681.848	1683.777	1683.777	1689.563	1683.777	1681.848	1681.848	1683.777
1672	1672.205	1672.205	1670.276	1670.276	1670.276	1672.205	1672.205	1672.205	1668.317	1674.133
1641	1641.345	1641.345	1639.416	1641.345	1643.274	1641.345	1639.416	1641.345	1641.345	1641.345
1620	1622.058	1620.129	1620.129	1620.129	1620.129	1620.129	1620.129	1620.129	1620.129	1620.129
1603	1602.771	1602.771	1602.771	1602.771	1602.408	1602.771	1602.771	1602.771	1602.771	1602.771
1570	1571.266	1571.568	1566.196	1571.911	1568.054	1569.982	1566.125	1573.84	1568.054	1568.054
1549	1544.909	1544.909	1548.766	1548.766	1550.695	1550.695	1544.909	1548.766	1552.552	1548.766
1531	1533.356	1531.408	1531.408	1533.336	1527.55	1529.479	1531.408	1531.408	1529.479	1529.479
1510	1510.192	1508.263	1508.263	1506.334	1508.263	1512.12	1510.192	1510.192	1508.283	1512.12
1456	1454.259	1456.187	1454.259	1454.259	1456.187	1458.118	1456.187	1452.33	1456.187	1456.187
1431	1431.114	1429.185	1433.043	1431.114	1433.943	1431.114	1431.114	1431.114	1431.114	1431.114

Appendix D: Additional information about student and thesis

D.1: Thesis plan of work

Plan of Work

Applied Physics

DE HAAGSE HOGESCHOOL | Larsen Lab | UCDAVIS UNIVERSITY OF CALIFORNIA

Student & Internship information

Student information | *1e Coach* | *2e Coach*

Student:	*Jasper Franse*	Name:	*R.A. Mantel*	Name: *A.J. Lock*
Student Number:	*12114979*	E-mail:	*r.a.mantel@hhs.nl*	E-mail: *a.j.lock@hhs.nl*
Education:	*Applied Physics*			
Period:	*08-02-16 t/m 03-06-16*			
E-mail Student:	*jasperfranse@hotmail.com*			

Internship Information

Name of company:	*Larsen Lab, University of California Davis*
Building Location:	*Chemistry Annex, Room 0450*
Department:	*Chemistry*
Intern Mentor:	*Prof. D.S. Larsen*
E-mail:	*dlarsen@ucdavis.edu*

Description of UC Davis & Larsen Lab

The University of California, Davis (UC Davis or UCD), founded in 1905, is a large public university and one out of 10 campuses of the University of California system. Established in Davis, California, about 20 km west of Sacramento, with 5300 hectares of land, which makes it the second largest UC campus in terms of land and has more than 50.000 students. UC Davis has also the third largest enrollment within the UC system after UCLA and UC Berkeley.
UC Davis is classified as a comprehensive doctoral research university with a medical program, and a high research activity. UC Davis faculty consists of many Science / research, laws and art groups. Including: National Academic of Science, the American Academy of Arts and Sciences, American Law Institute and the National Academy of Engineering.

The laboratory of Prof. D. Larsen is located within the Chemistry department of UC Davis. The laboratory is also referred to as Larsen lab.
The research done at Larsen lab extends across many scientific disciplines which includes: biophysics, physical chemistry, molecular biology and computational modeling. All these disciplines have in common that, within Larsen lab, they are investigated and characterized on rapid condensed phase dynamics. (Source: *http://larsenlab.ucdavis.edu/*).
The main focus of Larsen Lab is to explore the ultrafast processes (fs-ns) of photoreceptors and other light sensitizing proteins which serve central roles in light activated biological functions. A fundamental question for many photoreceptors is how the absorption of a photon within a protein is transformed into the complex response required for biological functions.

Global assignment description

The project involves what the lab refers to as "FTIR cyrokinetics." This project extends on the previous characterization of the primary dynamics of light sensitive photoreceptor proteins by tracking the propagation of the primary dynamics (on the ultrafast times <10 ns) through the secondary timescale to the generation of the terminal photo state. In these measurements, photosensitive samples are cryocooled within an Optical Cryostat (to 77 K) and irradiated to generate trapped intermediates of the photocycle. Increasing the temperature then advances the trapped photo generated populations into subsequent intermediates over activation barriers, providing a wealth of information about secondary dynamics for comparison to secondary dynamics studies. Spectral changes during approach to equilibrium can be analyzed using global analysis and transition state theory to derive microscopic forward and reverse rate constants as the sample equilibrates. The fractional occupations at thermal and chemical equilibrium are related by respective enthalpy differences (ΔH) via the van't Hoff equation. The current progress in this effort has focused on the visible probing of the cryotrapped intermediates.

The primary goal of this research would be to extend this effort into characterizing the vibrational spectra of intermediates with FTIR. This includes modifying the existing FTIR and cryostat to handle infrared light and optimizing the setup to measure the proper temperature dependent signals. Once solid data is collected, it is needed to master multi-dimensional analysis of the temperature and time dependent spectra to correlate the extracted population dependent spectra with the known visible cryokinetics and ns-ms room temperature kinetics.

Plan of approach

First of all, it's necessary to do a literature review on: FTIR, Vibrational energy/spectra, Cyrokinetics, what was discovered in earlier research, how was this done, what kind of equipment would be needed.

After that, a good global idea of what one should know and can expect is required. One should examine the equipment needed for the measurements. This includes knowing what affects could occur in the spectra, how to recognize them and to know which would have interest and which not.

Once there is a good understanding of the theory and equipment the set-up shall be build and adjusted for the measurements. When tests on the equipment and set-up seems sufficient the measurements on the proteins can start.

Finally, after collecting the data, it will be correlated with the known visible cryokinetics. When this is done I'll start finishing my paper, presentation and poster to hand in for my graduation.

Temporary chapters of Thesis report

- Cover page
  - title
  - Name & information
- Abstract + Dutch summary
- Table of contents
- Introduction
  - Problem description
  - Objectives of assignment
  - Expectations
- Theory
  - What is FTIR and spectroscopy

    - Cryokinetics
    - Cooling proces
    - Multi-dimensional analysis
    - Van 't Hoff
    - Special theory to be known for the equipment
    - Which factors can affect the measurements
- Measuring methods, work and materials
- Results
    - Experiment results
    - Calculations
    - Inaccuracy
- Conclusion
    - What is there to conclude
    - Discussion
    - Future suggestions
- References
- Appendices

Plan of work activities

Table D-1 shows a temporary plan of activities, which is divided in different periods. Most activities are a global description and other activities will be specified during the research, this includes data on presentation, visits and handing in papers.

Table D-1: Temporary plan of activities. Period of work against type of work and expected results.

Period	***Type of Work***	***Expected result/products (achieved on last date in period)***
08-02-16 t/m 15-02-16	**Beginning of internship, Collecting and understanding the theory, introductions to new environment and laboratory**	**Get familiar with the lab, people, used theories in the lab, procedures and safety in the lab.**
22-02-16	**Hand in plan of work**	**Report**
15-02-16 t/m 07-03-16	**Theory, equipment understanding (simulations?) Global analysis, FTIR, photocycles**	**More knowledge on equipment, theories and what can be expected and what not in future experiments**
07-03-16 t/m 25-03-16	**Equipment set up and adjustment**	**Best settings for the FTIR: lowest SNR, purge & start up time, best way for sample preparation**
28-03-16 t/m 29-04-16	**Set-up + experiments + processing**	**Build one or two set ups + 'manual' for experiment. Have solid data of sample + global analysis of data for comparison**
29-04-16	**Hand in concept work to 1e coach**	**Report containing: front page, introduction, theory, work and set up, few experiment results, partial conclusions and references/appendices**
29-04-16 t/m 23-05-16	**Last experiments, adjustments and processing**	**If found necessary better results. Finding a correlation between known data and FTIR data.**
23-05-16 t/m 27-05-16	**Checking data, finish thesis and prepare for presentation + making a poster**	**A finished report + poster + a set up presentation for the HHS in The Netherlands**
03-06-16	**Hand in Thesis + poster and give presentation at internship?**	**Report (3x hardcopy 2x digital), poster (A3) and a good mark**

End result expectations

In the end, I hope to be able to say something about the vibrational states of the measured proteins. For example, what are they made of (only isomerization or something else happening), what happens to the atom distribution within or having a better understanding on the vibrational energies. I also expect to say something about the similarities or differences between the FTIR and the visible measurements of the used proteins.
Other than that, it's hard to say what can be expected. This research (besides the FTIR) is all about getting a better understanding of the intermediate states of the photoreceptors of proteins. So, the best thing to expect would be: To know more about the proteins and see some similarities between different data results (visible, primary/secondary, ultrafast and FTIR studies).

Personal Goals

My personal goals during my graduation internship abroad are:

- Getting a better understanding of the use of physics in photonics and applying them in the field.
- I want to learn more about study fields crossing each other. For instance, this research work where spectroscopy, photonics and chemistry all meet in one study.
- Have a better idea of working on an international basis.
- Jacking up my English skills.
- Enhancing my planning skills. Also, enhancing my information-collecting skills on the needed equipment. Including to know what to expect and what not.
- Getting to know more about university research at an actual university.
- Try to do more research work on my own.